IL
NUOVO CIMENTO
ORGANO DELLA SOCIETÀ ITALIANA DI FISICA
SOTTO GLI AUSPICI DEL CONSIGLIO NAZIONALE DELLE RICERCHE

VOL. XVII, N. 1 *Serie decima* 1° Luglio 1960

Meteorological Coefficients and Solar Daily Variation of the Cosmic Radiation Measured Underground.

T. SÁNDOR, A. SOMOGYI and F. TELBISZ

Central Research Institute of Physics, Cosmic Ray Laboratory - Budapest

(ricevuto il 7 Marzo 1960)

Summary. — We have been registering the intensity of the penetrating component of the cosmic radiation since the 20-th February 1958. The absorption and decay coefficients as well as the total barometric coefficient were determined from the data of the first year of the observation. We determined further the amplitude of the fluctuation of the primary radiation for each month and the amplitude of the solar daily variation.

1. – Introduction.

Within the framework of the I.G. Year and the I.G. Co-operation 1959, we have been registering the penetrating component of the cosmic radiation at a depth of about 18 m underground (*i.e.* about 40 m w.e.). The primary aim of this work was to determine the atmospheric coefficients of the penetrating component and to investigate the solar diurnal variation of the intensity (*).

The measuring apparatus consisted of two identical, semicubical meson telescopes operating independently of each other. A detailed description of the telescopes may be found in (1).

(*) Part of the results published in this paper have been presented at the IUPAP Conference for Cosmic Rays held in Moscow, July 1959.

(1) T. SÁNDOR, A. SOMOGYI and F. TELBISZ: *Suppl. Nuovo Cimento*, in press.

The experimental station is situated in Budapest, at a geographical latitude 47.5° N, longitude 18.9° E and at 410 m a.s.l. It has been operating since the 20-th February 1958.

2. – The atmospheric coefficients.

We solved the regression equation of the following type:

$$\frac{\Delta I}{I_0} = A\,\Delta p + D\,\Delta h\,, \tag{1}$$

denoting by I_0 the average sum of the two fluxes measured by the two telescopes, by ΔI the deviation of this sum from I_0, by Δp the deviation of the barometric pressure from its mean, by Δh the analogous quantity for the height of the 200 mb isobaric level and by A and D the relative absorption and decay coefficients, respectively.

We determined further the total barometric coefficient (B), defined by the equation

$$\frac{\Delta I}{I_0} = B\,\Delta p\,.$$

TABLE I.

Month	k	r	A % per cm Hg	D % per km	B % per cm Hg	σ_{PG}/I_0 ‰
1958 March	178	0.77 ± 0.02	− 0.54 ± 0.05	− 0.92 ± 0.27	− 0.69 ± 0.03	2.1 ± 0.2
April	156	0.84 ± 0.01	− 0.84 ± 0.04	− 1.87 ± 0.20	− 0.84 ± 0.04	2.8 ± 0.3
May	234	0.54 ± 0.03	− 0.77 ± 0.05	− 0.45 ± 0.10	− 0.73 ± 0.05	2.4 ± 0.2
June	148	0.66 ± 0.03	− 0.50 ± 0.04	− 1.43 ± 0.23	− 0.52 ± 0.04	2.3 ± 0.3
July	96	0.86 ± 0.03	− 0.96 ± 0.07	− 0.55 ± 0.25	− 1.04 ± 0.06	1.2 ± 0.2
Aug.	181	0.78 ± 0.02	− 1.66 ± 0.07	− 0.83 ± 0.18	− 1.72 ± 0.05	5.4 ± 0.4
Sept.	108	0.37 ± 0.04	− 0.32 ± 0.12	− 1.02 ± 0.18	− 0.45 ± 0.12	4.7 ± 0.4
Oct.	50	0.70 ± 0.05	− 0.35 ± 0.09	− 1.51 ± 0.21	− 0.45 ± 0.08	1.9 ± 0.4
Nov.	98	0.79 ± 0.02	− 0.72 ± 0.04	+ 0.36 ± 0.39	− 0.71 ± 0.04	2.4 ± 0.3
Dec.	66	0.89 ± 0.02	− 0.71 ± 0.05	− 2.04 ± 0.32	− 0.72 ± 0.04	1.4 ± 0.3
1959 Jan.	119	0.88 ± 0.01	− 0.99 ± 0.04	− 0.67 ± 0.16	− 1.11 ± 0.03	2.9 ± 0.3
Febr.	188	0.88 ± 0.01	− 0.90 ± 0.04	− 0.51 ± 0.18	− 0.97 ± 0.02	2.9 ± 0.3
1-3-1958-28-2-1959	1622	0.83 ± 0.004	− 0.78 ± 0.01	− 1.20 ± 0.02	− 0.92 ± 0.01	4.6 ± 0.1

2210

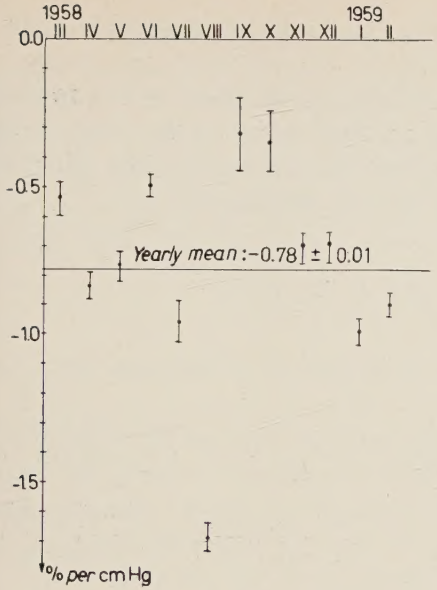

Fig. 1. – Absorption coefficients.

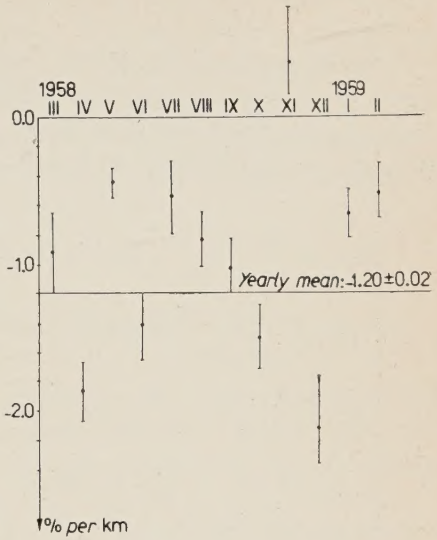

Fig. 2. – Decay coefficients.

A, D and B have been determined separately for each month, as well as for the one-year interval beginning with the 1-st March 1958. The results may be seen in Table I and in Figs. 1, 2 and 3.

Data concerning the isobaric layers were taken from the Daily Report of the Hungarian National Institute of Meteorology. At the radio sounding station situated 20 km south-east from our laboratory, balloons are flown up twice daily. The barometric pressure data were obtained from the readings of a barometer at the place of observation and from microbarograph data placed at our disposal by the National Institute of Meteorology.

In calculating the coefficients given in Table I only those bi-hourly intervals were used during which both telescopes functioned properly and the appropriate radio sounding

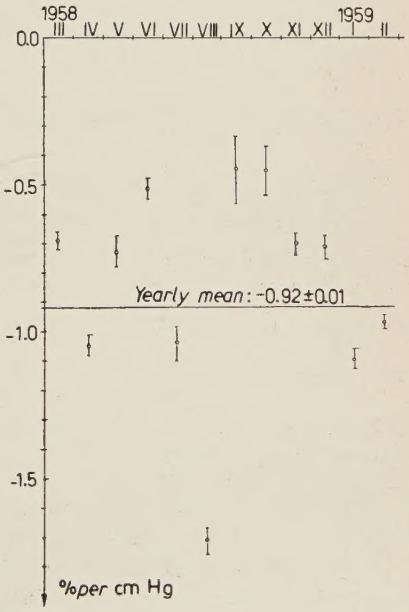

Fig. 3. – Total barometric coefficients.

data were also available (*). The total number (k) of such intervals is also shown in Table I.

The errors shown in Table I were calculated on the basis of the method outlined in papers ([1-3]). We modified the method so as to take into consideration also the measuring errors of the atmospheric factors. The following formulas were obtained and used in the present calculations:

$$
(2)\quad
\begin{cases}
\delta r = \dfrac{1}{\sigma_{II}} \cdot \dfrac{\sqrt{1-r^2}}{r} \left[r^2 (\delta I_0)^2 + A^2 I_0^2 (\delta p_0)^2 + D^2 I_0^2 (\delta h_0)^2 \right]^{\frac{1}{2}}, \\
\delta B = \dfrac{1}{I_0} \dfrac{\sigma_{II}}{\sigma_{pp}} \left[\left(\dfrac{\delta I_0}{\sigma_{II}} \right)^2 + \left(\dfrac{\delta p_0}{\sigma_{pp}} \right)^2 \right]^{\frac{1}{2}}, \\
\delta A = \dfrac{1}{I_0} \cdot \dfrac{\sigma_{II}}{\sigma_{pp}} \cdot \dfrac{1}{\sqrt{1-r_{ph}^2}} \left[\left(\dfrac{\delta I_0}{\sigma_{II}} \right)^2 + \dfrac{1-r_{Ih}^2}{1-r_{ph}^2} \left(\dfrac{\delta p_0}{\sigma_{pp}} \right)^2 + \left(-1 + r^2 + \dfrac{1-r_{Ip}^2}{1-r_{ph}^2} \right) \left(\dfrac{\delta h_0}{\sigma_{hh}} \right)^2 \right]^{\frac{1}{2}}, \\
\delta D = \dfrac{1}{I_0} \cdot \dfrac{\sigma_{II}}{\sigma_{hh}} \cdot \dfrac{1}{\sqrt{1-r_{ph}^2}} \left[\left(\dfrac{\delta I_0}{\sigma_{II}} \right)^2 + \left(-1 + r^2 + \dfrac{1-r_{Ih}^2}{1-r_{ph}^2} \right) \left(\dfrac{\delta p_0}{\sigma_{pp}} \right)^2 + \dfrac{1-r_{Ip}^2}{1-r_{ph}^2} \left(\dfrac{\delta h_0}{\sigma_{hh}} \right)^2 \right]^{\frac{1}{2}},
\end{cases}
$$

where r denotes the total correlation coefficient of the equation of regression (1); r_{Ip}, r_{Ih}, r_{ph} denote the simple correlation coefficients between the quantities I and p, I and h, p and h, resp.; σ_{II}, σ_{pp} and σ_{hh} are the second central moments of the variables I, p and h, resp., *i.e.* for instance $\sigma_{pp}^2 = (1/(k-1)) \sum (\Delta p)^2$. Furthermore,

$$
\delta I_0 = \sqrt{\frac{I_0}{k}}, \qquad \delta p_0 = \frac{\delta p}{\sqrt{k}}, \qquad \delta h_0 = \frac{\delta h}{\sqrt{k}}.
$$

where δp and δh denote the measuring error of one bi-hourly value p and h, resp.

The errors in the atmospheric coefficients due to the uncertainty in measuring the barometric pressure and the isobaric heights turned out to be insignificant (**) as compared to the errors due to statistical fluctuations in the measured fluxes, although errors as high as 0.3 mm Hg and 40 m, resp. were assumed in the barometric pressures and isobaric heights.

(*) The appropriate isobaric heights were determined by linear interpolation between the data obtained by the two radio soundings preceding and following the bi-hourly time intervals.

(2) L. JÁNOSSY and G. D. ROCHESTER: *Proc. Roy. Soc.*, A **183**, 786 (1944).

(3) L. JÁNOSSY, T. SÁNDOR and A. SOMOGYI: *Suppl. Nuovo Cimento*, **8**, 701 (1958).

(**) The errors of the decay coefficient turned out to be larger by 15%, when the errors in the measurement of the atmospheric data were taken into account, the errors of the absorption and total barometric coefficient remained nearly unchanged.

The coefficients obtained show a much greater spread than would be expected on the basis of their statistical errors. A χ^2 test yields a probability less than 10^{-3} for these spreads to be of purely statistical origin. We have inclined to ascribe these large fluctuations in the meteorological coefficients, at least partly, to correlations between meteorological factors and other (*e.g.* geomagnetic) quantities influencing the cosmic ray intensity. An example clearly demonstrating such a case is given in paper [4].

3. – The amplitude of fluctuation in the primary radiation.

In paper [1] we have shown a method suitable for the determination of the mean amplitude of fluctuations due to instrumental effects as well as for the determination of the mean amplitude of the real fluctuations (σ_c), including atmospheric effects.

If we carry out the same calculations using the fluxes corrected for atmospheric effects instead of the uncorrected ones, we get an average amplitude (σ_{PC}), which—as far as the procedure given in paper [1] is justified—is neither of instrumental nor of atmospheric origin, and which amplitude, consequently may be regarded as that of the primary radiation.

There are several ways for obtaining σ_{PC}, according to the different modes in which the correction for atmospheric effects can be carried out.

1) If we reduce our measured fluxes by the coefficients defined by equation (1) we have simply

$$\sigma_{PC}^2 = \sigma_c^2 - \tfrac{1}{4} r^2 \sigma_{II}^2 . \tag{3}$$

2) If we calculate the meteorological coefficients separately from the fluxes measured by the two telescopes we are able to reduce the data of each telescope with its own coefficients.

In this case

$$\sigma_{PC}^2 = \sigma_c^2 - a_2 \sigma_{1p}^2 - d_2 \sigma_{1h}^2 \equiv \sigma_c^2 - a_1 \sigma_{2p}^2 - d_1 \sigma_{2h}^2 ,$$

where a_i and d_i, resp. are the (not relative) absorption and decay coefficients belonging to the data of telescope No. i ($i = 1, 2$); σ_{ip}^2 and σ_{ih}^2, resp. are the second mixed central moments formed by the (uncorrected) rates of telescope

---

[4] T. Sándor, A. Somogyi and F. Telbisz: *Acta Phys. Hung.*, **11**, 205 (1960).

No. i and the meteorological data p and h, resp. For instance

$$\sigma_{2p}^2 = \frac{1}{k-1} \sum \Delta I^{(2)} \Delta p \,,$$

where $I^{(2)}$ denotes the uncorrected flux registered by telescope No. 2.

3) If we use meteorological coefficients other than those calculated by means of the appropriate equations of regression, we get

$$\sigma_{PC}^2 = \sigma_c^2 - a(\sigma_{1p}^2 + \sigma_{2p}^2) - d(\sigma_{1h}^2 + \sigma_{2h}^2) + a^2\sigma_{pp}^2 + 2ad\,\sigma_{ph}^2 + d^2\sigma_{hh}^2 \,,$$

where a and d are the given meteorological coefficients.

The values of σ_{PC} shown in Table I were calculated on the basis of the formula (3). Their errors are given by the formula

$$\delta\sigma_{PC}^2 = \sqrt{2\sigma_{PC}^2 + \sigma_{1-2}^2} \cdot \delta I_0 \,,$$

which was obtained in the same way as the formulas (2), neglecting errors due to uncertainties in the atmospheric data. σ_{1-2} has the following meaning:

$$\sigma_{1-2}^2 = \frac{1}{k-1} \sum [\Delta I^{(1)} - \Delta I^{(2)}]^2 \,.$$

4. – Solar daily variation.

After having corrected the bi-hourly data for the absorption and the decay effects we determined the amplitude and the phase of the solar daily variation

TABLE II.

Month	k'	A (‰)	T_{max} (U.T.)
1958 March	295	1.1 ± 0.2	1240 ± 0040
April	300	1.6 ± 0.2	1020 ± 0030
May	355	1.0 ± 0.2	0920 ± 0040
June	291	2.8 ± 0.2	1230 ± 0020
July	282	1.1 ± 0.3	1540 ± 0110
August	293	0.6 ± 0.2	1550 ± 0130
September	347	0.8 ± 0.3	1830 ± 0120
October	314	1.0 ± 0.4	2150 ± 0120
November	277	1.4 ± 0.3	1150 ± 0050
December	318	0.5 ± 0.3	1550 ± 0220
1959 January	308	1.1 ± 0.3	1610 ± 0100
February	304	0.8 ± 0.2	1000 ± 0110
1-3-1958 - 28-2-1959	3 684	0.68 ± 0.08	1700 ± 0030

2214

for each monthly period as well as for the whole year of observation. The values obtained are shown in Table II and Fig. 4. Every such bi-hourly

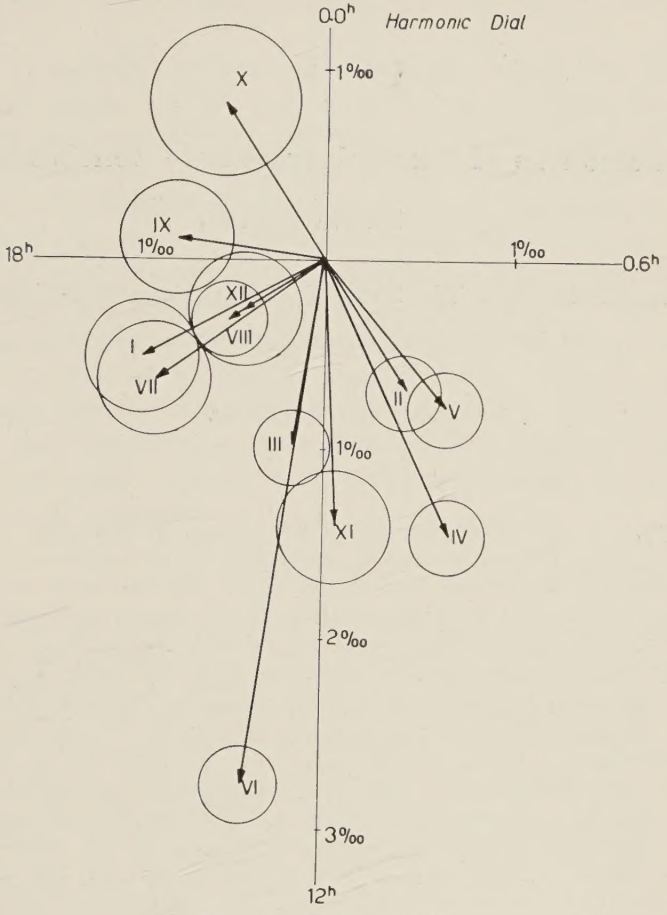

Fig. 4. – Harmonic dial.

interval was used during which at least one of the telescopes functioned properly. The total number (k') of these intervals is also shown in Table II.

RIASSUNTO (*)

Sin dal 20 Febbraio 1958 siamo andati registrando l'intensità della componente penetrante della radiazione cosmica. I coefficienti di assorbimento e decadimento, come anche il coefficiente barometrico totale, sono stati determinati in base ai dati del primo anno di osservazioni. Abbiamo inoltre determinato l'ampiezza della fluttuazione della radiazione primaria per ogni mese e l'ampiezza della variazione solare giornaliera.

(*) *Traduzione a cura della Redazione.*

2215

IL NUOVO CIMENTO Vol. XVII, N. 1 1° Luglio 1960

Interactions of 6.2 GeV Protons in Emulsions.

I. – General Results.

H. Winzeler, B. Klaiber, W. Koch, M. Nikolić and M. Schneeberger (*)

Physikalisches Institut der Universität - Bern

(ricevuto l'11 Marzo 1960)

Summary. — About 700 interactions were found by following 6.2 GeV protons « along the track ». An interaction mean free path of (38.2 ± 1.5) cm was obtained. 42 possible proton-free proton collisions were separated and the cross section for meson production was found to be 23^{+7}_{-6} mb. We found an average multiplicity for charged secondary tracks in inelastic p-p collisions of 2.8 ± 0.3 and the branching ratio of 2 prong to 4 prong events was about 2. These values were compared with the predictions of the statistical theory and with a modification of it. The results of this investigation would be consistent with a model which assumes that at these energies about 50% of all collisions are « peripheral » ones which lead to (nucleon) isobar ($\mathcal{N}\mathcal{N}^*$ or $\mathcal{N}^*\mathcal{N}^*$) formation only. The angular distribution of all thin secondary tracks in the L system have been measured and the formula of Castagnoli *et al.* has been applied to a reasonably selected sample of stars. This gave an overestimation by a factor of about 2 for the primary energy. Other investigators have obtained a similar value at 10^{12} eV.

Introduction.

A large amount of experimental work has been performed in the field on $\mathcal{N}$-$\mathcal{N}$ collisions at different energies. Several experimental data in the $(1 \div 10)$ GeV

(*) Now at CERN, Genève.

region have been published ([1-11]), at 10^{12} eV the available statistics is still considerable ([12,13]) and single events up to 10^{15} eV have been described ([14,15]). The appearance of singly charged particles with even higher energies is probable ([16]).

In ref. ([8,9]) and in the present work the proton energy was 6.2 GeV. The Dubna machine reaches 10 GeV and the CERN proton synchrotron provide us with 28 GeV protons. All these energies can be considered as passage to cosmic ray-jet energies (*). Pion, strange-particle and anti-particle production increases and, in the framework of general program, the study of its energy dependence is of high interest. Unfortunately the average number of particles produced is still small even for the highest machine energies and this in some sense complicates the situation. However, with machines one can have practically any particle flux and the primary energy is precisely known. Emulsion has the disadvantage of being a complex nuclear mixture, but it seems to us, that this difficulty can be overcome and that one can separate, for example, the collisions with free protons in a quite satisfactory manner. Besides this, even collisions with bound nucleons can give much information about the nature of p-$\mathcal{N}$ collisions.

([1]) W. B. Fowler, R. P. Shutt, A. M. Thorndike and W. L. Whittemore: *Phys. Rev.*, **103**, 1479 (1956).

([2]) M. M. Block, E. M. Harth, V. T. Cocconi, E. Hart, W. B. Fowler, R. P. Shutt, A. M. Thorndike and W. L. Whittemore: *Phys. Rev.*, **103**, 1484 (1956).

([3]) W. B. Fowler, R. P. Shutt, A. M. Thorndike, W. L. Whittemore, V. T. Cocconi, E. Hart, M. M. Block, E. M. Harth, E. C. Fowler, J. D. Garrison and T. W. Morris: *Phys. Rev.*, **103**, 1489 (1956).

([4]) R. Cester, T. F. Hoang and A. Kerman: *Phys. Rev.*, **103**, 1443 (1956).

([5]) R. E. Cavanough, D. M. Haskin and M. Schein: *Phys. Rev.*, **100**, 1263 (1955).

([6]) U. Haber-Schaim: *Nuovo Cimento*, **4**, 669 (1956).

([7]) F. N. Holmquist: UCRL 8559 (1958), p. 7.

([8]) R. M. Kalbach, J. J. Lord and C. H. Tsao: *Phys. Rev.*, **113**, 325, 330 (1959).

([9]) R. R. Daniel, N. Kameswara Rao, P. K. Malhotra and Y. Tsuzuki: preprint (Bombay, 1959).

([10]) E. M. Friedländer: *Nuovo Cimento*, **14**, 796 (1959).

([11]) N. P. Bogachev, S. A. Bunjatov, I. P. Merekov and V. M. Sidirow: *Dokl. Akad. Nauk*, **121**, 615 (1958).

([12]) M. Teucher: *Conference on High Energy Accelerators* (CERN, 1959), p. 13.

([13]) *Proc. of the 1958 Conference on Elementary Particles* (CERN, 1958). Report of Piccioni.

([14]) W. B. Fowler: *Proc. of the VII Annual Rochester Conference* (1957), p. xi-18.

([15]) M. W. Teucher, E. Lohrmann, D. M. Haskin and M. Schein: *Phys. Rev. Lett.*, **2**, 313 (1959).

([16]) G. Clark, J. Earl, W. Kraushaar, J. Linsly, B. Rossi and F. Scherb: *Nuovo Cimento*, **10**, 630 (1957).

(*) In the following called also « ultra high » energies. Energies above 10^{12} eV.

2217

Theoretical predictions can be made according to various theories [17-19]. Numerical calculations for the above mentioned machine energies, following the Fermi statistical theory, have been performed [20-25]. In its application to different primary energies the statistical model is practically limited, since with increasing primary energy the number of final states to be taken into account increases rapidly. Therefore at cosmic ray energies Fermi applies the « thermodynamical » (*) treatment.

For. 6.2 GeV protons, involving certain assumptions, reaction rates for pion, strange-particle, anti-baryon production and their energy spectra can be calculated with the low energy theory [20], and it is interesting to compare these with the experiment. Furthermore angular distributions can be used to get indications about the geometrical side of the $\mathcal{N}$-$\mathcal{N}$ interaction models, and in this connection one has probably to distinguish between head-on and peripheral collisions. Correlated to this and of a certain practical importance is also the average fraction of primary energy spent in the creation of particles, the « inelasticity ».

For cosmic ray energies, on the other hand, the situation is kinematically (all β's ≈ 1) and perhaps theoretically (thermodynamical treatment) less complicated than in the low energy cases, but much more undetermined on the experimental side, since the primary energies are not known *a priori*. In addition, in most cases, scattering measurements are not sufficient to determine the energies of *all* charged secondary particles and there exist many jets where no scattering measurements on the secondary tracks have been possible at all. In those cases the main way to determine the primary energy is via the angular distribution of the secondary tracks. The formula used by CASTAGNOLI *et al.* [26], for instance, gives relatively reliable results for the average energy of a larger sample of similar interactions, but in a single case it can

---

[17] W. HEISENBERG: *Zeits. f. Phys.*, **126**, 569 (1949); **133**, 65 (1952).

[18] E. FERMI: *Progr. Theor. Phys.*, **5**, 570 (1950).

[19] L. D. LANDAU: *Dokl. Akad. Nauk*, **17**, 51 (1953); S. Z. BELEN'KIJ and L. D. LANDAU: *Suppl. Nuovo Cimento*, **3**, 15 (1956).

[20] R. HAGEDORN: *Nuovo Cimento*, **15**, 246 (1960).

[21] J. VON BEHR and F. CERULUS: private communication (1960).

[22] R. HAGEDORN: CERN 59-25.

[23] F. CERULUS and R. HAGEDORN: CERN 59-3.

[24] R. HAGEDORN: preprint CERN (1959). A new derivation of the statistical theory of particle production with numeral results for p-p collisions at 25 GeV.

[25] S. Z. BELEN'KIJ, V. M. MAKSIMENKO, A. J. NIKISOV and J. L. ROZENTAL: *Fortschr. Phys.*, **6**, 524 (1958).

[26] C. CASTAGNOLI, G. CORTINI, C. FRANZINETTI, A. MANFREDINI and D. MORENO: *Nuovo Cimento*, **10**, 1539 (1953).

(*) Since the Stephan Boltzmann law is applied.

fail by an order of magnitude ([27]). This can partially be ascribed to statistical fluctuations in the charged particles angulary symmetry, (forward-backward symmetry is assumed in the derivation of the « Castagnoli » formula, it is evident in the C.M. system for p-p but not for p-n collisions), and to the fact that the complete formula contains corrections which depend on the energies of the produced particles. The large fluctuations are also due to a lack of absolute selection criteria for p-free p collisions in emulsions. Such topics will be stressed in the present paper. Especially the « white » stars (stars with no gray and black prongs) and stars with only one or two gray and black prongs will be discussed.

With respect to the present work two different ways of investigation are available.

a) Scattering measurements can be performed on the secondary tracks. Particle identities are assumed and the kinematics are transformed into the C.M. system. This gives the maximum information and naturally questions like that of the inelasticity can be answered in this manner.

b) If one does not perform scattering measurements one can still make use of the lab-angular distribution, but then one has to assume certain distinct models for meson production and to compare its predictions with the experimental curves, which in this case exist as angular distributions for different shower particle multiplicities. On the average for lower multiplicities the produced particles are much more strongly collimated than for larger multiplicities. This might give means to approach the geometrical aspect of the interaction, namely to distinguish between peripheral and head-on collisions.

In the present paper we have proceeded according to method *b*). Scattering measurements are in progress and the results will be published in a forthcoming paper.

1. – Experimental procedure.

6 plates Ilford G-5, (10×15) cm^2, 600 μm thick, exposed to the 6.2 GeV Berkeley internal proton beam, were scanned by the usual « pick-up and following along the track » method. The average proton density in the plan perpendicular to the beam entering the emulsions was $1.1\cdot10^5$ protons per cm^2. The vertical projection of the angular distribution of the beam where it entered the plates and after having penetrated 7.6 cm is shown in Fig. 1. The tracks were extremely flat. Their average potential path per plate was more than 6 cm. The tracks, being slightly inclined from glass to surface, were picked up near the glass, noted individually and followed until they either left the

([27]) M. W. TEUCHER: private communication (1959). Derived for ultra high energies.

plate or led to an interaction. The speed of following through was so fast that the scanner observed only the motion picture of the track. Every « scattering » with more than 1° in projection was noted.

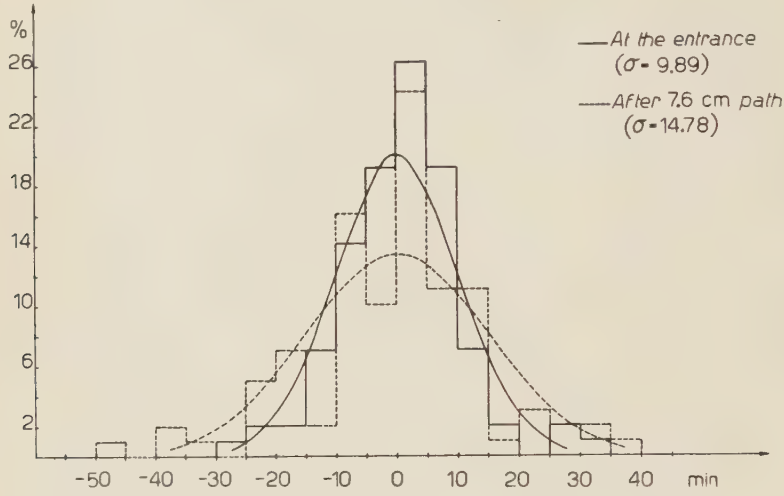

Fig. 1. – Projected angular distribution of the beam tracks.

Sometimes the scanner jumped to an already followed track while following through which resulted in 28 of the 699 stars being found twice. This fact has no further influence on the considerations if taken into account in the right manner. The 28 events are not included twice in the diagrams.

2. – Results.

Four approximately equivalent samples obtained from 5 scanners contributed to the statistics and a total path of 261 m has been followed. Table I

TABLE I. – *Raw observed values.*

Scanner	Number of interactions	Path (m)	Average interaction length (cm)	Possible elastic p-free p collisions
B.A.	199	72.51	36.4	2
Ch.P.	150	56.80	37.9	1
B.D. + E.B.	201	74.96	37.3	3
H.W.	149	56.97	38.2	3
Total	699	261.24	37.37 (*)	9

(*) Uncorrected, see sub-sections 2·2.1 and 2·2.3.

2220

contains the raw observed values. As can be seen, the individual fluctuations are small. This indicates that the influence of « human failure » is probably also small.

2·1. *The* p-*free* p *collisions.* – A first cut was made in order to separate the p-free-p collisions. We observed:

a) 315 stars with more than 10 prongs;

b) 347 events with less than 11 prongs and

c) 9 possible elastics p-free p collisions.

2·1.1. Elastic p free p collisions. – Table II shows the angles of the 9 events of class *c*). They were selected according to the following criteria:

1) Coplanarity;

2) $\operatorname{tg} \vartheta_1^L \cdot \operatorname{tg} \vartheta_1^L = 1 - \beta_{\mathrm{CM}}^{L^2}$;

3) Energy of the slower proton.

TABLE II. – *Angles in the* CM *system of* 9 *possible* p-*free* p *elastic collisions.*

Event	Angle in the CM system
H 84	4.5°
B 144	5°
Ch 19	5.5°
Br 71	10.5°
H 137	10.5°
H 10	17°
B 29	18°
Br 28	18°
Li 34	22°

Unfortunately there is a strong collimation in the forward-backward direction and this smoothes out the selectivity of the 3 checks. If most deflections have small angles, test 1 is very rough for geometrical reasons. Concerning test 2, a small angle deflection of the fast particle corresponds to an $80° \div 85°$ deflection (in the L system) of the slow proton. Small linear distortions in the emulsion (which, for instance, deform a square into a rhombus in the horizontal plane) can cause a larger error in the tangent of the larger angle, even though the angle itself may be measured quite precisely ($\pm 0.1°$). The same is valid for test 3. Relation 3) is the correlation between the momentum of the (slow) proton and its scattering angle:

$$P^L = P^L_{\text{pr.mary proton}} \cdot \frac{\cos \vartheta^L}{1 + ((\gamma^L_{\text{prim. proton}} - 1)/2) \sin^2 \vartheta^L} .$$

2221

In 5 of the 9 cases the proton came to rest in the emulsions. Possibly some of the 9 events are only quasielastic collisions, but no statistical separation can be made here.

2·1.2. Inelastic p-free p collisions. – Table III demonstrates how the events in class *b*) have been handled in order to separate the inelastic p-free p collisions. An inelastic p-free p collision is, by definition, a collision in which at least one particle has been created.

TABLE III. – *Separation of inelastic* p-*free* p *collisions.*

Number of Charged secondary tracks	Number of observed events	N_2 Stars with less than 3 certain nucleonic tracks	N_3 «p-free p elastic» criterion applied	N_4 Stars with 2 slow p's excluded	N_5 Ellipsoid test applied	n_s 0	1	2	3	4	5	6	7	
0	1													
1	40													
2	26	26	24	24	21	2	9	5						clean
							3	2						dirty
3	55	54	38	35			1	5	6					clean
								12	11					dirty
4	45	32	16	13	11				4	3				clean
									2	2				dirty
5	33	19	7	4					2	1				clean
										1				dirty
6	37	14	4	3	1									clean
										1				dirty
7	25	7	3	1										clean
													1	dirty
8	32	1	1	0										
9	28	2	1	0										
10	25	0	0	0										

N_2 is the number of stars with less than 3 certain nucleonic tracks.

N_3 Comparison with the p-free p elastic kinematics has been made and all events with a proton faster than the same-angle elastic proton have been eliminated.

N_4 remains if those cases in which each of the two protons have less than 195 MeV kinetic energy are excluded. One can easily show that this is a limiting value for inelastic p-free p collisions.

Up to this column even- and odd-prong stars have been treated equally. The next criterion is only applied to the even-prong events.

N_5 Many of the remaining stars still show a slow proton. N_5 remains if all events have been excluded in which the proton momentum vector did not fulfill a certain angular condition. This means: if an event did not belong to an elastic collision and if it occurred on a free proton, at least one pion must have been produced. Consequently for such cases a validity volume for the endpoint of the proton momentum vector can be calculated, which gives a stronger condition than that obtained for N_3. The L momentum vector of a proton with a given C.M. energy E_p^{CM} describes an ellipsoid defined by:

$$P_p^L = \gamma_{CM}^L \cdot \frac{E_p^{CM}\beta_{CM}^L \cos\vartheta^L \pm \sqrt{(P_p^{CM})^2 - (\beta_{CM}\gamma_{CM}^L m_p)^2 \sin^2\vartheta^L}}{1 + (\beta_{CM}^L\gamma_{CM}^L)^2 \sin^2\vartheta^L}.$$

Upper indices denote the frame of reference, E is the total energy, P the momentum, β and γ are the velocity parameters and ϑ^L is the angle between L momentum vector and primary direction. If $E_1^{CM} > E_2^{CM}$, the ellipsoid corresponding to E_2^{CM} lies entirely within the one for E_1^{CM}. So all protons with $0 < E_p^{CM} < E_{max}^{CM}$ must have L momentum vectors which lie within the ellipsoid for E_{max}^{CM}. For a given pion multiplicity n_π, P_{max}^{CM} is determined by:

$$E_{max}^{CM} = \frac{(E_{total}^{CM})^2 + m_p^2 - (m_p + n_\pi m_\pi)^2}{2E_{total}^{CM}}.$$

The pion multiplicity n_π can be replaced by the minimum number n_s of the charged pions. The presence of neutral pions causes a decrease of E_{max}^{CM} and the criterion is fulfilled *a fortiori*. Thus two-prong stars which were not in agreement with the elasticity test were subjected to the ellipsoid test with $n_c = 1$. For the 4-prong stars one can insert $n_c = 2$, etc.

33 stars are left which can belong to inelastic p-free p collisions. We distinguished between « clean » and « dirty » events. In our terminology a clean event is neither accompanied by a blob nor by an electron. As one sees from Table III there still exists a high fraction $b = 15/40$ of clean events among

2223

the odd prong stars (which certainely belong to collisions with bound nucleons). This indicates that a certain number of clean events among the even-prong stars can belong to complex nuclei collisions. On the other hand one must also assume a certain number of spurious blobs and electrons among the inelastic p-free p collisions, (about $(0 \div 10)\%$ (*), see f.i. ref. [28]). Thus the fraction f of clean events among the p-free p collisions is smaller than 1. With the knowledge of f and b one can calculate in a statistical manner the real number x_f of inelastic p-free p collisions using the equations:

$$x_f + x_b = \text{Number of even-prong stars} = \text{possible inelastic p-free p collisions.}$$

$$f x_f + b x_b = \text{Number of clean even-prong stars.}$$

With $b = 0.37$ and $f = 0.95$ (**) we obtained: $x_f = 19$. With this the inelastic cross-section for p-free p collisions becomes:

$$\sigma_{\text{in}} = 23^{+7}_{-6} \text{ mb} .$$

The method of separation applied here is a statistical one and does not enable us to decide in detail which of the 33 possible p-free p inelastic collisions are true p-free p collisions. So far the branching ratio (see Table III) of charged particle multiplicities—f.i. the ratio 2-prong stars/4-prong stars $= 21/11$ — necessarily contains a contamination from p-bound nucleon collisions.

Thin track multiplicities and angular distributions for the 33 possible inelastic p-free p collisions are given in the next sub-section.

2·2. *The collisions with bound nucleons.* – Fig. 2 shows the frequency distribution of 662 stars with n_h (grey+black) prongs. 319 stars show more than 6 grey+black prongs. With the rough assumption that most of the grey+black prongs belong to nucleonic particles (protons, deuterons, tritons, alphas, etc.) one can say that most of these 319 stars are due to the heavy emulsion nuclei (Ag and Br), which contribute about 70% to the total geometrical cross-section. We differentiate roughly in the following between heavy and light

---

([28]) Y. EISENBERG, W. KOCH, E. LOHRMANN, M. NIKOLIĆ, M. SCHNEEBERGER and H. WINZELER: *Nuovo Cimento*, **8**, 664 (1958).

(*) In principle this percentage can be obtained from the elastic p-free-p collisions. Among our 9 cases only one event had an associated blob.

(**) Naturally f depends on the kind of stack, *i.e.* on exposure and development, but the results are insensitive to its precise value since it is large anyway.

nuclei by attributing the stars with $n_h > 6$ to p-bound nucleon collisions in heavy nuclei. (Concerning Fig. 2 it must be said that usually such distributions are plotted on a semilogarithmic scale ([29,30]), but our available statistics is not large enough to expect additional information from this.) Fig. 2 also contains the distribution of n_h for stars with one thin track ($n_s = 1$).

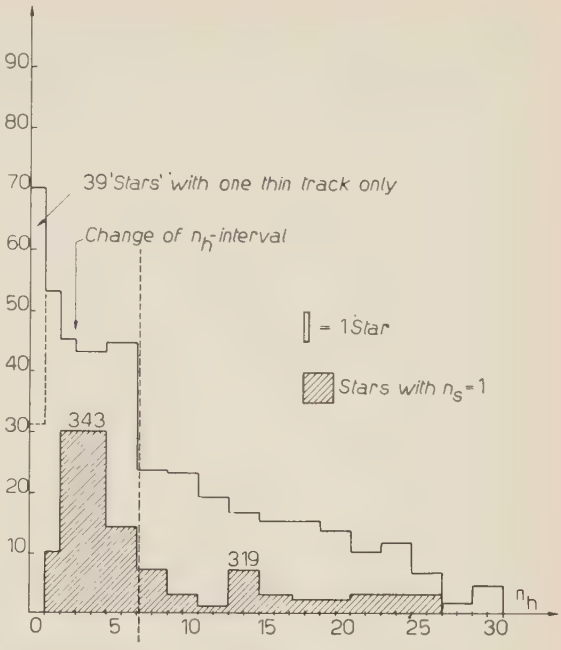

Fig. 2. – Frequency of stars with n_h gray+black prongs.

2·2.1. Thin track multiplicities. – Table IV shows the thin track multiplicity distribution for the 33 possible inelastic p-free p collisions and for 94 stars with $n_h = 0$, 1 and 2 (see discussion). The corresponding average n_s are 2.06 and 2.09. In the latter 94 stars p-free p collisions are not included.

TABLE IV. – *Thin track multiplicities for the* 33 *possible inelastic* p-*free* p *collisions and for the stars with* $n_h = 0, 1, 2$.

n_s	0	1	2	3	4	5	6	7
Inelastic p-free p collisions	2	12	7	6	6	0	0	0
stars with $n_h = 0, 1, 2$, excluding p-free p collisions	0	20	30	35	5	3	0	1

A summary of the raw observed number of thin tracks emerging from 662 stars is given in Table V. An increase in thin track multiplicity with increasing number of gray+black prongs is indicated. The effect, which must

([29]) M. W. TEUCHER: *Zeits. f. Naturfor.*, **8***a*, 131 (1953).
([30]) W. HEISENBERG: *Vorträge über kosmische Strahlung* (1953), p. 79.

2225

be due to secondary collisions inside the hit nuclei, becomes more obvious from Fig. 3 which shows the frequency distribution of the stars as a function of the thin track number n_s for heavy ($n_h > 6$) and light ($n_h < 7$) nuclei. For $n_h < 7$ and > 6, $\overline{n}_s$ becomes 2.27 and 3.04 respectively.

TABLE V. – *Thin track statistics as function of gray+black prong number (9 possible p-free p not included).*

n_h	Number of stars	Thin tracks, total	Average number of thin tracks
0	70	131	1.86
1	53	107	2.02
2	45	95	2.11
3/4	86	192	2.23
5/6	89	257	2.89
7/8	47	123	2.62
9/10	46	147	3.20
11/12	38	128	3.37
13/14	33	101	3.06
15/16	30	89	2.97
17/18	30	93	3.10
19/20	27	80	2.96
21/22	20	50	2.50
23/24	23	74	3.22
25/30	25	89	3.56
Total	662	1753	2.65

It seems to us necessary to make some remarks about the notions « stars » and « interaction ». In the case of the p-free p collisions the terminology is clear. We have distinguished between elastic and inelastic collisions as discussed in subsection 2·1.2. For proton collisions with complex nuclei, however, there is some arbitrariness. We call « star » every event which has at least one gray+black or at least 2 thin secondary tracks. We have also noted 39 « scatterings », the projected scattering angles of which are $> 1°$. In a certain fraction of these events the only difference between the « stars » with $n_s - 1$ and $n_h > 0$ is that neutrons have replaced the charged evaporation products. For uniqueness of definition of an « interaction » we perform a suitable extrapolation by using Table V. As can be seen from this table the average number of thin tracks for events with $n_h = 0$ is lower than the neighbouring values for stars with $n_h = 1$, 2 and more. We perform here an extrapolation by postulating the average thin track multiplicity for the events with $n_h = 0$ to be 2.1, which is an average value for the stars with $n_h = 1$, 2

2226

and 3. This extrapolation results in only 55 instead of 70 events with $n_h = 0$ having to be taken as « stars ». Thus this procedure can be used for defining the notion of « star ».

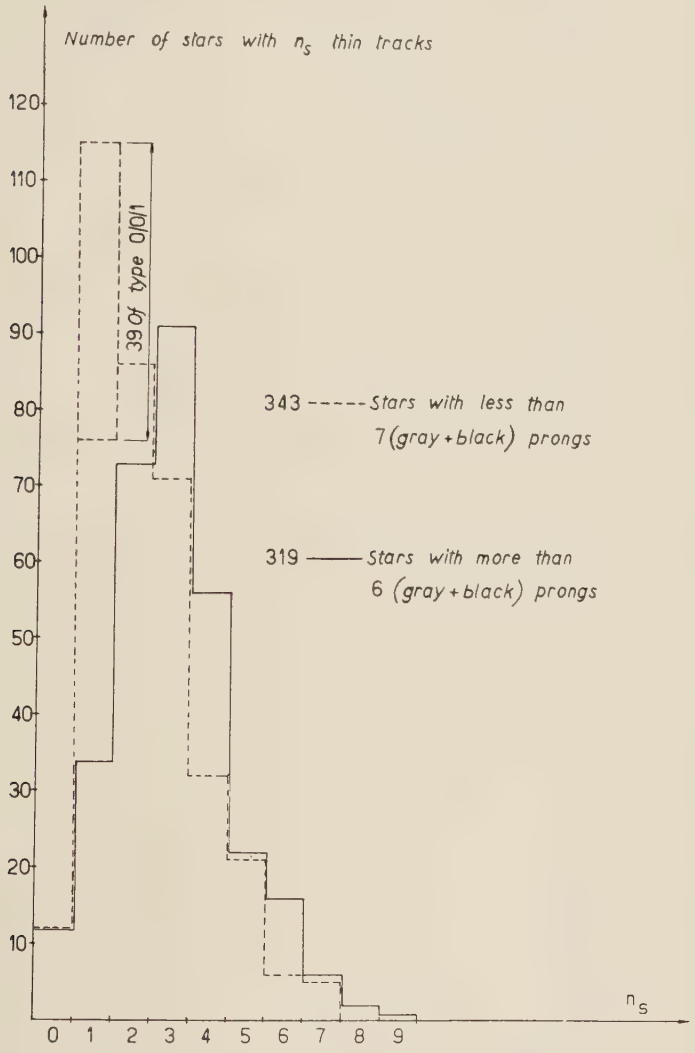

Fig. 3. – Frequency distribution of 662 stars with n_s thin tracks (excluded 9 possible p-free p elastic collisions).

2·2.2. Thin track angular distributions. – Fig. 4-*a* show the lab-angular distributions for different thin track multiplicities separately for heavy and light nuclei. Fig. 4-*b* correspond to the thin tracks of the 33 pos-

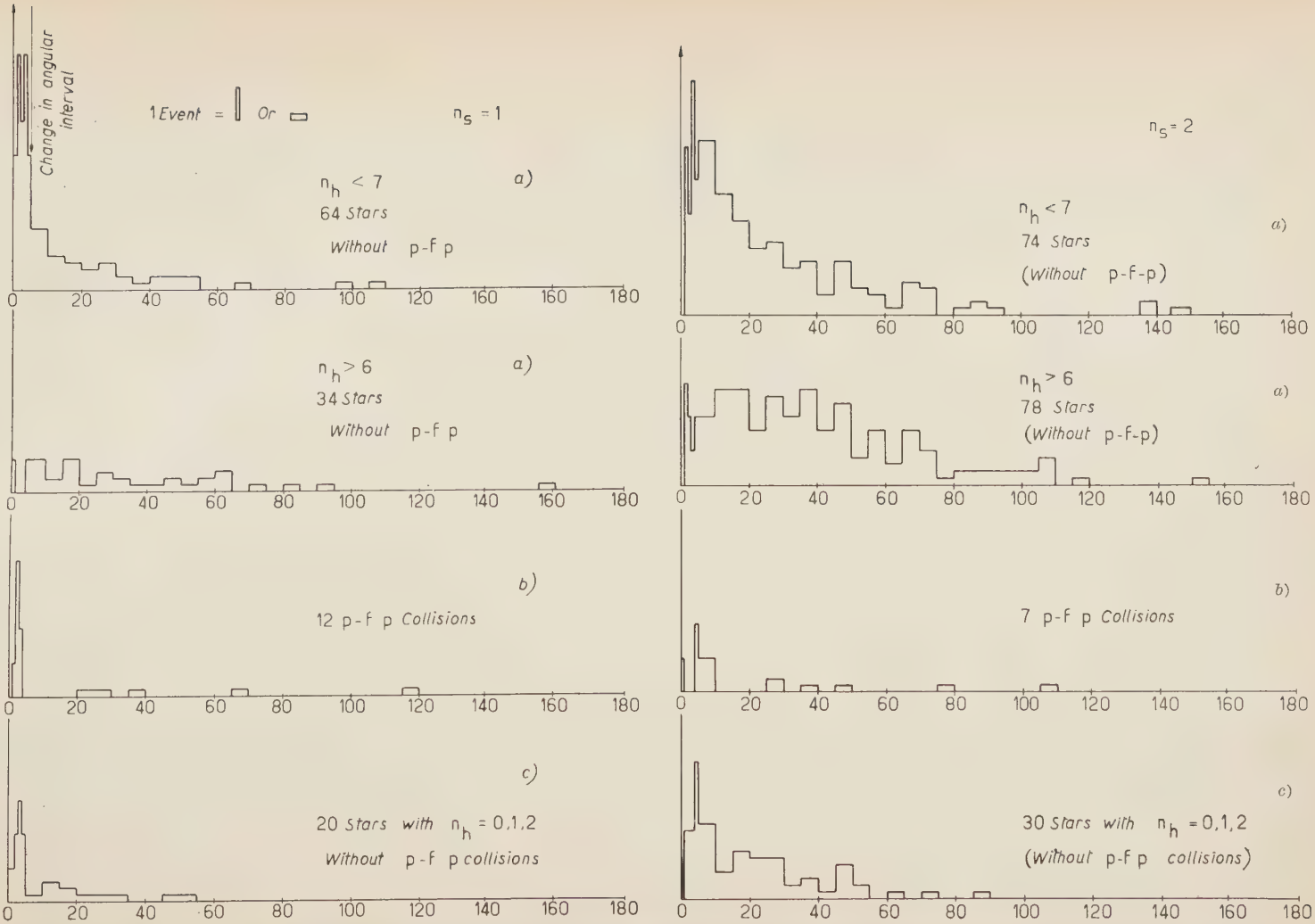

Fig. 4. – L-angular distributions of thin tracks.

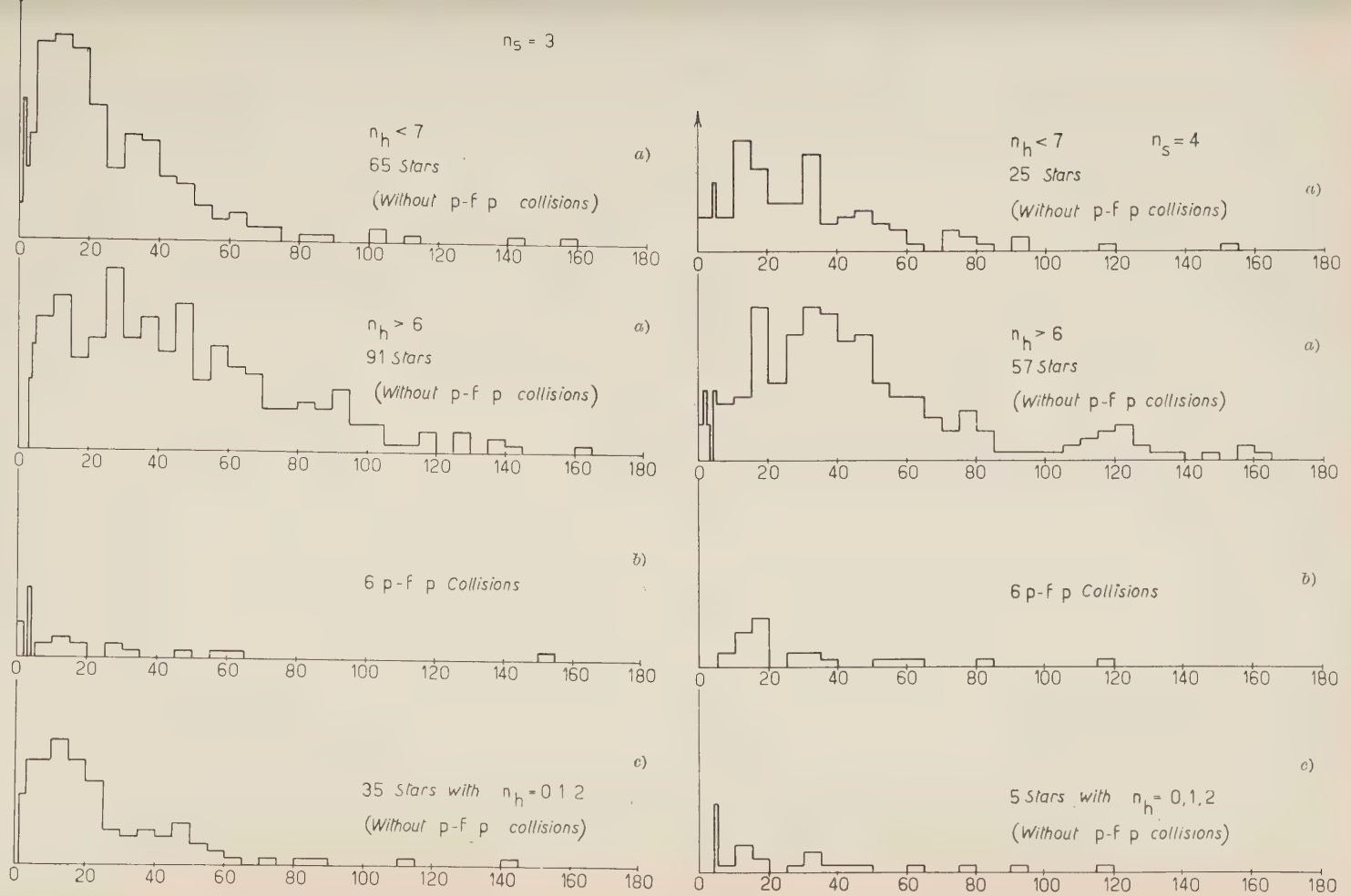

Fig. 4. – *L*-angular distributions of thin tracks.

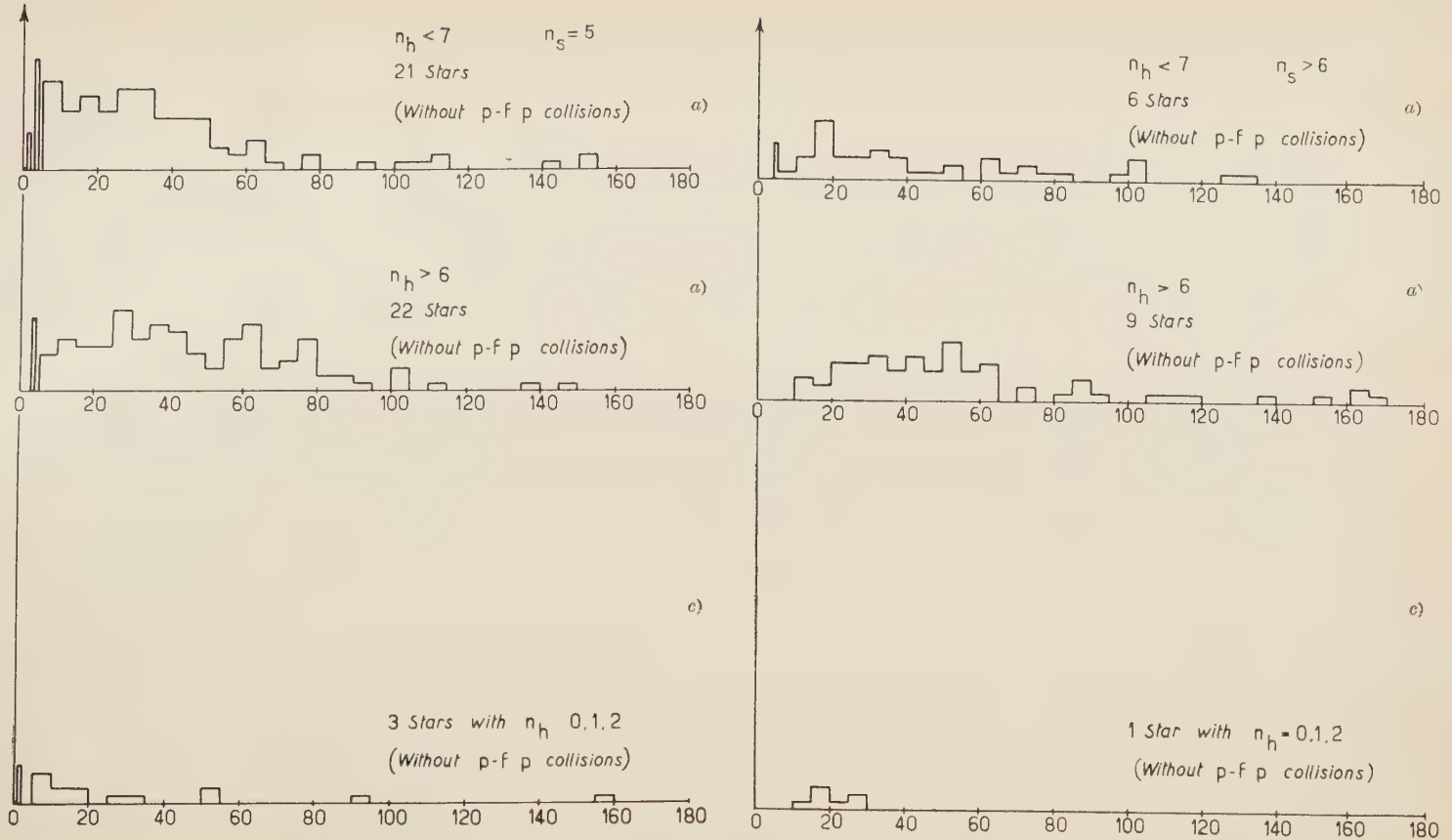

Fig. 4. – L-angular distributions of thin tracks.

sible inelastic p-free p collisions. Fig. 4-*c* consist of the angular distributions of the thin secondary tracks of the stars with $n_h = 0$, 1 and 2. Such stars are

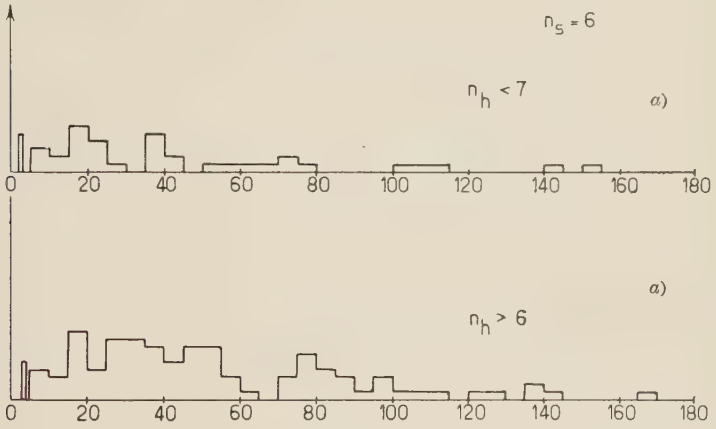

Fig. 4. – *L*-angular distributions of thin tracks.

often in the analysis of cosmic ray induced jets as representative for « pseudo-nucleon » collisions. The distributions will be discussed in detail in Section 3·2.

2·2.3 Interaction mean free path. – We observed 699 interactions in a total path of 261 m. After subtraction of 15 events with one thin track only (see sub-section 2·2.1), we get an interaction mean free path of

$$\lambda = (38.2 \pm 1.5) \text{ cm} .$$

3. – Discussion.

In the following we compare the results obtained from the p-free p collisions with numerical results of calculations according to the statistical model. In addition a rough « velocity » test on the secondary particles is performed.

The collisions with bound nuclei, their thin track angular distributions and number of gray+black tracks are discussed in sub-section 3·2.

3·1. *The* p-*free*-p *collisions.* – The statistics obtained for the p-free p collisions is small but within its limits the elastic and the inelastic cross-section of 23 mb agrees with a corresponding value obtained by KALBACH *et al.* [8] who applied a completely different scanning method. For the relative frequencies of 2 and 4 prong events however we obtained approximately the

22·31

reciprocal of their ratio; namely 15 mb and 7 mb, respectively. This point has to be clarified with better statistics.

On the other hand we can compare our values with the results of extensive numerical calculations for 6.2 GeV protons performed by CERULUS and HAGEDORN [23].

These authors used the Fermi theory in the low energy form (statistical model) with the expression:

$$P_b = W^b_{r,s,t}(T) \left\{ \frac{\pi(2Sj+1)^{\sigma_j}}{\pi N_i!} \right\} \Omega^{a-1} \varrho_b(E, m_1 \ldots, m_n, p = 0) ,$$

P_b is the probability for a distinct final state b. W takes account of the isotopic spin T conservation. It is the probability for r particles of $T = \frac{1}{2}$, s particles of $T = 1$ and t particles of the $T = \frac{3}{2}$ to form the state of total isotopic spin T. The next factor stands for the spin multiplicity, Ω for the interaction volume and ϱ for the phase space weight.

The calculations available [21] yield different results if the pion-pion isobar is included or not. The corresponding average multiplicities for charged secondary particles become 3.71 and 3.21. The observed average was 2.8, which might indicate that the Fermi theory overestimates the multiplicities at these energies. Furthermore the Fermi theory predicts reaction rates of 2, 4 and 6 prong events which do not agree with the experimentally observed ones. The reaction rates predicted with the Fermi theory (we shall call the Fermi theory model A) for charged particle multiplicities as calculated by HAGEDORN, v. BEHR and CERULUS are shown in Table VI.

TABLE VI. – *Branching ratios for the emission of charged secondary particles according to the statistical theory.*

	Predicted percentages	
	with nucleon isobar, without pion-pion isobar	with nucleon isobar and pion-pion isobar
2-prong stars	43.4	25.5
4-prong stars	52.6	63.5
6-prong stars	4.0	11.0

The bad agreement between theory A and the experiment indicates that an interaction of the Fermi type alone is probably not able to reproduce the experimental observation satisfactorily.

A more refined model (model B) was considered by v. BEHR and CERULUS [21]. In that case the validity of the Fermi theory was presumed for « head-on collisions » which in this model contribute, by definition, a certain

fraction a to the total inelastic cross-section. Peripheral collisions were treated differently. They were only allowed to form one or two nucleon isobars ($\frac{3}{2}$-$\frac{3}{2}$). The relative frequencies of the 3 types of interactions (Fermi, two isobars: $\mathcal{N}^*\mathcal{N}^*$, one isobar: $\mathcal{N}\mathcal{N}^*$) are called a, b and c.

There exist different possibilities to evaluate a, b and c from the experiment. With sufficient statistics this model will easily prove or disprove itself.

A first method to get an idea about a, b and c uses the reaction rates of the charged secondary prongs. According to v. Behr and Cerulus a, b and c could be completely determined by the following equation system.

Without pion-pion isobar, but with nucleon isobar:

$$0.434\,a + 0.8\,b + c = \text{fraction of 2-prong stars} = 21/33 = 0.64$$

$$0.526\,a + 0.2 \qquad = \text{fraction of 4-prong stars} = 11/33 = 0.33$$

$$0.040\,a \qquad = \text{fraction of 6-prong stars} = 1/33 = 0.03$$

With pion-pion isobar:

$$0.255\,a + 0.8\,b + c = 0.64$$

$$0.635\,a + 0.2\,b = 0.33$$

$$0.110\,a = 0.03$$

Contrib. from Fermi-part $\mathcal{N}^*\mathcal{N}^*$ $\mathcal{N}\mathcal{N}^*$

The six prong events apparently are so rare that one cannot make use of the third equation. Since our main interest is directed to the magnitude of a,

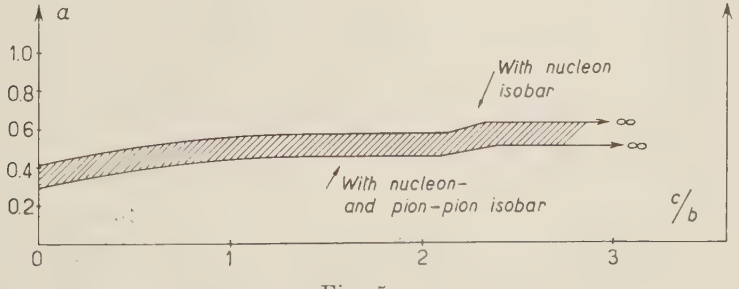

Fig. 5.

which stands for the abundance of the Fermi part, we plotted a as a function of c/b in Fig. 5. The figure shows (according to our small statistics) that a

2233

can vary from 0.30 to 0.63. With the reasonable assumption that c/b is about unity and presuming the validity of model B one can say that head-on collisions contribute only about 50%. So much for the analysis of the branching ratios.

There exist other possibilities for getting a, b and c from the experiment. For discussing one of them we consider the situation in the C.M. system according to model B. Fig. 6 shows a diagram with β^{CM} and ϑ^{CM} on the axes.

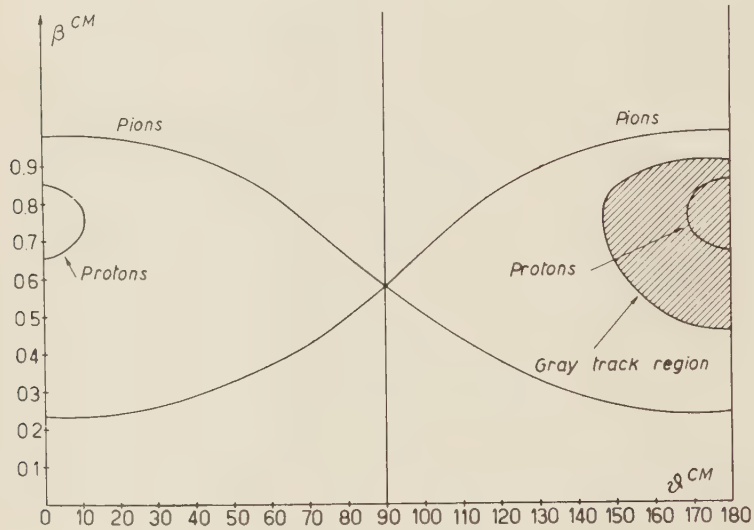

Fig. 6.

The shadowed area on the right contains those particles which lead to gray or black prongs in the L system (meaning that $\beta^L < 0.7$). For head-on collisions isotropy in the CM system is assumed. For $\mathcal{N}\mathcal{N}^*$ and $\mathcal{N}^*\mathcal{N}^*$ formation isotropic decay in the system of the isobars is assumed and further that the transverse momentum of these isobars in the CM system is small, *i.e.* that their line of flight is practically identical with the primary direction. With this crude picture one gets the CM angular kinematics for peripheral collisions shown in Fig. 6. According to this the nucleon of the backward isobar (or also the backward nucleon in the case of $\mathcal{N}\mathcal{N}^*$ formation) always produces a gray or black track in the L system. For head-on collisions, on the other hand, with isotropy in the CM system, 98% of all tracks should be thin in the L system.

We now make use of the real observed percentage of gray+black prongs from the p-free p collisions in estimating a, b and c. V. Behr and Cerulus

give the following reaction rates for the decay of $\mathcal{N}^*\mathcal{N}^*$ and $\mathcal{N}\mathcal{N}^*$:

TABLE VII. – *Branching ratios for the isobar decay.*

$\mathcal{N}^*\mathcal{N}^*$	$p+p+\pi^0+\pi^0$:	0.18
	$p+p+\pi^+ +\pi^-$:	0.20
	$p+n+\pi^+ +\pi^0$:	0.58
	$n+n+\pi^+ +\pi^+$:	0.04
$\mathcal{N}\mathcal{N}^*$	$p+p+\pi^0$:	0.17
	$p+n+\pi^+$:	0.83

One can easily see that with the above considerations one gets the two equations:

$$0.98a' + 0.72b' + 0.71c' = 0.74 = \text{fraction of observed thin tracks},$$

$$0.98a' + 0.33b' + 0.42c' = 0.37 = \text{fraction of observed white stars},$$

We distinguished between a, b, c and a', b', c'. If really, as it was assumed, all reactions from head-on collisions had lead to isotropic particle emission the primed and unprimed values should be equal. If one obtained a much smaller value for a' than for a this would indicate that not all interactions of the « Fermi-part » could show isotropic particle emission. The first equation is not very sensitive to the real value of a'. The second one looks better but there the number of white stars on the right is only 12 in our case. It is thus meaningless to calculate a' from these equations. We can only say that the observed fractions on the right hand of the equations seem mostly to be determined by b' and c' and this might indicate a small value for a'.

The method applied above is some kind of integrate velocity test. It was performed visually and can thus only be considered as an estimate. While for scattering measurements only flat tracks can be taken into consideration one could here use all tracks. (In our experience a practiced scanner can judge relatively reliably whether a track is gray or thin, and moreover there are only a few « border line » tracks.)

According to V. BEHR and CERULUS 20 % of the fraction b decay into $p+p+\pi^+ +\pi^-$, and practically all these events should yield stars of the type $n_h = 1$ and $n_s = 3$. We observed 5 events of this type among 33 possible p-free p collisions. If the Fermi-part shows throughout isotropic emission, we can estimate b to be $\sim 25/33$. These cases will be investigated in more detail in a forthcoming paper. The events $n_h = 1$ and $n_s = 3$ will serve especially to study $\mathcal{N}^*\mathcal{N}^*$ formation.

2285

Finally in Fig. 7 we show the L angular distribution of the 3 thin tracks from the reaction: $p+p \rightarrow \mathcal{N}^*+\mathcal{N}^* \rightarrow p+p+\pi^++\pi^-$ as calculated with the model discussed above. The strong peak in the forward direction arises from the protons of the forward isobars, while, as already mentioned, the protons of the backward isobars, lead to gray tracks. We shall use this figure in the discussion of the angular distribution of the thin tracks from all stars in the next section.

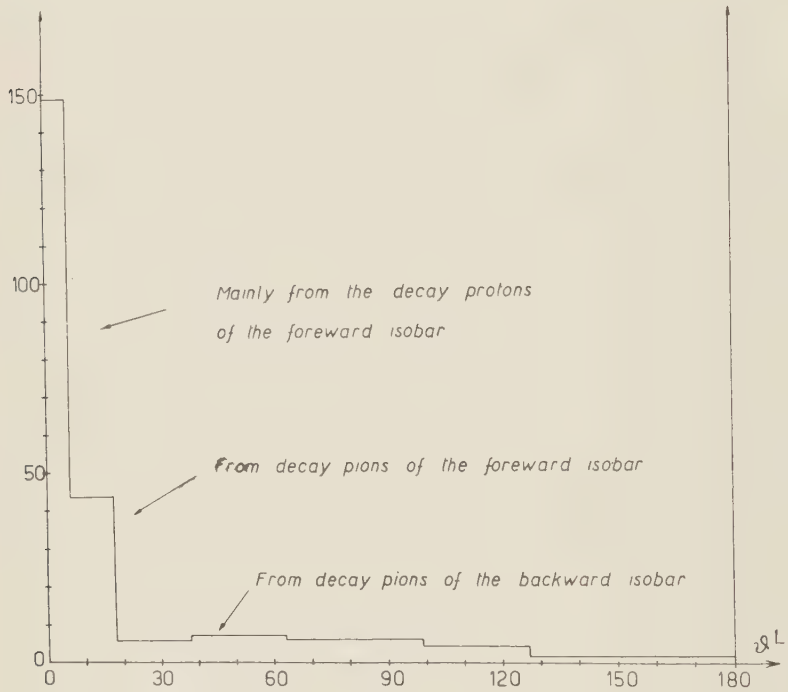

Fig. 7. – Calculated L-angular distribution of thin tracks for $\mathcal{N}^*\mathcal{N}^*$ formation according to model B.

Concerning this sub-section, we cannot decide definitely whether the observed facts indicate a high abundance of $\mathcal{N}\mathcal{N}^*$ and $\mathcal{N}^*\mathcal{N}^*$ from peripheral collisions or whether they indicate a strong deviation from isotropy for protons in head-on collisions. If in the Fermi-part the protons tend to keep their primary directions, one could obtain the observed percentage of gray tracks without the assumption of a large fraction of nucleon isobars. However with better statistics it should then be possible to decide by means of the observed average multiplicities of charged secondary particles which of the effects is predominant.

3·2. p-*bound-nucleon collisions.*

3·2.1. Mean free path for interaction. – We begin with a consideration that makes use of the mean free path in the emulsions for a derivation of the cross-section for « star production » of a single nucleon. With the assumption of uniform nucleon density, of Hofstadter's nuclear radii and standard emulsion composition one obtains a mean free path in nuclear matter and thus a cross-section of 38 mb for the single nucleon. (Interaction m.f.p. 38.2 cm).

This value has to be compared with the p-free p data. We obtained 9 elastic and 19 inelastic p-free p collisions (see sub-section 2·1.2) and a reasonable assumption is that every elastic and inelastic p-bound nucleon collision has lead to a star. One would therefore say with this approximation, that the 38 mb obtained indirectly must be compared with the 34 mb total p-free p cross-section. The only assumption is that p-p collisions and p-n collisions are equivalent at these energies.

3·2.2. The angular distribution of thin tracks and the application of the « Castagnoli formula ». – In Figs. 4 the L angular distributions for different thin track number are shown. Obviously we have stronger collimation for lower multiplicities and for small n_h. This effect, on the one side, must be ascribed to the nature of the p-nucleon collision and on the other hand, to secondary collisions inside the struck nucleus. Since the difference between the stars with $n_h < 7$ and $n_h > 6$ is so evident, one can separate the whole sample of observed stars into two groups. The one consists mainly (if $n_s < 5$) of such events which, in first approximation, can be considered as representative of the angular distribution of the p-free nucleon collisions while the other group consists mainly of stars in which secondary interactions happened. At the moment we are not much interested in the latter sample. If we compare the angular distribution of the stars with $n_h < 7$ with that from the p-free p collisions, we see that both show a similar sensitive dependence on n_s, while the corresponding angular distributions for the stars with $n_h > 6$ are highly insensitive to n_s. It therefore seems to be justified for the purpose of this discussion to accept the angular distribution of the thin tracks of the stars with $n_h < 7$ as a p-free nucleon like angular distribution.

For the stars with $n_h < 7$ the formula used by Castagnoli *et al.* [26] has been applied. The general expression is

$$\log \gamma_{\mathrm{CM}}^{L} = -\frac{1}{n}\sum_{i=1}^{n} \log \operatorname{tg} \vartheta_i^{L} + \log C\,,$$

and we took the first order approximation with $\log C = 0$. The « derived » energies for the primary proton are given in Table VIII. In principle this formula is « valid » when $\beta_{\mathrm{CM}}^{L} \gg \beta_{\mathrm{meson}}^{\mathrm{CM}}$. In our case β_{CM}^{L} is 0.88 while $\beta_{\mathrm{meson}}^{\mathrm{CM}}$

can vary within relatively wide limits. In addition a necessary condition is forward/backward symmetry in the CM system. But here we are considering a mixture resulting from p-p and p-n collisions. For the latter type of interaction symmetry is a poorly fulfilled assumption ([31]), not a logical necessity as for the p-p collisions. Several other objections can be made but now we are interested only in qualitative results.

TABLE VIII. – *Primary energies as calculated with the formula of Castagnoli et al.*

n_s ($n_h < 7$)	$E^L_{\text{prim. proton}}$ (GeV)
1	470
2	26
3	15.7
4	9.5
5	7.4
6	2.2

Looking at Table IV one can conclude that for the p-free p collisions at these energies more than 4 thin prongs are rather infrequent. One can therefore see that the stars with $n_s \geq 5$ are no longer typical ones. Probably the « Castagnoli » formula gives the best approach for stars with $n_s = 3$ and $n_s = 4$. In spite of this the primary energy for $n_s = 3$ is overestimated by a factor of 2, and for $n_s = 4$ the overestimation is still about 30 %. The deviation between the energy obtained in the first order approximation and the real energy can be expressed by the magnitude of C. The value of C for the stars with $n_s = 3$ is 0.7 and for $n_s = 4$ it becomes 0.9. At energies of 10^{12} eV SCHEIN *et al.* obtained $C = 0.7$ ([32]).

The energy value obtained for $n_s = 1$ is wrong by orders of magnitude. This can be understood if one compares the angular distribution of the thin tracks from the stars with $n_s = 1$ with the calculated distribution as shown in Fig. 7. The two distributions look similar. This is possibly a chance coincidence and does not necessarily mean that these stars mostly belong to events in which nucleon isobars only have been produced. Nevertheless this comparison serves well to illustrate the real situation. It shows that the stron peak in the forward direction belongs to « penetrating » protons. One can expect that, on the average, the « other » proton was slow and produced a

([31]) W. F. FOWLER, R. P. SHUTT, A. M. THORNDIKE and W. L. WHITTEMORE: *Phys. Rev.*, **95**, 1026 (1954).

([32]) M. SCHEIN, D. M. HASKIN, E. LOHRMANN and M. W. TEUCHER: *Multiple Meson Production in $\mathcal{N}$-$\mathcal{N}$ Collision at* 10^{12} eV, preprint (Chicago, 1959).

gray track (see discussion in Section 3·1). These protons can not be distinguished from the evaporation tracks and, using the « Castagnoli » formula, one is thus biased in favor of an overestimation of the energy.

3·2.3. Frequency distribution of thin tracks. – In Fig. 2 we plotted separately the frequency distribution of stars with $n_s = 1$ as a function of their gray+black prong number. One can observe a shift to lower n_h: (This effect has already been found in early works ([29,30])). For $n_s = 1$ the average n_h is $\overline{n}_h = 7.2$ while for the rest of the stars it is 10.5. This could be explained by means of two different effects. Once, we are biased if we take only the stars with $n_s = 1$ since, for stars with larger n_s the probability of secondary interactions is larger and therefore more evaporation tracks are expected. Two, this shift can arise from the effect that, as stated above, the nucleon which was emitted backwards in the CM system had a low kinetic energy in the L system (especially in quasielastic collisions) and, if it has made an interaction, that should result in a lower excitation energy for stars with $n_s = 1$.

Concerning secondary interactions we want to make more remarks. As can be seen from Fig. 3 the stars with larger n_h show, on the average, a larger n_s. This must be due to secondary interactions for a twofold reason. First, if n_s is larger the chance for secondary interactions increases and, second, fast particles undergoing secondary interactions still have some chance to lead to additional thin tracks by producing other fast particles. That the latter effect really happens can be deduced from a comparison of the average n_s of the inelastic p-free p collisions ($\overline{n}_s = 2.06$) with the total average number of thin tracks (which is 2.65).

3·2.4. Frequency distribution of heavy tracks, the star size. – We want to say a few words about the distribution of gray+black prongs. In a paper of Camerini *et al.* ([33]) the star size distribution (represented in our notion by n_s and n_h) has been studied as a function of the primary energy. These authors find no indication for a saturation in the average n_h with increasing primary energy. Our average n_h is 9.7 as compared with their 18 (for 6 GeV). This is a remarkable difference which is probably due to an essential loss of small stars in their area scan. According to measurements of Birnbaum *et al.* ([34]), n_h at higher energies is no longer a good measure for the primary energy. Our statistics are not sufficient to decide if there also

([33]) U. Camerini, J. H. Davies, P. H. Fowler, C. Franzinetti, H. Muirhead, W. O. Lock, D. H. Perkins and G. Yekutieli: *Phil. Mag.*, **42**, 1254 (1951).

([34]) M. Birnbaum, M. M. Shapiro, B. Stiller and F. W. O'Dell: *Phys. Rev.*, **86**, 86 (1952).

6339

exists some kind of « knee » for our case of constant primary energy (see f.i. refs. [29] and [35]). In ref. [29] a detailed discussion of the physical reason for this « knee » is given. Of course n_h does not only depend on the primary energy but also on the atomic number, *i.e.* on the number of charged nucleons per nucleus available for evaporation and is therefore influenced by the composition of the emulsion.

3·2.5. Selection criteria, stars with small visible excitation energy. – In Table III we have demonstrated how the different separation steps, in order to separate the p-free p collisions, have influenced the number in the columns. Events with odd and even prong numbers were treated equally and use was made of the appearance of slow electrons or blobs. This procedure finally gave us the necessary additional information to deduce the *real* number of p-free p collisions among the *possible* ones.

About $\frac{2}{3}$ of the 33 possible inelastic p-free p collisions had to be attributed to p-bound nucleon collisions (Table III column N_5 and sub-Section 2·1.2). In this connection it is of interest to ask whether or not the fact that, after, strong selection, the sample left still has an indistinguishable contamination of p-bound n collisions can influence results which were derived for p-free p collisions only. This is of special interest for jets produced by ultra high energy particles. There one generally does not know the primary energy and mainly the angular distributions of white stars serve to estimate the primary energy. In the following we shall discuss preferentially the white star or stars with small visible excitation energy. Certainly it will not be possible to compare our 6.2 GeV stars throughout with ultra high energy jets, but at least some points can be discussed qualitatively.

The total number of white stars (excluding « scatterings » but including p-free p collisions) is 30, which makes about 5% of all observed stars. This is rather low as compared with the 10 ÷ 15% for stars at ultra high energies [32]. One probable explanation is that (in p-free p collisions at 6.2 GeV) some of the meson and one nucleon produce gray tracks, while at ultra high energies most tracks are thin. (Backward protons from $N^*.N^*$ formation can there still produce gray tracks, but $N^*.N^*$ formation becomes much more infrequent with increasing energy). In the following we shall briefly extrapolate from our stars to cosmic ray jets.

The fraction of white stars among the 33 possible p-free p inelastic collisions is about 0.4. If one believes this fraction to be about 1 at energies of 10^{12} eV one can extrapolate roughly (*) to higher energies with our 30 white stars. Assuming that there are enough cases, where the proton collided with

[35] M. W. TEUCHER: *Zeits. f. Naturfor.*, **7a**, 61 (1952).

(*) The influence of secondary interactions is neglected here.

only one bound nucleon without giving visible excitation energy to the rest nucleus. The extrapolated number of white stars at 10^{12} eV is $30/0.4 = 75$, which in fact makes about 11 % and which is in agreement with the (10÷15)% obtained directly at that energy. Only about $\frac{1}{3}$ of these (10÷15)% belong to real inelastic p-free p collisions. The rest must belong to complex nuclei leading to odd and even prong stars, and one question is whether the angular distribution of the (thin) secondaries from these stars looks very different from the angular distribution obtained from p-free p collisions alone. The same may be asked of the average multiplicities and the reaction rates of the (thin) secondary tracks. Often the appearance of a white star as an even-prong event has been attributed to p-free p collisions, and for odd-prong events white stars are believed to show angular distributions and multiplicities still representative for p-free nucleon collisions, since one has concluded that the average excitation energy given to the rest-nucleus in white stars is small.

The average thin track multiplicity of 33 possible p-free p collisions is 2.06, for the stars with small visible excitation energy ($n_h = 0, 1, 2$) it is 2.09; and the total average is 2.65. Thus at first sight it seems that the stars with small visible excitation energy do not show a considerable contamination with stars in which secondary interactions happened, but we believe that this, in reality, is not true. For the calculation of $\bar{n}_s = 2.09$ the 24 stars with 1 thin track only have been included (see sub-section 2·2.1). Therefore 2.09 is certainly not the right value to compare wity 2.06 from p-free p collisions. If we leave out the 24 critical stars we get 2.50. This indicates that already the stars with small visible excitation energy have a considerable contamination with stars in which secondary interactions happened.

From multiplicity considerations alone we believe that even the white stars contain a non-negligible fraction of stars in which secondary interactions happened. On the other hand one can see from Figs. 4 that the angular distributions of thin tracks for p-free p collisions, for the stars with small visible excitation energy and for all stars with $n_h < 7$ do not differ significantly. Therefore we can conclude that if one performs a strong selection (as in sub-Section 2·1.2) of possible p-free p collisions the selected sample is representative of p-free p collisions as regards multiplicity and angular distribution. At higher energies it can happen that occasionally white stars occur in which secondary interactions were made. Such single events naturally are no longer representative for the correspokding p-free nucleon collision.

* * *

We are highly indebted to Prof. SCHEIN for making the plates available to us and to Drs. HEARD, LOFGREN, TEUCHER, LOHRMANN and to the Bevatron crew for providing us with this excellent exposure.

Section 3·1 grew out of discussions which we had at CERN with Drs. v. BEHR, CERULUS and HAGEDORN and we are very grateful to Drs. v. BEHR and CERULUS for communicating parts of their results to us prior to publication.

Dr. TEUCHER made many useful suggestions especially concerning Section 3·2.

Our special thanks are due to Prof. HOUTERMANS for his support and encouragement, to Prof. PEYROU for valuable criticism and to Dr. Y. EISENBERG for critical remarks.

The scanning team did efficient work. We are grateful to Mrs. B. ALBRECHT, E. BLASER, B. DZIUMBLA, CH. PLUMETTAZ and I. RITSCHARD.

Our further thanks are due to the Schweizerische Studienkommission für Atomenergie, to the Kommision für Atomwissenschaften and to the Schweizerischer Nationalfonds for financial support of this work.

RIASSUNTO (*)

Si sono trovate 700 interazioni seguendo protoni di 6.2 GeV «lungo la traccia». Si ottenne un percorso libero medio di interazione di (38.2 ± 1.5) cm. Si separarono 42 possibili collisioni protone-protone libero trovando che la sezione trasversale per la produzione di mesoni è 23^{+7}_{-6} mb. Abbiamo trovato una molteplicità media per tracce di secondari carichi in collisione anelastiche p-p di 2.8 ± 0.9 ed il rapporto di branching fra eventi a 2 e 4 rami era circa 2. Questi valori vennero paragonati a quelli predetti dalla teoria statistica e da una sua modificazione. I risultati di queste ricerche sarebbero in accordo con un modello che suppone che a queste energie circa il 50% di tutte le collisioni sono «periferiche» portano solo alla formazione di isobare (di nucleoni) ($\mathcal{N}\mathcal{N}^*$ o $\mathcal{N}^*\mathcal{N}^*$). Si sono misurate le distribuzioni angolari di tutte le tracce secondarie sottili nel sistema L e si è applicata la formula di Castagnoli *et al.* ad un campione di stelle ragionevolmente selezionato. Questo porta ad una stima per eccesso dell'energia primaria per un fattore di circa 2. Altri ricercatori hanno ottenuto a 10^{12} eV un valore simile.

(*) *Traduzione a cura della Redazione.*

IL NUOVO CIMENTO Vol. XVII, N. 1 1° Luglio 1960

On the Two Fluid Model in Multiple Production of Mesons.

M. Hamaguchi

Department of Physics, Kyoto University - Kyoto

(ricevuto il 12 Marzo 1960)

Summary. — The mechanism of multiple particle production in high energy nucleon-nucleon collisions is investigated using the two fluid model. The theoretical inelasticity is numerically calculated.

1. – Introduction.

The present note describes a picture of the dissipating system using the two fluid model [1], in which the core part of the incident nucleon behaves as the perfect fluid, while the cloud part surrounding the core behaves as the viscous fluid. We may imagine that the latter part is composed of π-mesons, K-mesons and nucleon-antinucleon pairs, etc. At the first stage of the expansion, various fluids produced by high energy nucleon-nucleon collisions are enclosed in the flat-circular volume, where each constituent of these fluids is near thermal equilibrium at extremely high temperature. These fluids expand into the outer space with the development of time, keeping up the local uniformity of the energy. Since the core part does not contain the viscous effect, it may be easy to find its conspicuous distribution at the fronts of fluid motion. Although the cloud parts are lagging a little behind the core fluid in the expansion process because of the viscosity, they will also show the distribution concentrated intensely in the vicinity of the fronts of the expanding cloud in a one dimensional fluid motion.

Here, we shall remember the empirical model [2] proposed by Cocconi, but not further discuss the connection between our model and Cocconi's one.

[1] R. P. Feynman: *Phys. Rev.*, **91**, 1291, 1301 (1953); **94**, 262 (1954).
[2] G. Cocconi: *Phys. Rev.*, **111**, 1699 (1958).

To express the covariant energy-momentum tensor ([3]), we have used

$$(1) \qquad T^{\mu\nu} = \sum_{k=i(\text{core}),\, j(\text{cloud})} \{p_k g^{\mu\nu} + (\varepsilon_k + p_k) v^\mu v^\nu\} - \\ - \sum_{j(\text{cloud})} \eta_j \{\partial_\mu v^\nu + \partial_\nu v^\mu + (v^\mu \dot{v}^\nu + v^\nu \dot{v}^\mu)\} - \sum_{j(\text{cloud})} \zeta_j \{g^{\mu\nu} + v^\mu v^\nu\} \partial_\varrho v_\varrho ,$$

where $\dot{v}^\mu = v_\nu \cdot \partial_\nu v^\mu$, $g^{\alpha\alpha}(\alpha = 1, 2, 3) = 1$, $g^{00} = -1$ and $C = 1$. $\sum_{k=i,j}$ represents the sum of each component of the core and the cloud specified by the indices i, j.

In Section 2, we have solved the equation of motion $\partial_\nu T_{\mu\nu} = 0$ in hydrodynamical expansion process, where Reynolds number is very large $\mathscr{R} > 1$. Analogously to Heisenberg-Landau's ([4]) idea, we think that the use of a turbulent flow is most favorable for the hydrodynamic description of multiple particle production. In the domain considered, there is only a small fluctuation due to the viscosity. Therefore, an asymptotic expansion with respect to viscous coefficients will be used.

On the other hand, the dependence on the temperature of the viscous coefficient should be directly taken into account, but we must keep in sight the all-over description of the phenomena in excess of our stress on this point only. So, we should turn our attention to the large Reynolds numbers mentioned above, even if there is a slight fluctuation of viscosity with temperature.

In Section 3, we have obtained an expression of inelasticity using the (0, 0)-components of energy-momentum tensor at the critical time, and made out a few tables. As a consequence, the trend of the deviation of inelasticity in the two fluid model will be investigated.

2. – Equation of motion.

From the fundamental equation in relativistic hydrodynamics $\partial_\nu T_{\mu\nu} = 0$, we have the following simultaneous equations (*) of a one dimensional motion

---

([3]) G. A. KLUITENBERG: *Relativistic Thermodynamics of Irreversible Processes* (Leiden); E. C. G. STUECKELBERG and G. WANDERS: *Helv. Phys. Acta*, **26**, 307 (1953); C. ECKART: *Phys. Rev.*, **58**, 919 (1940).

([4]) W. HEISENBERG: *Zeits. f. Phys.*, **133**, 65 (1952); L. D. LANDAU: *Izv. Akad. Nauk SSSR*, **17**, 51 (1953).

(*) In the derivation of eq. (2), we have omitted the derivative of viscous coefficients with respect to space and time. The volume of the system at a given time is $V \approx \pi a^2 x$ (a, linear dimension of system), so the energy density $\varepsilon \sim E/\pi a^2 x \sim T^4$. Here, the T-dependence of viscosity being assumed as an example η, $\zeta \propto T^3$, we can decide automatically an x-dependence of viscosity $\eta, \zeta \sim D/x^3$, (D, a numerical const). There-

in the direction of positive x-axis,

$$(2)\quad \begin{cases} \dfrac{4}{3}\dfrac{\partial}{\partial t}(\varepsilon v^2)+\dfrac{1}{3}\dfrac{\partial \varepsilon}{\partial \xi}=\sum\limits_{j\,(\mathrm{cloud})}\eta_j\left\{\dfrac{\partial}{\partial t}\left[2(1+v^2)\dfrac{\partial v}{\partial t}+3\dfrac{\partial v}{\partial \xi}\right]+\dfrac{\partial}{\partial \xi}\left[\dfrac{\partial v}{\partial t}+2\dfrac{\partial v}{\partial \xi}\right]\right\}+ \\ \qquad +\sum\limits_{j\,(\mathrm{cloud})}\zeta_j\left\{\dfrac{\partial}{\partial t}\left[v^2\dfrac{\partial v}{\partial t}-\dfrac{1}{2}\dfrac{\partial v}{\partial \xi}\right]-\dfrac{1}{2}\dfrac{\partial}{\partial \xi}\left[\dfrac{\partial v}{\partial t}-\dfrac{1}{2v^2}\dfrac{\partial v}{\partial \xi}\right]\right\}, \\ \dfrac{1}{3}\dfrac{\partial \varepsilon}{\partial t}+\dfrac{1}{3}\dfrac{\partial}{\partial \xi}\left(\dfrac{\varepsilon}{v^2}\right)=\sum\limits_{j\,(\mathrm{cloud})}\eta_j\left\{\dfrac{\partial}{\partial t}\left[\dfrac{\partial v}{\partial t}+2\dfrac{\partial v}{\partial \xi}\right]-\dfrac{1}{2}\dfrac{\partial}{\partial \xi}\left[\dfrac{3}{v^2}\dfrac{\partial v}{\partial t}+\dfrac{4}{v^2}\dfrac{\partial v}{\partial \xi}\right]\right\}- \\ \qquad -\sum\limits_{j\,(\mathrm{cloud})}\zeta_j\left\{\dfrac{1}{2}\dfrac{\partial}{\partial t}\left[\dfrac{\partial v}{\partial t}-\dfrac{1}{2v^2}\dfrac{\partial v}{\partial \xi}\right]-\dfrac{1}{4}\dfrac{\partial}{\partial \xi}\left[\dfrac{1}{v^2}\dfrac{\partial v}{\partial t}-\dfrac{1}{2v^4}\dfrac{\partial v}{\partial \xi}\right]\right\}, \end{cases}$$

introducing the new variable co-ordinate $\xi = t - x$. In the derivation of the above expression, we have imposed the ultra-relativistic condition upon the four velocity,

$$(c)\qquad v_0 \sim v_1 \equiv v \gg 1, \qquad v_0 - v_1 \approx 1/(2v)\ , \qquad t \gg \xi \gg \Delta\ ,$$

where Δ is a Lorentz contracted width of the system. To solve the above simultaneous equations under the condition (c), we make use of the method of asymptotic expansion with respect to η, ζ,

$$v^2 = (v^0)^2 + \sum_{j\,(\mathrm{cloud})}\eta_j (v_j^1)^2 - \sum_{j\,(\mathrm{cloud})}\zeta_j (v_j^2)^2\ ,$$

$$\varepsilon = \varepsilon^0 + \sum_{j\,(\mathrm{cloud})}\eta_j \varepsilon_j^1 - \sum_{j\,(\mathrm{cloud})}\zeta_j \varepsilon_j^2\ ,$$

where higher order terms of η_j and ζ_j were omitted due to the assumption of small viscosity fluctuation. At first sight, the propriety of application of asymptotic expansion is not always obvious for higher order derivatives of eq. (2). But, we will not meet with any difficulty, if only convergence of this series

---

fore, the derivatives of momentum transfer in the equation of motion are estimated as follows:

$$\frac{\partial \eta}{\partial \xi}\left(\frac{\partial v}{\partial \xi}\right) \approx \frac{\eta}{(t-\xi)}\left(\frac{\partial v}{\partial \xi}\right),\quad \eta\frac{\partial}{\partial \xi}\left(\frac{\partial v}{\partial \xi}\right) \approx \frac{\eta}{\xi}\left(\frac{\partial v}{\partial \xi}\right).$$

In the domain of $t \gg \xi \gg \Delta$, the former is negligible as compared with the latter. It will be also proved that in a general way this conclusion does not depend on the above special example.

and non-singularity are satisfied. This kind of method had been used by Heisenberg in past years (5).

The solution of the above equations can be carried out quite similarly after the method of Sections 1, 2, in I (6), in which at first a power function of (t/ξ) was assumed as the velocity, and after the simultaneous equations of ε with respect to t, ξ were solved. Finally, the lengthy calculation gives a set of solutions,

$$(3)\ (*)\qquad \begin{cases} v^2 \approx f^0 \dfrac{t}{\xi} + \sum\limits_{j\,(\text{cloud})} (f_j^1 \eta_j - f_j^2 j_j) \left(\dfrac{t}{\xi}\right)^{\alpha}, \\ \varepsilon \approx \varepsilon^{0*} \exp\left[-\dfrac{4}{3}\left(\ln\dfrac{t}{\Delta} + \ln\dfrac{\xi}{\Delta} - \sqrt{\ln\dfrac{t}{\Delta}\cdot\ln\dfrac{\xi}{\Delta}}\right)\right] + \\ \qquad + \sum\limits_{j\,(\text{cloud})} (\eta_j \varepsilon_j^{1*} - \zeta_j \varepsilon_j^{2*}) \left(\dfrac{t}{\xi}\right)^{\beta} + \sum\limits_j \eta_j \cdot O_1(t, \xi, \Delta) + \sum\limits_j \zeta_j \cdot O_2(t, \xi, \Delta), \end{cases}$$

where $\varepsilon = \sum\limits_{k=i\ (\text{cloud}),\, j\,(\text{cloud})} \varepsilon_k$, $\quad \varepsilon^{0*} = \sum\limits_{k=i,j} \varepsilon_k^{0*}$.

Both of the last two terms O_1, O_2 of the energy density are negligible compared with the second term, therefore these additional terms will be omitted in the following calculation. ε^{0*} is an initial value of the solution in the non-viscous equation, and ε^{1*}, ε^{2*} are also those in the 1-st order equations with respect to viscosity. f^0, f_j^1 and f_j^2 are given by $f^0 - \frac{1}{2}\sqrt{\ln(t/\Delta)/\ln(\xi/\Delta)}$, $f_j^1 \approx -0.83\varepsilon_j^{1*}/\varepsilon^{0*}$, etc. As is clearly seen from the region in which our solution is applicable, if we expediently assume $f^0 \approx 1$ and $\varepsilon_j^{1*} \approx \varepsilon_j^{2*} \cdots - l^2 \varepsilon_j^{0*}$, though a suitable method to determine the latter quantity does not exist, (l means the dimension of the length of order 1), $f_j^1 \approx f_j^2 \approx 0.83\, l^2 \varepsilon_j^{0*}/\varepsilon^{0*} \equiv \gamma_j < 1$ will be obtained. Then, the expression (3) is also written

$$(3')\qquad \begin{cases} v^2 \approx \dfrac{t}{\xi} + \sum\limits_{j\,(\text{cloud})} \gamma_j (\eta_j - \zeta_j) \left(\dfrac{t}{\xi}\right)^{\alpha}, \\ \varepsilon \approx \sum\limits_{i\,(\text{core})} \varepsilon_i^{0*} \exp\left[-\dfrac{4}{3}\left(\ln\dfrac{t}{\Delta} + \ln\dfrac{\xi}{\Delta} - \sqrt{\ln\dfrac{t}{\Delta}\cdot\ln\dfrac{\xi}{\Delta}}\right)\right] + \\ \qquad - \sum\limits_{j\,(\text{cloud})} \varepsilon_i^{0*} \left\{\exp\left[-\dfrac{4}{3}\left(\ln\dfrac{t}{\Delta} + \ln\dfrac{\xi}{\Delta} - \sqrt{\ln\dfrac{t}{\Delta}\cdot\ln\dfrac{\xi}{\Delta}}\right)\right] - l^2 \cdot (\eta_j - \zeta_j) \left(\dfrac{t}{\xi}\right)^{\beta}\right. \end{cases}$$

(5) W. HEISENBERG: *Ann. d. Phys.*, **74**, 577 (1924).

(6) M. HAMAGUCHI: *Nuovo Cimento*, **4**, 1242 (1956); **5**, 1622 (1957), hereafter quoted as I, II respectively.

(*) $\alpha = 4.54$ and $\beta = 2.21$ are the numerical values given in I.

2246

From this, we see that the energy densities of the cloud grow gradually during the expansion process due to the viscosity effect ($\eta_j < 0$, $\zeta_j > 0$).

Applying now the same method to this case as in the derivation of the limit of a one dimensional motion in I, we can also obtain the following limit using the velocity mentioned above,

$$t_1 \approx \frac{a^2}{\xi}\left[1 + \sum_{j\,(\text{cloud})} \gamma_j(\eta_j - j_j)\left(\frac{a}{\xi}\right)^{2(\alpha-1)}\right]. \tag{4}$$

Then, the expression of critical energies in the conical flight is also given by

$$\varepsilon_k = \varepsilon_k^{0*}\left(\frac{t_1}{t}\right)^4\left\{\exp\left[-\frac{4}{3}\left(\ln\frac{t_1}{\Delta} + \ln\frac{\xi}{\Delta} - \sqrt{\ln\frac{t_1}{\Delta}\cdot\ln\frac{\xi}{\Delta}}\right)\right] - l^2(\eta_k - \zeta_k)\left(\frac{t_1}{\xi}\right)^{\beta}\right\}, \tag{3''}$$

where $k = i$ (core), j (cloud), and $\eta_i = \zeta_i = 0$. Applying $\sqrt{\ln(t_1/\Delta)/\ln(\xi/\Delta)} \approx 2$ derived from $f^0 \approx 1$ to the above expression, we can rewrite it in a favorable form for the following discussion,

$$\varepsilon_k = \varepsilon_k^{0*}\left(\frac{\xi^{\frac{4}{3}}\cdot t_1^{\frac{8}{3}}}{t^4}\right)\left\{1 - l^2(\eta_k - \zeta_k)\left(\frac{t_1}{\xi}\right)^{\beta+\frac{4}{3}}\right\}. \tag{5}$$

By inserting the limit (4) of a one dimensional motion into (5), we obtain the respective critical energy densities for the cloud particles (viscous) and the core particles (non-viscous),

$$\varepsilon^c_{j\,(\text{cloud})} = \varepsilon_j^{0*}\left(\frac{a^{\frac{4}{3}}}{t_c\,\xi^{\frac{1}{3}}}\right)^4\cdot\left[1 + \frac{8}{3}\sum_{j\,(\text{cloud})}\gamma_j(\eta_j - \zeta_j)\left(\frac{a}{\xi}\right)^{2(\alpha-1)}\right]\cdot\left[1 - l^2(\eta_j - \zeta_j)\left(\frac{a}{\xi}\right)^{2\beta+\frac{8}{3}}\right], \tag{6_1}$$

$$\varepsilon^c_{i\,(\text{core})} = \varepsilon_j^{0*}\left(\frac{a^{\frac{4}{3}}}{t_c\,\xi^{\frac{1}{3}}}\right)^4\cdot\left[1 + \frac{8}{3}\sum_{j\,(\text{cloud})}\gamma_j(\eta_j - \zeta_j)\left(\frac{a}{\xi}\right)^{2(\alpha-1)}\right], \tag{6_2}$$

where t_c is a critical time in free particle scattering. Here, we pay attention to $2(\alpha-1) \approx 2\beta + \frac{8}{3}$ and $\eta_j \equiv \eta$, $\zeta_j \equiv \zeta$.

We can generally expect that the existence of viscous effect of the cloud results in an increase of the total entropy which is covered by the decrease of internal energy of the system. Here, assuming local equilibrium in the elements of mixing fluids, we may assume that this decrease of internal energy is covered also by the decrease of the energy density of non-viscous core parts. This fact differs from our concrete concept in treating of the energy density of the usual perfect fluid. A matter of primary concern for us is that the critical energy of the cloud shows an increase larger than that of the core in the course of the development of the system, due to the viscous effect of the last

term on the right hand side of (6_1). Then, we have

$$\frac{\varepsilon_j^c}{\varepsilon_j^{0*}} = \frac{\varepsilon_i^c}{\varepsilon_i^{0*}}\left[1 - l^2(\eta - \zeta)\left(\frac{a}{\xi}\right)^{2\beta+\frac{8}{3}}\right], \tag{6'}$$

$$viz. \qquad \varepsilon_j^c/\varepsilon_j^{0*} > \varepsilon_i^c/\varepsilon_i^{0*}\ . \tag{6''}$$

As we do not know the suitable quantitative estimation of η, ζ, we cannot definitely settle the above inequality, but discuss about it to a certain extent in due consideration of the different critical temperatures of the core and the cloud (see Section 3). The inequality is also a mathematical expression which characterizes the properties of mixing fluids viewed from the two fluid model.

3. – Hydrodynamic expression of the inelasticity.

In this section, we calculate the mean energy densities of the core particles and of the cloud particles at the end stage of the collision process in the centre of mass system, and then express theoretically the inelasticity with these quantities.

The (0, 0)-components of the energy-momentum tensor follow from the relation (**1**),

$$T_k^{00} - \frac{4}{3}\varepsilon_k r^2 - 2\eta_k\left[(1+r^2)\frac{\partial v}{\partial t} + \frac{3}{2}\frac{\partial v}{\partial \xi}\right] - \zeta_k\left[r^2\frac{\partial v}{\partial t} - \frac{1}{2}\frac{\partial r}{\partial \xi}\right]. \tag{1'}$$

The velocity of the fluid element in the conical flight is also given by

$$v \sim t/a \tag{7}$$

which is obviously valid for the mixing fluid (see eq. (47) in I). Substituting relation (7) into (1'), we obtain

$$T_k^{00} = \frac{4}{3}\varepsilon_c\left(\frac{t}{a}\right)^2 - 2\eta_k\left(\frac{1}{a}\right) - \zeta_k^v\left(\frac{t^2}{a^3}\right), \tag{1''}$$

using the volume viscosity $\zeta_k^v = \zeta_k + 2\eta_k$.

Here, the mean values of T_k^{00} at the critical point $t = t^c$ satisfying the relations (6_1), (6_2), are well defined by

$$\langle T_k^{00}\rangle_\xi = \int_A^a T_k^{00}(t_k)\,\mathrm{d}\xi \Big/ \int_A^a \mathrm{d}\xi \quad (*)\ .$$

(*) See eqs. (41), (48) in I as to the integral domain.

Then, we have for the core and cloud particles,

$$(8)\quad \begin{cases} \langle T^{00}_{i(\text{core})}\rangle \approx 4(\varepsilon_i^c \varepsilon_i^{0*})^{\frac{1}{2}} \left[1 - \dfrac{4}{9[\frac{1}{3} - 2(\alpha-1)]} \sum\limits_{j(\text{cloud})} \gamma_j(\bar\eta - \bar\zeta) \left(\dfrac{a}{\Delta}\right)^{2(\alpha-1)-\frac{1}{3}}\right] \equiv 4(\varepsilon_i^{c'} \varepsilon_i^{0*})^{\frac{1}{2}}, \\ \langle T^{00}_{j(\text{cloud})}\rangle \approx 4(\varepsilon_j^c \varepsilon_j^{0*})^{\frac{1}{2}} \cdot \left[1 - \dfrac{4}{9[\frac{1}{3} - 2(\alpha-1)]} \cdot \sum\limits_{j(\text{cloud})} \gamma_j(\bar\eta - \bar\zeta) \left(\dfrac{a}{\Delta}\right)^{2(\alpha-1)-\frac{1}{3}} - \right. \\ \qquad \left. - \dfrac{l^2(\bar\eta - \bar\zeta)}{2[2\beta + \frac{7}{3}]} \left(\dfrac{a}{\Delta}\right)^{2\beta+\frac{7}{3}}\right] + O_3(\bar\eta, \bar\zeta_v) \equiv 4(\varepsilon_j^{c'} \varepsilon_j^{0*})^{\frac{1}{2}}, \end{cases}$$

respectively (*). As is easily verified, the viscous term $O_3(\bar\eta, \zeta^v)$ induced from last two terms of (1″) should be neglected according to the relation

$$l^2 \bar\eta \left(\frac{a}{\Delta}\right)^{2\beta+\frac{7}{3}} \varepsilon_j^c > \bar\zeta^v \frac{1}{a}, \qquad (\bar\eta \approx \bar\zeta^v).$$

$\bar\eta$, $\bar\zeta^v$ represent the mean values of viscous coefficient in the domain considered.

Now, we shall define the theoretical inelasticity by a quantity K, which means the ratio between the energy of cloud particles and the energy of the total system,

$$(9)\quad \frac{1-K}{K} = \frac{\sum\limits_{i(\text{core})} \langle T_i^{00}\rangle_\xi}{\sum\limits_{j(\text{cloud})} \langle T_j^{00}\rangle_\xi} = \frac{\sum\limits_{i(\text{core})} (\varepsilon_i^{c'} \varepsilon_i^{0*})^{\frac{1}{2}}}{\sum\limits_{j(\text{cloud})} (\varepsilon_j^{c'} \varepsilon_j^{0*})^{\frac{1}{2}}}.$$

(*) The quantity $\varepsilon^{c'}_{k=i,j}$ defined by (8) is closely connected with ε_k^c. By straightforward calculation and omission of higher order terms of η, ζ, we have

$$(\varepsilon_j^{c'}/\varepsilon_j^c) = (\varepsilon_i^{c'}/\varepsilon_i^c)\left[1 - \frac{l^2(\bar\eta - \bar\zeta)}{(2\beta + \frac{7}{3})}\left(\frac{a}{\Delta}\right)^{2\beta+\frac{7}{3}}\right].$$

If we fix together this expression and the inequality (6″), a relation $(\varepsilon_j^{c'}/\varepsilon_j^{0*}) > (\varepsilon_i^{0'}/\varepsilon_i^{0*})$ is also obtained. Remembering that the viscous contribution cannot affect the non-dissipative term, that is, Reynolds number $\mathscr{R} > 1$, we can easily find

$$\tfrac{1}{2} \leqslant (\varepsilon_i^{c'} \varepsilon_j^{0*})/(\varepsilon_i^{0*} \varepsilon_j^{c'}) \leqslant 1.$$

Assuming the relation between energy-density and temperature $\varepsilon_k^{c'} \propto T^4$ which holds in a way approximately analogous to black body radiation, we have

$$\frac{1}{\sqrt[4]{2}} \leqslant T_c^0/T_c \leqslant 1,$$

where T_c^0 and T_c are respective critical temperatures of the core and the cloud, and the initial stage of the total system is regarded as about $T \approx \infty$.

In our model, the cloud particles surrounding the core nucleon form the mixing fluids consisting of the π-mesons and the K-mesons. The ratios of initial energy densities of these particle are given as follows:

$$(10)\qquad \begin{cases} (\varepsilon_{\pi}^{0*}/\varepsilon_{\mathcal{N}}^{0*}) = (g_{\pi}\varphi(0)/g_{\mathcal{N}}\tilde{\varphi}(0)) \approx 0.857\,, \\ (\varepsilon_{\theta}^{0*}/\varepsilon_{\mathcal{N}}^{0*}) = (g_{\theta}\varphi(0)/g_{\mathcal{N}}\tilde{\varphi}(0)) \approx 1.143\,. \end{cases}$$

Here, we have used the relation

$$\varepsilon_{k}^{0*} = \frac{g_k}{2\pi^2}\frac{T^4}{(\hbar c)^3}\varphi(m_k c^2/T)\big|_{T\to\infty}\,,$$

together with the statistical weights $g_{\pi}=3$, $g_{\theta}=4$ and $g_{\mathcal{N}}=g_{\bar{\mathcal{N}}}=4$. Let us now replace the energy in eq. (9) by the particle density through the medium of the relation (7)

$$(10')\qquad \begin{cases} \varepsilon_{i(\mathrm{core})}^{c'} = n_i^c \cdot T_c^0 \cdot \dfrac{\tilde{\varphi}(x_i^0)}{\tilde{F}(x_i^0)}\,, \\ \varepsilon_{j(\mathrm{cloud})}^{c'} = n_j^0 \cdot T_c \cdot \dfrac{\varphi(x_j)}{F(x_j)}\,, \end{cases}$$

where $x_i^0 = M_i c^2/T_c^0$, $x_j = m_j c^2/T_c$, and $T_c^0 (\equiv T_c^{\mathcal{N}} = T_c^{\bar{\mathcal{N}}}) < T_c (\equiv T_c^{\pi} = T_c^{\theta})$, in which T_c^0, T_c are the critical temperatures of the core- and the cloud-particles, respectively.

By inserting the relation (10), (10′) into (9) we finally obtain an expression which after a simple, but lengthy, calculation may be written in the following form,

$$(11)\qquad \frac{1-K}{K} = \frac{(2n_{\mathcal{N}}^c)^{\frac{1}{2}}\cdot\left(\dfrac{T_c^0}{T_c}\cdot\dfrac{\tilde{\varphi}(x_{\mathcal{N}}^0)}{(\tilde{F}x_{\mathcal{N}}^0)}\right)^{\frac{1}{2}}}{(n_{\pi}^c)^{\frac{1}{2}}\left(0.429\,\dfrac{\varphi(x_{\pi})}{F(x_{\pi})}\right)^{\frac{1}{2}} + (n_{\theta}^c)^{\frac{1}{2}}\left(0.571\,\dfrac{\varphi(x_{\theta})}{F(x_{\theta})}\right)^{\frac{1}{2}}}\,.$$

Here, we shall compute the inelasticity in the special case in which the cloud temperature is $T_c \approx 1.1\, m_{\pi}c^2$ and the core temperature shows a change of $T_c^0 = T_c \sim T_c/\sqrt[4]{2}$. The stage of $T_c^0 \approx T_c/\sqrt[4]{2}$ corresponds to the extreme case in which the viscous effect of the cloud has a maximum contribution to critical energy $\varepsilon_j^{c'}$; in that case our perturbational calculation may be destroyed.

(7) Functions (φ, F) and $(\tilde{\varphi}, \tilde{F})$ were given by Belenkij-Landau-Milehin for the boson and the fermion, respectively. S. Z. Belen'kij and L. D. Landau: *Usp. Fiz. Nauk*, **56**, 309 (1955); S. Z. Belen'kij and S. A. Milehin: *Žurn. Ėsp. Teor. Fiz.*, **29**, 20 (1955).

2250

For the numerical values of $F(x)$ and $q(x)$, we have used the Table given in reference (7).

The following table gives the results of our numerical computation for the inelasticity.

TABLE I. – K = *inelasticity*.

$T_c = 1.1 m_\pi c^2$	K	Composition of various particles			Model
		n_N^c	n_θ^c	n_π^c	
$T_c^0 = T_c$	0.73	0.04	0.35	1	one fluid
$T_c^0 = T_c/\sqrt[4]{2}$	0.84	0.0115	0.35	1	two fluid

From Table I, we can understand the tendency to fluctuation of the inelasti city in the two fluid model. K value for $T_c^0 < T_c$ is generally larger than that of $T_c^0 = T_c$.

In the case of $T_c < 1.1 m_\pi c^2$, the inelasticity increases gradually with the decrease of the critical temperature T_c (and also T_c). We shall expressly point out the fact that this value attains the order of magnitude of $K \sim 0.9$ at $T_c = 0.8 m_\pi c^2$.

If we apply the high critical temperature $T_c > 1.1 m_\pi c^2$ to our model, it may be possible to make a forecast of the low value of inelasticity. In fact, at the critical temperature $T_c^0 = T_c = 1.3 m_\pi c^2$, we could obtain $K \approx 0.64$ from eq. (11), after we made use of the appropriate quantities required for the calculation. In conclusion, we can expect a fluctuating value of inelasticity $K = 0.6 \sim 0.9$ for the critical temperature $T_c = (0.8 \sim 1.3) m_\pi c^2$ considered.

4. – Discussion.

We have here discussed the mechanism of multiple particle production based upon the two fluid model and sought for the plausible expression of inelasticity of this model. This expression is of the form containing the energy densities at the initial and the critical times. As is clearly known from (6'), if it were possible to suppose $\varepsilon_j^{0*}/\varepsilon_j^{c'} = \varepsilon_i^{0*}/\varepsilon_i^{c'}$ (*i.e.* $\eta = \zeta = 0$) we have a simple expression for the one fluid model, $K = \sum_{j(\text{cloud})} \varepsilon_j^{0*}/\varepsilon^{0*} = \sum_{j(\text{cloud})} \varepsilon_j^{c'}/\varepsilon^{c'}$, ($\varepsilon^{c'}$; critical energy of the total system). We cannot, however, approve the above assumption owing to the essence of two fluid model, in which the critical temperature of the core is not equal to that of the cloud. Then, we have had to use the relations (9), (11) for calculation of inelasticity. That is to say, such a treatment gives enough ground for intervention of our two fluid model.

2251

* * *

I wish to thank Professors H. YUKAWA and T. INOUE for their continual encouragement.

RIASSUNTO (*)

Si analizza il meccanismo di produzione multipla di particelle nelle collisioni nucleone-nucleone di alta energia, usando il modello a due fluidi. Si calcola numericamente l'anelasticità teorica.

(*) *Traduzione a cura della Redazione.*

6252

The Excited Nucleon's Model of Meson Production (*).

U. Maor and G. Yekutieli

Department of Physics, The Weizmann Institute of Science - Rehovoth

(ricevuto il 12 Marzo 1960)

Summary. — A model of meson production from excited nucleons is described for both nucleon-nucleon and nucleon-nucleus collisions induced by cosmic ray particles. The results are compared with observations in photographic emulsions, and reasonable agreement is found.

1. – Introduction.

A few years ago Tokagi (1) and Kraushar and Marks (2) suggested that at high energy nuclear collisions, mesons are produced from two centers. According to Kraushar and Marks (2), in nucleon-nucleon collisions two excited nucleons are formed that live longer than nuclear reaction time; later on they decay independently into mesons and nucleons. Observations of Lindenbaum and Yuan (3) at lower energies ($(0.5 \div 3.0)$ GeV) suggest a similar process of meson production in nucleon-nucleon collisions. At this range of energy one or two nucleons are excited to the first $(\frac{3}{2}\,\frac{3}{2})$ isobar level found in π^+-p scattering experiments. The isobars have a resonance-like mass distribution with a peak at 1.230 GeV and a life time longer than 10^{-23} s. Subsequently each excited nucleon decays spontaneously into a nucleon and a pion. These observations were successfully extended by Lindenbaum and

(*) This work has been sponsored in part by the Geophysics Research Directorate of the Air Force Cambridge Research Center, Air Research and Development Command, United States Air Force under contract AF61(052)-58 through the European Office ARDC.

(1) S. Takagi: *Progr. Theor. Phys.*, **7**, 123 (1952).

(2) W. L. Kraushaar and L. J. Marks: *Phys. Rev.*, **93**, 326 (1954).

(3) S. J. Lindenbaum and L. C. L. Yuan: *Phys. Rev.*, **93**, 917 and 1431 (1954); **103**, 404 (1956).

STERNHEIMER [4] and by HOLMQUIST [5] up to energies of few GeV, with the conclusion that mesons are produced predominantly from excited nucleons. The recent discovery of second and third resonance levels in photomeson-production [6] and π-p scattering experiments [7,8] indicate the possibility of extending this theory to even higher energies. Further analysis of nuclear events produced by cosmic ray particles by COCCONI [9] and CIOK *et al.* [10] gave new evidence for meson emission from two centers. At the same time several authors [11-14] observe that in these collisions mesons are produced with a low transverse momentum with a peak at about $P_T = 0.4$ GeV/c. Both of these observations are compatible with a model of meson production from excited nucleons. These recent developments make it worthwhile to explore the possibility of extending the excited nucleon's model of meson production to cosmic ray energies.

The purpose of this paper is an attempt to describe meson production by cosmic ray particles in terms of an excited nucleon's model. We shall assume that in a nucleon-nucleon collision two excited nucleons are produced with masses M_1 and M_2 and momenta P_1 and P_2 given by an excitation function $W(M_1 P_1 M_2 P_2 | E_c)$ where E_c is the total energy in C.M.S. of the collisions. The two excited nucleons have a life time longer than the collision time, and leave the reaction range as two free particles. Subsequently each excited nucleon decays independently into a number of low energy pions, and a single nucleon.

A model of meson production in nucleon-nucleus collision will be described as follows: The energetic incident nucleon sees the nucleus as a gas of A independent nucleons. The first phase of the reaction is a nucleon-nucleon collision between the incident nucleon and one nucleon of the nucleus. From this

---

[4] S. J. LINDENBAUM and R. M. STERNHEIMER: *Phys. Rev.*, **105**, 1874 (1957).

[5] F. N. HOLMQUIST: *Ph. D. Thesis* (University of California, 1958).

[6] R. R. WILSON: *Phys. Rev.*, **110**, 1212 (1958).

[7] H. C. BURROWES, D. O. CALDWELL, D. H. FRISCH, D. A. HILL and D. M. RITSON: *Phys. Rev. Lett.*, **2**, 119 (1959).

[8] R. R. CRITTENDEN, J. H. SCANDRETT, W. D. SHEPARD and W. D. WALKER: *Phys. Rev. Lett.*, **2**, 121 (1959).

[9] G. COCCONI: *Phys. Rev.*, **111**, 1699 (1958).

[10] P. CIOK, T. COGHEN, J. GIERULA, R. HOŁYŃSKI, A. JURAK, M. MIĘSOWICZ, T. SANIEWSKA and J. PERNEGR: *Nuovo Cimento*, **10**, 741 (1958).

[11] S. HASEGAWA, J. NISHIMURA and Y. NISHIMURA: *Nuovo Cimento*, **6**, 979 (1957).

[12] O. MINAKAWA, Y. NISHIMURA, M. TSUZUKI, H. YAMANOUCHI, H. AIZU, H. HASEGAWA, Y. ISHII, S. TOKUNAGA, Y. FUJIMOTO, S. HOSEGAWA, J. NISHIMURA, K. NIU, K. NISHIKAWA, K. IMAEDA and M. KAZUNO: *Suppl. Nuovo Cimento*, **11**, 125 (1959).

[13] B. EDWARDS, J. LOSTY, D. H. PERKINS, K. PINKAU and J. REYNOLDS: *Phil. Mag.*, **3**, 237 (1958).

[14] E. G. BOOS, A. KH. VINITSKII, ZH. S. TAKIBAEB and I. IA. CHASNIKOV: *Journ. Exp. Theor. Phys.*, **34** (7), 430 (1958).

2254

primary collision two excited nucleons are emitted in a narrow cone in the direction of the incident particle. We shall assume that the excited nucleons have the same interaction mean free path in nuclear matter as an ordinary nucleon. This implies that the mean collision time of an excited nucleon in nuclear matter is of the order of the mean reaction time, and is smaller than the mean life time of an excited nucleon. Thus most of the energetic excited nucleons, will make another collision before they will have a chance to decay into mesons. We further assume that one more excited nucleon is produced in the next excited nucleon-nucleon collision. In this manner a cascade of excited nucleons is developed in the nucleus. When the cascade of excited nucleons leaves the nucleus the excited nucleons will decay independently into mesons and nucleons in a narrow cone. This narrow cone of energetic particles is the jet of shower particles associated with high energy cosmic ray eventsin photographic emulsion. Some of the slow excited nucleons will decay into pions and nucleons in the nucleus. These particles in further collisions transfer energy to the entire nucleus and produce the large star with grey and heavy prongs observed in nuclear emulsion.

2. – Meson production in nucleon-nucleon collisions.

According to the excited nucleon model, meson production is a two phase process: 1) creation of excited nucleons in nuclear reaction; and 2) decay of excited nucleons into mesons and nucleons. Both of these reactions are strong, and conserve among other things, isospin, strangeness and parity. In the most general case the excited nucleons and subsequently the mesons, may carry different quantum numbers of charge, angular momentum, isospin and strangeness. For the moment we shall ignore this specification and deal only with the simple neutral nucleons and pions. Later on, the theory may be modified to include the different charge and strangeness states.

Following LINDENBAUM and STERNHEIMER ([4]) the relative probability for creating two excited nucleons of masses M_1 and M_2 in a nucleon nucleon collision is: $|H|^2(|P_1|E_1E_2/(E_1+E_2))$, where H is the matrix element for this reaction, E_1P_1; E_2P_2 are the energies and momenta of the two excited nucleons in C.M.S. In this system $E_1+E_2=E$, the total energy of the system and $|P_1|=|P_2|$. At low energies $|H(M_1M_2)|^2$ has a resonance found in π^--p scattering experiments. At higher energies there are indications for second and third resonances corresponding to isobars of masses $M=1.750$ and $M=2.071$ GeV respectively ([6-8]).

The behaviour of $|H|^2$ at even higher energies is not yet known, and in order to apply the isobar model to cosmic ray energies we shall have to guess the general character of $|H|^2$. Later on by comparing the results of

2255

that model with experiment we can find out how well the average features of $|H|^2$ were pictured, and in this way learn something about its behaviour at higher energies.

The most simple assumption is that at high energies there are many isobar levels of the same strength and thus $|H|^2$ averaged over the different resonance levels is a constant. This assumption yields a meson multiplicity that rises like E_c with energy ([15]). Experimentally we know that meson multiplicity increases very slowly with energy, and thus $\langle|H^2|\rangle$ must be a decreasing function of the mass of the isobar. As a second attempt let us assume that in the energy range (1÷1600) GeV $|H(M_1M_2)|^2$ averaged over all resonance levels could be approximated by $\exp[-(M_1+M_2)/\alpha]$, where α is a free parameter to be adjusted so that the calculated multiplicity in the energy range (25÷1600) GeV will be as near as possible to the observed one. Furthermore we shall assume that the excited nucleons are produced isotropically in the C.M.S. of the collision.

For the decay of excited nucleons, we shall assume that mesons are emitted from excited nucleons, one after another isotropically and with a constant low energy E_π. A choice of E_π between 0.3 and 0.5 GeV is suggested by several authors ([14,16,17]). As we shall see later, this type of decay yields in the C.M.S. a narrow distribution for the transverse momenta of pions with a peak at $P_T \simeq \sqrt{E_\pi^2 - m_\pi^2}$.

3. – Monte-Carlo calculation of meson production in nucleon-nucleon collisions.

In order to study the excited nucleon's model of meson production in nucleon-nucleon collisions, a Monte-Carlo calculation was programmed for the WEIZAC electronic computer. The calculation was carried out for a given primary E_0. At this energy a number of collisions were followed. For each collision two excited nucleons of masses M_1 and M_2 were chosen according to the weighting function $W(M_1M_2) = \exp[-(M_1+M_2)/\alpha](|P|^2 E_1E_2)/(E_1+E_2))$, where $E_1^2 = P_1^2+M_1^2$ and $E_2^2 = P_2^2+M_2^2$ are the energies of the excited nucleons in their C.M.S.; $E_1+E_2 = E_c$ is the total energy of the collision in that system, and $|P_1| = |P_2|$. Both M_1 and M_2 are heavier than 1.230 GeV, the mass of the lowest excited nucleon that decays into a meson, the $(\frac{3}{2}\,\frac{3}{2})$ isobar. α is a free parameter to be found by comparison with experiment. The direction of each excited nucleon $\bar{P}_1$ $(= -\bar{P}_2)$ in the C.M.S. was chosen isotropically. Sub-

([15]) U. MAOR and G. YEKUTIELI: T.S.R. no. 1 (unpublished, 1959).
([16]) S. KANEKO and M. OKAZAKI: *Nuovo Cimento*, **8**, 521 (1958).
([17]) E. LOHRMANN: *Nuovo Cimento*, **5**, 1074 (1957).

2256

sequently each excited nucleon emits one after another n_π mesons. Each meson is emitted isotropically and with a constant energy E_π from the excited nucleon. Whenever a meson is emitted the excited nucleon recoils to conserve momentum. The last meson is emitted with a momentum chosen to insure that the last excited nucleon will go into a nucleon. Calculation of each collision gives the momenta in the Laboratory System of n created mesons and two outgoing nucleons. This output is used to study the following features of nucleon-nucleon collisions: 1) Meson multiplicity; 2) Energy distributions of mesons and nucleons, and 3) Transverse momentum (P_T) distribution of mesons and nucleons.

In order to find the values of the two free parameters of this model, α and E_π, several small samples with different values of α and E_π were tried out at seven different incident energies: $E_0 = 25$; 50; 100; 200; 400; 800; and 1600 GeV. The average numbers of mesons obtained in this way are presented in Table I. The P_T distributions of the different samples are all very

TABLE I. – *Meson production (n_π) in nucleon-nucleon collision for different values of E_π and α.*

Free parameters		Incident energies in GeV						
α (GeV)	E_π (GeV)	25	50	100	200	400	800	1600
3.0	.375	9	11.2	8.6	13			
3.5	.375	8.6	10.6			18.7	17.3	18.6
3.5	.400 (*)	7.4	10.7	13.4	14.9	16.5	17.4	17.3
4.0	.375							28.3
4.0	.400			18.3	21.0	22.3	20.8	17.6

All samples $N = 10$. (*) $N = 250$.

similar. The values of the transverse momenta are mostly below 1 GeV/c with a pronounced peak near 0.350 GeV/c. The peak of the P_T distributions in the different cases varies slowly between (320÷380) MeV/c and it is in reasonable agreement with the experimental observations. Therefore the average meson multiplicity in this model depends mainly on the choice of α, *i.e.* on the average mass of the excited nucleons. The only experimental information on meson production in this range of energy is from observations in nuclear emulsions. In using the nuclear emulsion data we made the assumption that the group of stars with $Nh \leqslant 2$ represent mainly nucleon-nucleon collisions. The energy of the incident particle is measured by the median angle and the CASTA-

GNOLI [18]) methods. The average numbers of shower particles n_s of nuclear events with $Nh \leqslant 2$ as observed by CASTAGNOLI *et al.* [18]), EDWARDS *et al.* [13]), GUREVICH *et al.* [19]), LOHRMANN [17]) and BRISBOUT *et al.* [20]) are presented in Table II.

TABLE II. – *Meson multiplicity n_π as function of incident energy E in stars with $N_h \leqslant 2$. n_s is average number of shower particles and n is the number of observed events.*

Emulsion data		Nucleon-nucleon collisions for $\alpha=3.5$ GeV and $E_\pi=.400$ GeV				
Energy range (GeV)	$\langle E_0 \rangle$ (GeV)	n_s	n_π	n	n_s	n_π
25÷ 150	70	7.8	10.2	12	9.9	13.4
150÷ 300	250	12.5	17.3	2	10.9	14.9
300÷ 600	560	10.0	13.5	1	12.0	16.5
600÷1200	905	15.5	21.7	2	12.5	17.3
1200÷2400	1050	11.7	16.1	7	12.7	17.5
25÷ 600	127	8.6	11.4	15	10.2	13.8
600÷2400	1790	12.5	17.2	9	12.5	17.3

The average number of mesons per event is given by $n_\pi = 1.5(n_s - 1)$ on the assumption that all mesons are pions. By comparing Table I to II it is evident that the best choice of the free parameters is $\alpha = 3.5$ GeV, $E_\pi = 0.4$ GeV.

Using these values an extensive calculation of 250 collisions at each of the seven incident energies was carried out. The results of these nucleon-nucleon collisions are preseted with those of the nucleon-nucleus collisions in Section **6**, **7** and **8**.

4. – Nucleon-nucleus interaction.

In Section **2** a model for nucleon-nucleon collision is described, we shall extend this model to nucleon-nucleus interactions.

([18]) C. CASTAGNOLI, G. CORTINI, C. FRANZINETTI, A. MANFREDINI and D. MORENO: *Nuovo Cimento*, **10**, 1539 (1953).

([19]) I. I. GUREWICH, A. P. MICHACOVA, B. A. NICKOSKII and L. V. SURAKOVO: *Journ. Exp. Theor. Phys.*, **34** (7), 185 (1958).

([20]) F. A. BRISBOUT, C. DAHANAYAKE, A. ENGLER, Y. FUJIMOTO and D. H. PERKINS: *Phil. Mag.*, **1**, 605 (1956).

The nucleus is pictured as a gas of free nucleons with a spherical symmetric distribution $\varrho(r)$. Observations by HOFSTADTER ([21]) and collaborators on electron nucleus scattering, show that heavy and medium nuclei can be described by a core of constant density ϱ_0 and a periphery around it in which the density decreases gradually. This type of nucleus can be approximated by a trapezoidal density distribution: $\varrho(r < R_1) = \varrho_0 = \text{constant}$, where $R_1 = -1.56 + 1.08 A^{\frac{1}{3}}$ is the radius of the core measured in units of 10^{-13} cm; and A is the number of nucleons in the nucleus, and $\varrho(R_1 < r < R_2) = \varrho_0(r - R_1)/(R_2 - R_1)$ in the periphery. The width of the periphery is constant $R_2 - R_1 = 3.12 \cdot 10^{-13}$ cm. For instance a nucleus of an AgBr « Atom » in photographic emulsion will have $A = 94$; $R_1 = 3.45 \cdot 10^{-13}$ cm and $\varrho_0 = 1.74 \cdot 10^{38}\,\text{cm}^{-3}$

The incident nucleon is of very high energy (above 20 GeV) and we shall assume that it interacts singly and independently with nucleons of the nucleus, with the same cross-section for nuclear interaction as in nucleon-nucleon collisions. According to BRENNER and WILLIAMS ([22]) the cross-section for nucleon-nucleon interaction between 20 and 50 GeV is 21 mb. We shall use this value for nucleon-nucleon collisions up to 1600 GeV. This cross-section corresponds to a mean free path for nuclear collision of $\lambda = 4.7 \cdot 10^{-13}$ cm in the core of an AgBr nucleus.

The first collision of the incident nucleon in the nucleus is a nucleon-nucleon interaction and is treated according to the model described in Section 2. In this collision two excited nucleons are produced. We shall assume that each excited nucleon has the same interaction mean free path in nuclear matter as ordinary nucleons. An excited nucleon has a mean life time longer than a nucleon-nucleon reaction time, and thus the mean time for nuclear collision in a nucleus is about 1.5 times longer than its reaction mean time (it is proportional to the ratio: « mean free path for collision in nuclear matter » over « range for nuclear collision »).

Now, the mean life time in the system of the nucleus of a very energetic excited nucleon is increased due to its large Lorentz factor γ, and it is certainly longer than its mean time for collision in the nucleus. Thus an energetic excited nucleon with a γ factor larger than a critical value γ_0 on the average makes a collision in the nucleus before it has a chance to decay. On the other hand a low energy excited nucleon (with $\gamma < \gamma_0$) will on the average decay inside the nucleus. The critical value of γ_0 depends on the ratio of the mean life time of an excited nucleon to its mean time for nuclear collision in the nucleus. Considering the assumptions made before on the nuclear interaction of excited nucleons we shall take $\gamma_0 = 1.4$ for the critical Lorentz factor

([21]) R. HOFSTADTER: *Rev. Mod. Phys.*, **28**, 214 (1956).
([22]) A. E. BRENNER and R. W. WILLIAMS: *Phys. Rev.*, **106**, 1020 (1957).

2959

of excited nucleons. This is the first condition for the development of a cascade of excited nucleons in the nucleus. Only excited nucleons with $\gamma < \gamma_0$ will participate in this cascade. We shall further assume that in excited-nucleon nucleon collisions, as in nucleon-nucleon collisions two excited nucleons M_1 and M_2 are produced with relative frequency $W(M_1 M_2) = \exp[-(M_1 + M_2)/\alpha] \cdot (|P_1| E_1 E_2/(E_1 + E_2))$ with the condition that the masses of each secondary excited nucleon is not smaller than that of the primary excited nucleon. To complete the conditions for the development of a cascade of excited nucleons in the nucleus, we assume that a target nucleon in the nucleus may interact only with one excited nucleon and that there is no mutual interaction between two excited nucleons. According to this model the incident nucleon will initiate a cascade of excited nucleons in the nucleus. Most of the excited nucleons (with $\gamma > 1.4$) will leave the nucleus and decay outside the nucleus into pions and ordinary nucleons. The decay of these particles will follow the same process as described for excited nucleons produced in nucleon-nucleon collisions. (See Section 2). These particles will constitute the jets observed in nuclear events produced by cosmic ray particles in photographic emulsions. Some of the excited nucleons (with $\gamma < 1.4$) will decay in the nucleus and give up their energy to excite the nucleus and to produce the cosmic ray star associated with high energy jets of cosmic ray events in nuclear emulsion.

5. – Monte-Carlo calculation of nucleon-nucleus interaction.

A Monte-Carlo calculation of the nucleon nucleus interaction was programmed for the WEIZAC electronic computer. The block diagram of this program is shown in Fig. 1. The actual calculations were carried out for two nuclei: a heavy nucleus with $A = 94$ representing the nuclei of Ag and Br atoms in the emulsion and a light nucleus with $A = 14$ representing the nuclei of the atoms C, N and O in the emulsion. For each nucleus the reaction was studied at five different incident energies: $E = 100$; 200; 400; 800 and 1600 GeV, and for every incident energy 100 cascades were followed. Throughout the calculation as in the nucleon-nucleon collisions the parameters $\alpha = 3.5$ GeV and $E_\pi = 0.4$ GeV were used. The output of this numerical calculation is used to study the following features of nucleon-nucleus interaction. 1) Meson multiplicity; 2) Energy distribution of mesons and nucleons; and 3) Transverse momenta distribution of mesons and nucleons. The results obtained in this way are presented in the next Section.

2260

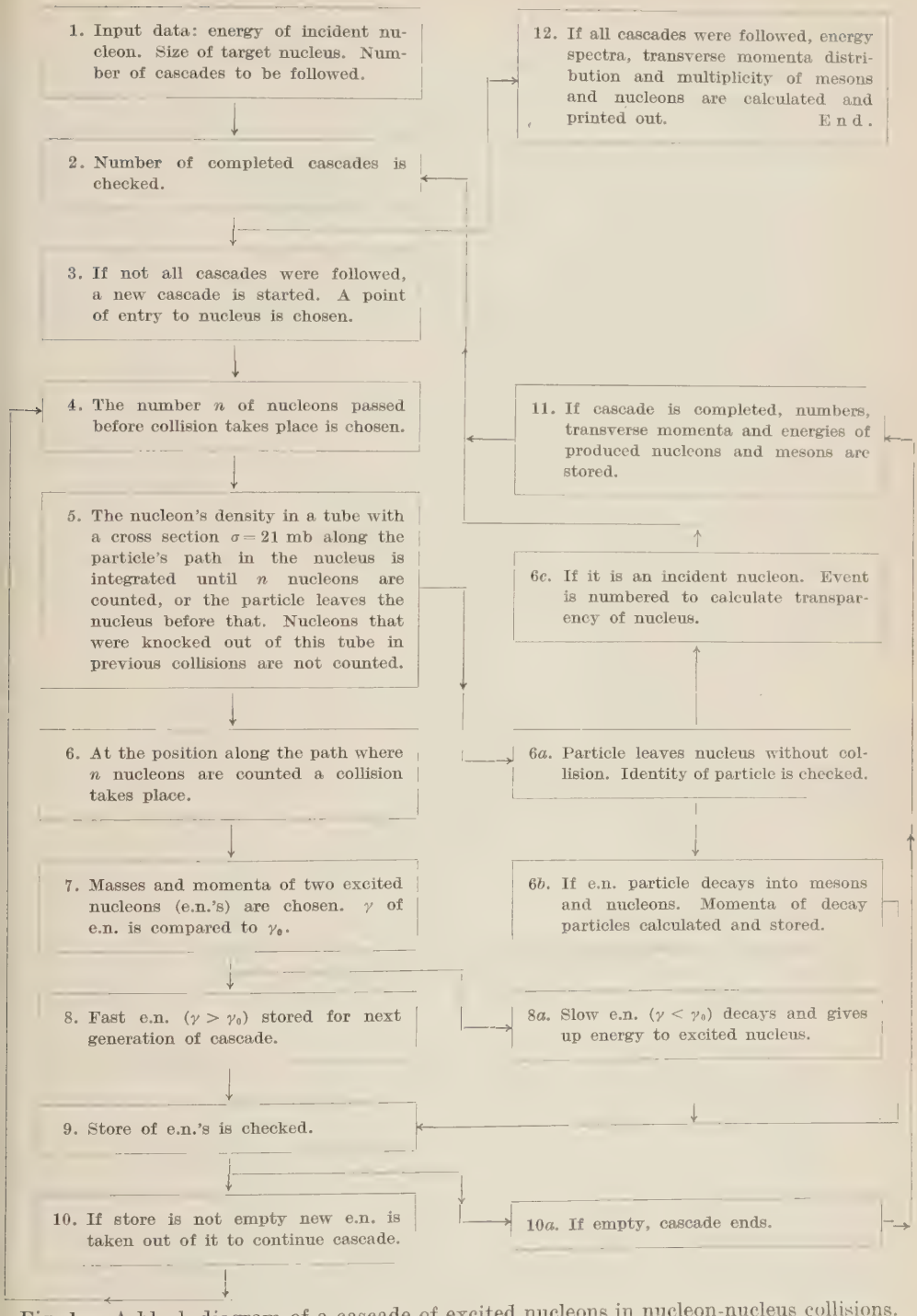

Fig. 1. – A block diagram of a cascade of excited nucleons in nucleon-nucleus collisions.

6. – Meson production in nucleon-nucleon and nucleon-nucleus collisions.

The average numbers of mesons n_π and shower particles n_s produced in nucleon-nucleon and nucleon-nucleus collisions as function of the incident energy are given in Tables II and III. Assuming that all mesons are pions, the average number of shower particles n_s is given by: $n_s = 0.5\, n_{\mathcal{N}'} + 0.66\, n_\pi$, where $n_{\mathcal{N}'}$ is the average number of relativistic nucleons produced per interaction. If there are 20% K-particles among mesons n_s is reduced by 4%.

The main features of the cascade of excited nucleons in AgBr and CNO « nuclei » are summarized in Table III.

TABLE III. – *Average numbers of energetic nucleons* ($N_{\mathcal{N}}$) *and mesons* (n_π) *in nucleon nucleus collisions.*

	AgBr $\sigma = 21$ mb			AgBr $\sigma = 40$ mb		
E (GeV)	$N_{\mathcal{N}}$	n_π	$n_\pi/N_{\mathcal{N}}$	$N_{\mathcal{N}}$	n_π	$n_\pi/N_{\mathcal{N}}$
100	4.8	18.9	6.0	7.13	38.9	5.5
200	5.1	38.6	7.6	8.11	54.9	6.8
400	5.2	46.7	9.0	8.17	69.5	8.2
800	5.1	50.4	9.9	8.83	85.2	9.7
1600	5.6	61.6	11.0	9.59	103.0	10.7
	CNO $\sigma = 21$ mb			$0.04\,[\mathrm{H}] = 0.16\,[\mathrm{CNO}] + 0.80\,[\mathrm{AgBr}]$ $\sigma = 21$ mb		
100	3.1	19.6	6.2	4.4	26.8	6.1
200	3.3	25.0	7.5	4.7	35.4	7.5
400	3.4	30.5	9.2	4.7	43.0	9.0
800	3.6	35.5	9.8	4.7	46.7	9.9
1600	3.3	34.5	10.5	5.1	55.4	10.9

Results are given for four different types of cascades: *a*) A cascade of excited nucleons in heavy nuclei of the emulsion, the AgBr group, with $\sigma = 21$ mb for nucleon-nucleon collisions. This value for the cross-section is the one measured by BRENNER and WILLIAMS ([22]) at the highest energy measured so far, 50 GeV. *b*) The same cascade but with $\sigma = 40$ mb to study the effect of the nucleon-nucleon interaction cross-section on the nucleon nucleus collisions. *c*) An excited nucleon's cascade in a light nucleus of the CNO group with $\sigma = 21$ mb, and *d*) The results of a cascade of an average nucleon nucleus

2962

interaction in photographic emulsion. The average interaction is given by $0.04\,[\mathrm{H}] + 0.16\,[\mathrm{CNO}] + 0.80\,[\mathrm{AgBr}]$, the relative contributions of the three types of collisions in emulsions were calculated as follows: $\sigma_{N',N'} = 21$ mb for the nucleon-nucleon collisions and the nucleon-nucleus cross-sections obtained from the Monte-Carlo calculation, for nucleon-CNO and nucleon-AgBr collisions.

The average number of fast nucleons produced per interaction $N_{N'}$ is equal to the average number of excited nucleons that participated in the cascads. It appears from Table III that $N_{N'}$ depends very much on the size of the nucleus and the cross-section for nucleon-nucleon collision of the cascade. At the same time the number of fast nucleons in the same nucleus increases slowly with increasing incident energy. The average number of pions produced per excited nucleon ($n_\pi/N_{N'}$) behaves the opposite way. It depends only on the incident energy E_0, and it is practically constant for different types of cascades induced by the same primary energy. Thus the total number of mesons produced in a given cascade depends on the primary energy through ($n_\pi/N_{N'}$) (the average number of pions produced per excited nucleon), on the size of the nucleus and on the nucleon-nucleon collision cross-section, through ($N_{N'}$) (the average number of nucleons produced per cascade).

7. – Observable features of nucleon-nucleus interactions.

Unfortunately we cannot compare directly the results of the excited nucleon's model with experimental observations. Most of the experimental observations between 100 and 1600 GeV were made in photographic emulsion exposed to the cosmic radiation. In these experiments it is impossible to measure directly the energy of the primary and the size of the target nucleus of each individual event.

Several methods ([23,18]) were used to estimate the primary energy of high energy nuclear events in photographic emulsion. They are based on the assumption that all mesons are produced in a single center from which they are emitted with a forward-backward symmetry. According to CASTAGNOLI *et al.* ([18]) the Lorentz factor of the emitting center γ_c, is related to the angular distribution of the shower particles in the laboratory system by:

$$\ln \gamma_c = n_s^{-1} \sum \ln \cot \theta = \langle \ln \cot \theta \rangle ,$$

where $\gamma_c^2 = (1 - \beta_c^2)^{-1}$ and β_c is the velocity of the emitting center.

([23]) N. M. DULLER and W. D. WALKER: *Phys. Rev.*, **23**, 215 (1954).

2203

Equivalent results are obtained by the median angle and the F-plot ([23]) methods. The $\langle \ln \cot \theta \rangle$ parameter was found very useful for estimating the primary energy E_0 in nucleon-nucleon collisions, where $E_0/m_p = \gamma_0 = 2\gamma_c^2 - 1$. The same method was applied to very high energy nucleon-nucleus collisions ([24,25]), on the assumption that all the N struck nucleons of the target nucleus form a single cluster, moving with a Lorentz factor γ_c, from which mesons are emitted with a forward-backward symmetry. In this case again $\ln \gamma_c = \langle \ln \cot \theta \rangle$ and the primary energy E_0 is given by:

$$E_0/m_p = \gamma_0 = N(\gamma_c^2 - 1) + \gamma_c \sqrt{N^2(\gamma_c^2 - 1) + 1} \, .$$

Thus the estimation of the primary energy E_0 in the nucleon-nucleus interactions depends on an additional assumption—the formation of a single cluster of struck nucleons, and on an extra parameter, N, the number of struck nucleons in the target nucleus.

According to the excited nucleon's model mesons are emitted from many different centers, thus one may think that the relation $\ln \gamma_c = \langle \ln \cot \theta \rangle$ is meaningless for this model. However as $\langle \ln \cot \theta \rangle$ can be evaluated for each event, we may use it to define a fictitious system of emission with Lorentz factor γ_c. The parameter γ_c so defined is treated as a stochastic variable, and an attempt is made to verify statistically the relation

$$\gamma_c = (\gamma_0 + N)(1 + 2\gamma_0 N + N^2)^{-\frac{1}{2}}$$

for different values of primary energy

$$E_0 = m_p \gamma_0 \, ;$$

where N is the number of the excited nucleons per interaction.

To this end the distributions of $\ln \gamma_c = \langle \ln \cot \theta \rangle$ as calculated by the Monte-Carlo program are studied for nucleon-nucleon, nucleon-CNO and nucleon-AgBr collisions at different incident energies E_0, and fixed number of struck nucleons N.

Some examples of $\langle \ln \cot \theta \rangle$ distributions evaluated by the excited nucleon's model for H, CNO and AgBr are shown on Fig. 2 and 3. The distributions of the nucleon-nucleon collisions have pronounced maxima and can be approximated by Gaussian curves with an averaged dispersion $\sigma = 0.2$. The mean values of $\ln \gamma_c$ for these distributions are summarized in Table IV.

([24]) G. COCCONI: *Phys. Rev.*, **93**, 1107 (1954).
([25]) E. M. FRIEDLÄNDER: *Nuovo Cimento*, **14**, 976 (1959).

In the same table the expected γ_c's $(=\sqrt{(\gamma_0+1)/2})$ are compared with the corresponding mean values

TABLE IV. – *Comparison between expected and calculated* $\ln \gamma_c$ *as function of incident energy.*

Incident energy E_0	Expected $\ln \gamma_c$	The mean $\ln \gamma_c$ of the distribution	$C = \frac{\gamma_c \text{ calculated}}{\gamma_c \text{ expected}}$
25	1.32	1.46	1.16
50	1.65	1.74	1.09
100	1.99	2.09	1.08
200	2.34	2.40	1.07
400	2.68	2.72	1.04
800	3.03	3.05	1.02
1600	3.48	3.40	1.02

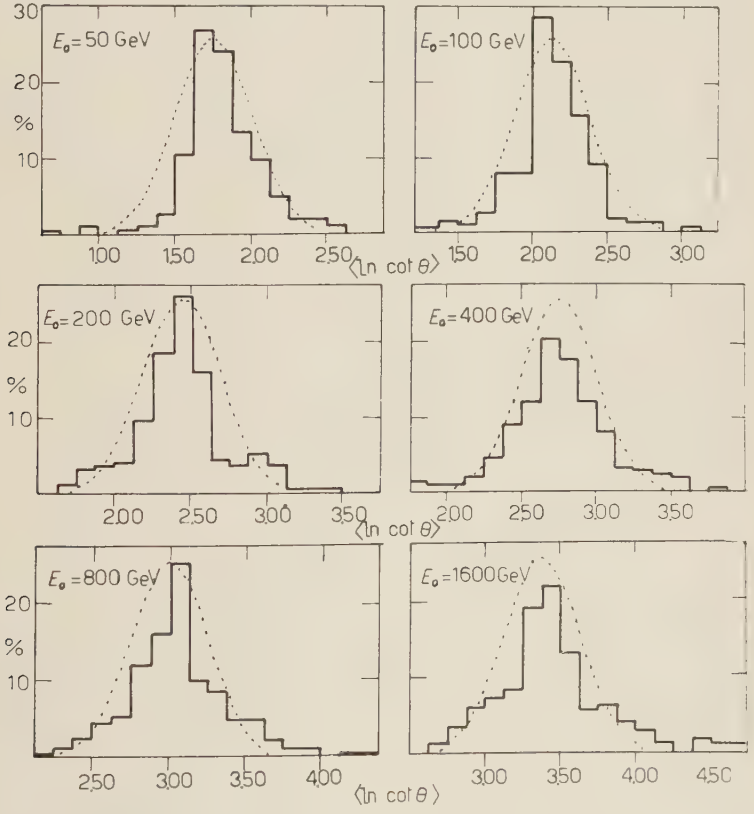

Fig. 2. – $\langle \ln \cot \theta \rangle$ in nucleon-nucleon collisions.

It appears that for the excited nucleon's model the relation $\ln(C\gamma_c) = \langle \ln \cot \theta \rangle$ holds, where C is a small correction factor that varies from 1.16

2265

to 1.02 between 25 and 1600 GeV. Thus the $\langle \ln \cot \theta \rangle$ parameter may be used to estimate the incident energy in nucleon-nucleon collisions.

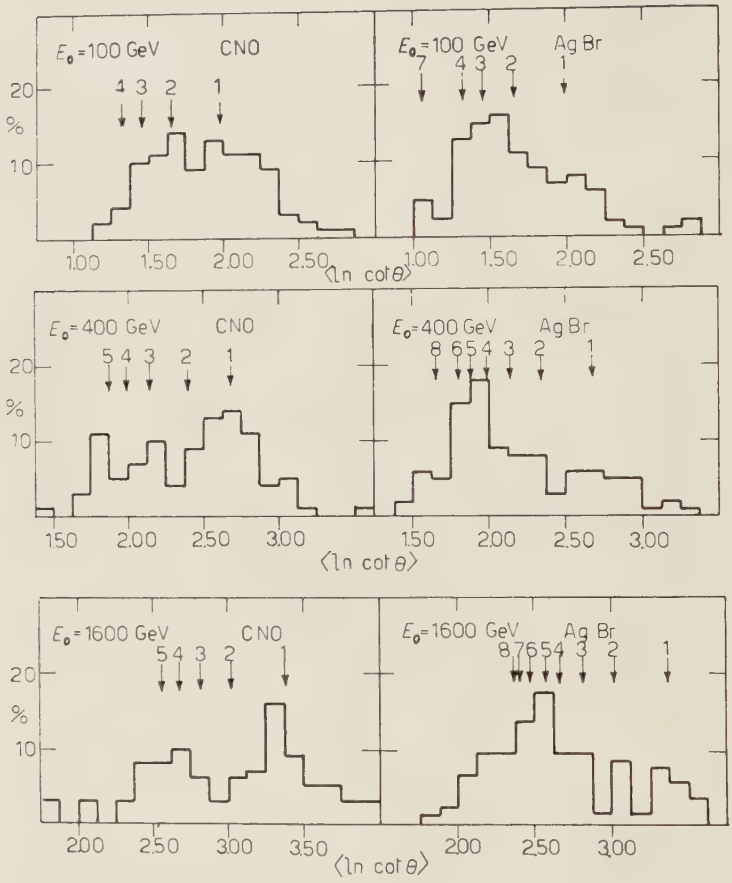

Fig. 3. – $\langle \ln \cot \theta \rangle$ in nucleon-CNO and nucleon-AgBr collisions.

The $\ln \cot \theta$ distributions of nucleon-nucleus collisions are more complicated. Each distribution is a superposition of several distributions of collisions with one, two or N struck nucleons. The arrows above each distribution show the expected $\ln \gamma_c$ for different numbers, N, of struck nucleons as calculated by the relation: $\gamma_c = (\gamma_0 + N)(1 + 2\gamma_0 N + N^2)^{-\frac{1}{2}}$. The corresponding maxima suggest that with good statistics the $\ln \cot \theta$ distribution can be used to estimate both the number of struck nucleons and the incident energy in nucleon-nucleus collisions (compare FRIEDLANDER [25]).

The average values of $\ln \cot \theta$ for cascades with the same number of struck nucleons N are plotted on Fig. 4. On the same figure the expected

2266

$\ln \gamma_c$ according to relation $\gamma_c = (\gamma_0 + N)(1 + 2\gamma_0 N + N^2)^{-\frac{1}{2}}$ is shown by full line. The good agreement demonstrated by Fig. 4 verifies the relation $\ln \gamma_c = \langle \ln \cot \theta \rangle$ for nucleon-nucleus collisions as well. Finally in order to estimate the dispersion of $\langle \ln \cot \theta \rangle$ in nucleon-nucleus collisions, several $\langle \ln \cot \theta$ histograms are plotted on Fig. 5 for cascades of fixed N, at $E_0 = 400$ GeV.

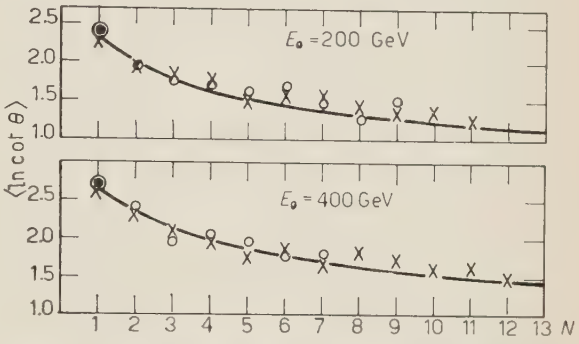

Fig. 4. – $\langle \ln \cot \theta \rangle$ as function of number of struck nucleons. Targets: • H, o CNO, x AgBr.

In spite of the small statistics the dispersion of the nucleon-N nucleons collisions is of the same order as that obtained for nucleon-nucleon collisions.

The results obtained with the help of the excited nucleons model for both nucleon-nucleon and nucleon-nucleus collisions show that the verification of the relation $\ln \gamma_c = \langle \ln \cot \theta \rangle$ does not prove meson emission from a single

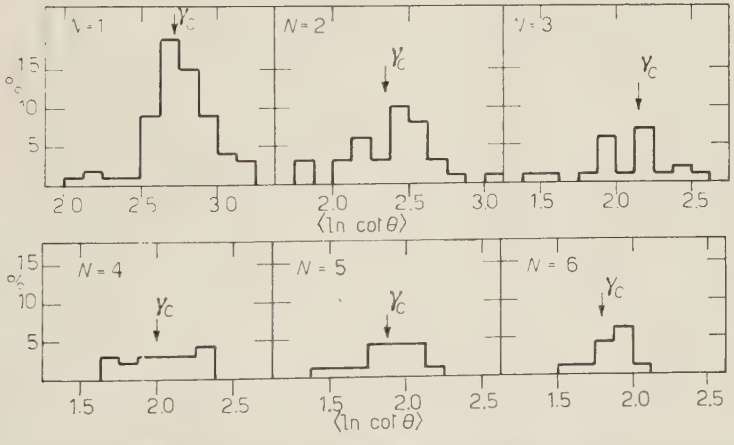

Fig. 5. – $\langle \ln \cot \theta \rangle$ distribution for cascades of different N in nucleon-CNO and nucleon-AgBr collisions at E_0=400 GeV.

center. On the other hand we believe that for a number of models similar to the excited nucleon's model this kinematical relation will hold. It expresses the fact that for these models, mesons are emitted from a number of centers fluctuating around a fictitious system moving with a Lorentz factor $\gamma_c = \exp \langle \ln \cot \theta \rangle$.

The above discussion shows that the Castagnoli parameter $\langle \ln \cot \theta \rangle$ can be used to estimate the incident energy in nucleon-nucleus collisions only when the number of struck nucleons N is known. According to the excited nucleon's model the number of struck nucleons in a nucleon-nucleus collision depends mainly on the nucleon-nucleon interaction cross-section and very little on the incident energy. The frequency of occurrence of struck nucleons in nucleon-CNO and nucleon-AgBr collisions, the transparencies of these nuclei, and their relative interaction cross-section in emulsion, are given in Table V.

TABLE V. – *Frequency of occurrence* (%) *of struck nucleons in nucleon*-CNO *and nucleon*-AgBr *collisions for* $\sigma_{NN} = 21$ mb.

	Relative occurrence (%) of N struck nucleons									Nuclear transparency (%)	Relative cross section in emulsion
	Target										
	1	2	3	4	5	6	7	8	9		
CNO	41	24	13	10	5	4	2	1	0	80	0.16
AgBr	22	14	12	12	11	9	7	5	8	46	0.80

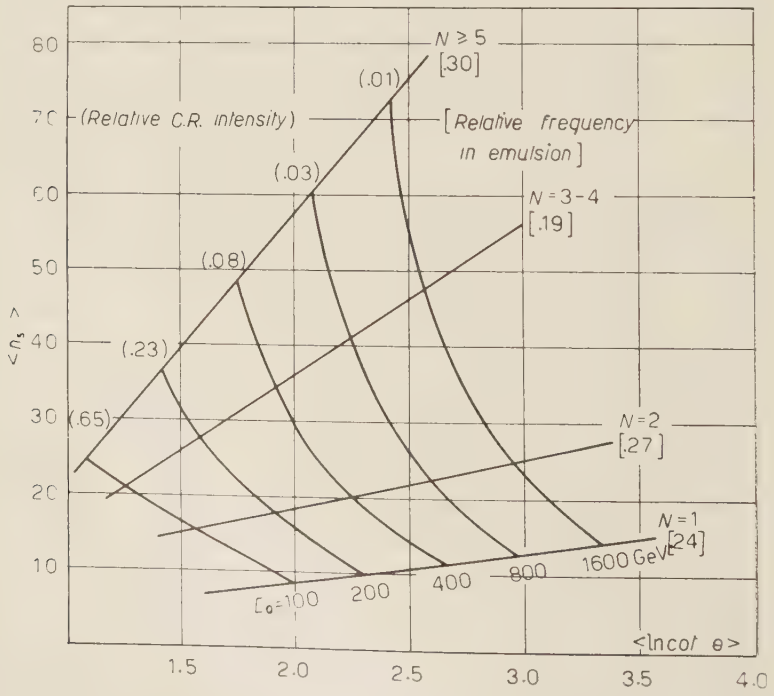

Fig. 6. – Average multiplicity $\langle n_s \rangle$ versus $\langle \ln \cot \theta \rangle$ for cascades of fixed N at different incident energies E_0.

Meson multiplicity in nucleon-nucleus collisions depends strongly on the number of nucleons, N, struck in each reaction. In order to study the correlation between shower multiplicity, n_s, and number of struck nucleons, N, we plot in Fig. 6 average n_s versus average $\langle \ln \cot \theta$ for cascades of the same incident energy E_0 and with the same number of struck nucleons N. Fig. 6 summarizes the average observable features of the excited nucleon's model. Each point on this plot represents a nuclear reaction given by its multiplicity n_s and its « effective logarithmic incident energy »: $\ln \gamma_0 = \langle \ln \cot \theta$. The vertical curves are lines of constant primary energy E_0, and the horizontal curves are lines of constant number of struck nucleons per collision, N. For the purpose of analysing nuclear events produced in photographic emulsions by cosmic radiation, the relative frequencies of collisions in photographic emulsions with N struck nucleons, and the relative primary cosmic ray intensities are also given in brackets. If the fluctuations around their means of both n_s and $\langle \ln \cot \theta \rangle$ were small, we could use Fig. 6 to find the incident energy (E_0) and the size of the nuclear cascade (N) of individual nuclear events in photographic emulsion. In reality the fluctuations of n_s and $\langle \ln \cot \theta$ are not small and do mix high energy large size cascades with low energy small size cascades, and thus only the average features of cosmic ray events can be analysed.

8. – Comparison with cosmic ray events in photographic emulsion.

Several authors observed high energy cosmic ray events in photographic emulsion. Each event was analyzed in terms of: 1) its charged multiplicity n_s, 2) the Lorentz factor of the emission center γ_c evaluated by the median angle or the Castagnoli *et al.* method, and 3) its star size N_h. The first two observables can be compared directly with the similar parameters of the excited nucleon's model. The relation between the star size N_h and the number of struck nucleons N is more complicated. Nuclear events observed in photographic emulsion are divided into three groups according to their star size N_h: 1) nucleon-nucleon collisions including $N = 1$ reactions in CNO and AgBr stars with $N_h \leqslant 2$; 2) nucleon-CNO collisions with probably some low excitation nucleon-AgBr collisions excluding nucleon-nucleon collisions in CNO and AgBr; —stars with $2 < N_h \leqslant 7$, and 3) all other nucleon-AgBr collisions—stars with $N_h > 7$.

For comparison with the excited nucleon's model, the $N_h < 2$ group is equivalent to cascades with $N = 1$ *i.e.* nucleon-nucleon collisions. All nucleon-CNO reactions with $N > 1$ are included in the second group of stars with $2 < N_h \leqslant 7$. Most of the nucleon-AgBr reaction with $N > 1$ belong to the third group. As we do not know how to distinguish a nucleon-AgBr col-

lision among events with $2 < N_h \leqslant 7$, we shall tentatively include all nucleon-AgBr reactions with $N > 1$ in the group of stars with $N_h > 7$.

On Fig. 7 the observed cosmic ray events are plotted according to their multiplicity n_s, $\langle \ln \cot \theta \rangle$ and star size N_h. The three curves on the same

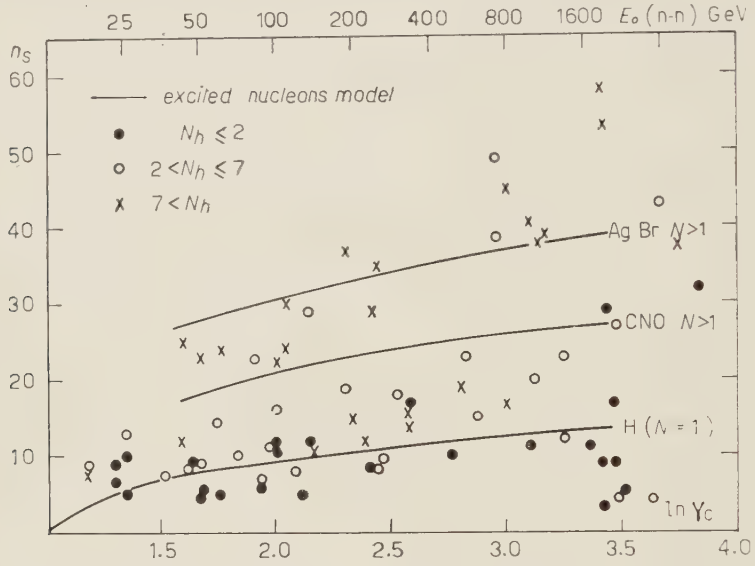

Fig. 7. – n_s as function of $\ln \gamma_c$ in photographic emulsion.

figure represent the expected $\langle n_s \rangle$ as function of $\langle \ln \cot \theta \rangle$ for three types of reactions as calculated by the excited nucleon's model. The curves correspond to nucleon-nucleon collisions *i.e.* $N = 1$, nucleon-CNO reactions with $N > 1$ and nucleon-AgBr reactions with $N > 1$ respectively. In evaluating these curves the incident energies E_0's weighed according to the primary cosmic ray spectrum $C \cdot E^{-2.5}$ ([26]), and a $\sigma_{N,N} = 21$ mb is used for the nucleon-nucleon interaction cross-section. The contributions of large size cascades are mainly at low γ_c's, thus when the incident energy is cut off at $E_0 = 1\,600$ GeV the averages $\bar{n}_s$ of the AgBr group is underestimated above $\ln \gamma_c = 2.5$. To overcome this difficulty, the incident energies are extended up to 3200 GeV. Together with $\ln \gamma_c$ the effective nucleon-nucleon incident energy $E_0(n-n) = m_p(2\gamma_c^2 - 1)$ is given also in GeV.

The individual events of the three groups observed in photographic emulsion are plotted on Fig. 7, and are seen to fall around their respective averaged curves as calculated by the excited nucleon's model. The average values of

([26]) V. L. GINZBURG: *Progress in Elementary Particles and Cosmic Ray Physics*, vol. **4** (1958), p. 343.

the observed multiplicities of stars with $N_h \leqslant 2$; $2 < N_h \leqslant 7$; $7 < N_h$ and all events are compared in Tables II and VI with the predictions of the excited nucleon's model.

TABLE VI. – *Comparison between n_s observed in nuclear emulsion and the results of the Monte-Carlo calculations* (M.C.).

Observed; $2 < N_h \leqslant 7$			M.C. CNO $N > 1$	Observed; $7 < N_h$			M.C. AgBr $N > 1$	Observed; all events			M.C. average collision
$\ln \gamma_c$	n_s	n	n_s	$\ln \gamma_c$	n_s	n	n_s	$\ln \gamma_c$	n_s	n	n_s
1.94	13.8	8	20.0	1.90	21.5	8	28.2	1.94	17	15	23.1
2.40	11.6	3	-23.5	2.38	29.2	5	33.0	2.4	20.8	10	25.6
				2.69	15.6	3	34.5				
2.80	28.4	5	25.2					2.90	26.2	16	28.2
3.45	27.0	1	27.5	3.18	38.7	4	38.0	3.48	10.3 (*)	13 (*)	31.4

(*) The n_s at this energy is underestimated, because 11 of the events are with $N_h \leqslant 2$.

It appears from these tables that the multiplicities predicted by the excited nucleon's model in general are in reasonable agreement with the observed values. The agreement between theory and experiment is fairly good at high and intermediate energies, but at lower energies the model predicts too high values. This defect can be corrected by using a smaller value of α in the excitation function of the excited nucleons. The effect of this change will be to reduce the inelasticity of the nuclear collisions. The same effect can be achieved by allowing semi-elastic collisions in which only one nucleon is excited.

The excited nucleon's model predicts a ratio of 1:10 of nucleons to mesons in an average collision in nuclear emulsion around 1 000 GeV. If we allow 10% (or 20%) K-particles among the produced mesons we shall find a value of $(1+1)/11 = 0.18$ (or $(1+2)/11 = 0.27$) for the fraction of non-pions among all produced particles, in good agreement with the value of 0.27 ± 0.8 observed by EDWARDS *et al.* [13].

9. – Transverse momentum distribution of mesons and nucleons.

The transverse momentum (P_T) distributions of mesons produced in nucleon-nucleon and nucleon-nucleus collisions were calculated by the excited nucleon's model. Few samples are shown in Fig. 8. All these distributions, for different types of nuclear collisions and over a wide range of incident ener-

gies are quite similar: most of the mesons have transverse momentum below 1 GeV/c with a peak around 0.350 GeV/c. However at higher incident energies, above 800 GeV, the P_T-distribution becomes flatter, with a lower peak and a

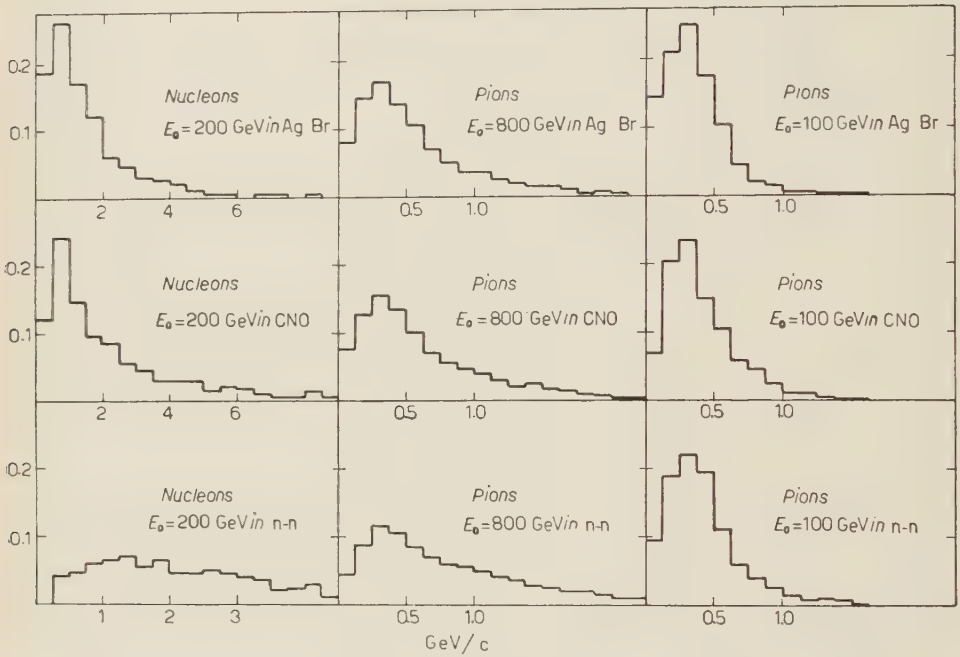

Fig. 8. – Transverse momentum distribution of nucleons and pions.

longer tail toward higher momenta. We believe that the P_T-distribution can be corrected by assuming that the excited nucleons are produced with an angular distribution collimated along the primary direction instead of the isotropic distribution used so far.

The experimental observations by EDWARDS *et al.* [13] and others [11-14] on the P_T distribution of mesons produced in nuclear interaction, agree well with the results of the Monte-Carlo calculations. A comparison between experimental and theoretical results is given in Table VI.

A few samples of the P_T distributions of nucleons in nucleon-nucleon and nucleon-nucleus collisions are shown in Fig. 8. It appears that while the nucleons produced in nucleon-nucleus collisions have a peak in their P_T-distributions, the P_T-distributions in nucleon-nucleon collisions are flat. However in all these cases most of the nucleons have transverse momentum between 1 and 2 GeV/c (compare Fig. 8) in good agreement with the experimental observations of EDWARDS *et al.*[13].

2272

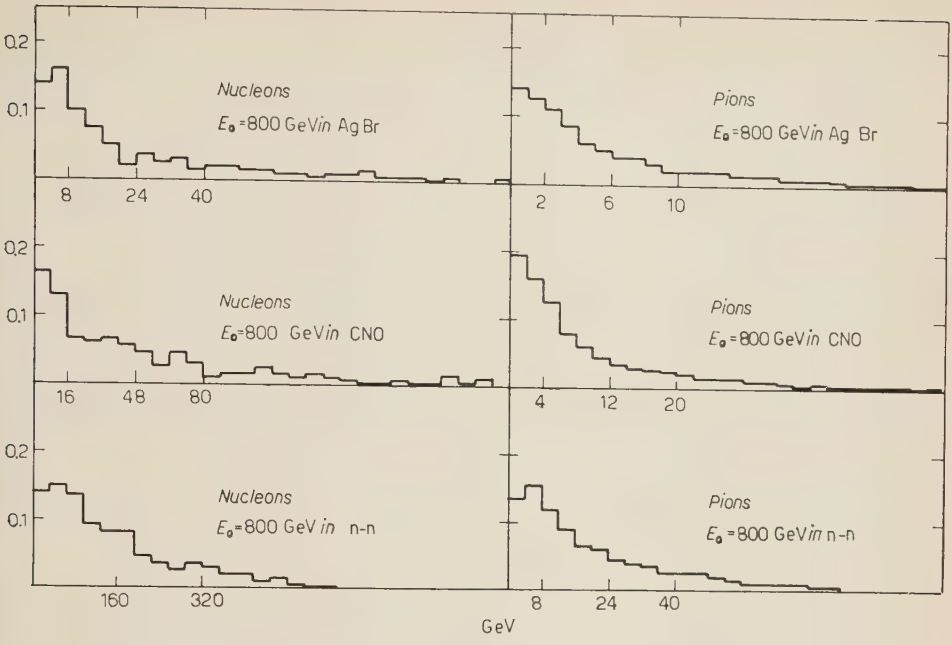

Fig. 9. – Energy spectrum of secondary nucleons and pions.

10. – Energy spectra of secondary mesons and nucleons.

Some examples of energy spectra of nucleons and mesons produced in nucleon-nucleon and nucleon-nucleus collisions are shown in Fig. 9. Of particular importance for the study of the attenuation of the hard component of the cosmic radiation in the atmosphere, are the energy

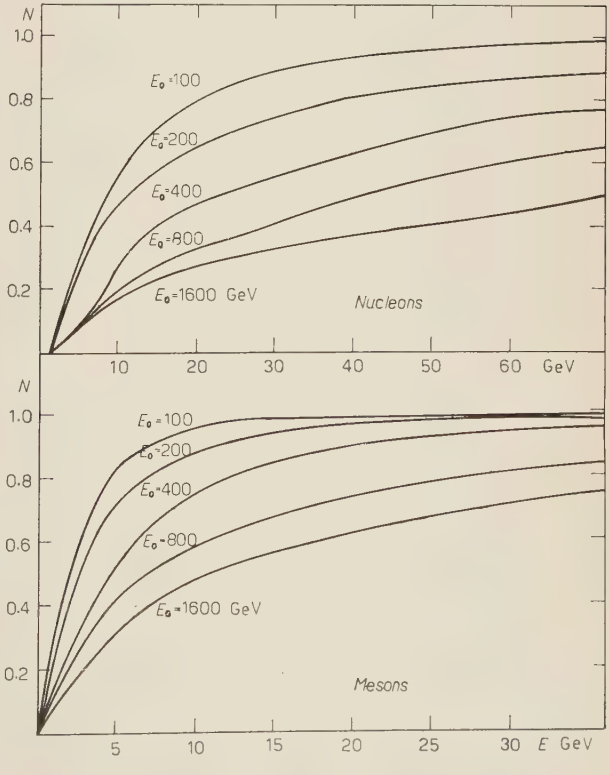

Fig. 10. – Integral energy spectra of secondary particles in CNO.

spectra obtained for the CNO target. The integral energy spectra of nucleons and pions produced in $\mathcal{N}$-CNO collisions are given in Fig. 10.

11. – Conclusions.

The excited nucleon's model offers a consistent theory for meson production in nucleon-nucleon and nucleon-nucleus collisions between 100 and 1600 GeV. It predicts with reasonable agreement the charge multiplicity and P_T distribution of secondaries in nuclear events induced by cosmic ray particles. Comparison between theory and experiment shows that the excited nucleon's model can be improved in the following ways: 1) Meson production, in nucleon-nucleus collisions mainly at low energies, could be reduced. This can be achieved either by using a lower value for α in the excitation function or, by allowing collisions in which only one excited nucleon is formed. 2) The P_T distribution of mesons above 800 GeV has to be more concentrated around its peak. This can be obtained by assuming that the excited nucleons in the C.M.S. of production, are emitted anisotropically, and with a strong collimation along the primary direction.

TABLE VII. – *Characteristic of P_T distribution of mesons.*

Incident energies (GeV)	Peak momentum (GeV/c)	Observed or calculated by
100 ÷ 500	0.300 ÷ 0.400	EDWARDS *et al.* [13]
500 ÷ 1000	0.300 ÷ 0.400	EDWARDS *et al.* [13]
30 000	0.500	EDWARDS *et al.* [13]
38 000	0.365 ± 0.030	MINAKAWA *et al.* [12]
84 000	0.407 ± 0.032	MINAKAWA *et al.* [12]
100	0.320	This model with $E_\pi = 400$ MeV

The study of the excited nucleon's model yields some results applicable to other models as well. The Castagnoli relation $\ln \gamma_c = \langle \ln \cot \theta \rangle$ will be valid for all models of meson production in which particles are emitted from one or more centers fluctuating around a system moving with a Lorentz factor γ_c. Therefore the experimental verification of the Castagnoli relation does not necessarily prove the emission of mesons from a single center. In a similar way the P_T distribution of mesons and nucleons at this range of energy seems to be rather a kinematical property, connected with the production of low energy mesons from fast moving centers. On the other hand, it appears that the real test for the validity of a theory of meson production is the

2274

experimental verification of its dynamical properties such as: 1) meson multiplicity as function of energy in nucleon-nucleon and nucleon-nucleus collisions; and 2) energy spectra of mesons and nucleons in nuclear reactions.

* * *

We would like to thank Prof. C. L. PEKERIS for making the WEIZAC electronic computer available for this work; the crew of the computer for their kind collaboration; and to Mr. R. YA'ARI who participated in the early stages of this work.

RIASSUNTO (*)

Si descrive un modello di produzione di mesoni da nucleoni eccitati per collisioni nucleone-nucleone e nucleone-nucleo prodotte da particelle di raggi cosmici. I risultati vengono confrontati con le osservazioni nelle emulsioni fotografiche, e si trova un accordo ragionevole.

(*) *Traduzione a cura della Redazione.*

Theory of Low Energy Nucleon-Nucleon Scattering - I.

D. Amati, E. Leader (*) and B. Vitale (**)

CERN - Geneva

(ricevuto il 21 Marzo 1960)

Summary. — The nucleon-nucleon interaction at energies below the threshold for inelastic processes, is studied using a method based on the Cini-Fubini approach to the Double Integral Representation technique. The essential idea is to treat all the singularities of the amplitudes, for values of the variables lying near their physical region, taking full advantage of the symmetry of the Mandelstam representation. The spectral functions are calculated using unitarity, both in the nucleon-nucleon and in the nucleon-antinucleon channels. In the latter the two pion contribution is calculated in terms of pion-nucleon scattering and contains amplitudes characterising the low waves of the $\mathcal{N}\overline{\mathcal{N}} \to 2\pi$ process. The construction of integral equations for the partial wave amplitudes is discussed. The nucleon-nucleon amplitude is developed in terms of linear combinations of the Fermi operators chosen to have simple properties under crossing, and whose invariant coefficients are shown to satisfy a Mandelstam representation in 4th order perturbation theory.

1. – Introduction.

We shall develop in this paper a theoretical study of the nucleon-nucleon interaction at low energies; *i.e.* valid for energies below the threshold of pion production, and perhaps for energies at which the inelastic scattering is still negligible.

The method we shall use is based on the two dimensional spectral representation proposed by Mandelstam [1] and follows a more simplified approach

(*) Elsie Ballot Fellow on leave of absence from St. John's College, Cambridge.
(**) On leave of absence from Istituto di Fisica Teorica, Università di Napoli.
[1] S. Mandelstam: *Phys. Rev.*, **112**, 1344 (1958).

introduced recently by CINI and FUBINI [2]. This approach consists mainly in taking correctly into account only the contributions to the causal amplitudes due to singularities near the physical region of the variables; the contribution of higher singularities being expressed by some free parameters in the final results. In the Cini-Fubini paper the case of the scattering of scalar neutral nucleons is discussed; the physical case of interaction of two fermions through a charged pseudoscalar meson field is dealt with in the present paper by a suitable extension of the Cini-Fubini method.

Application of dispersion relation techniques to $\mathcal{N}$-$\mathcal{N}$ scattering was first developed by GOLDBERGER, NAMBU and OEHME [3]. They made use of dispersion relations, for the coefficients of a particular set of invariant operators at fixed momentum transfer. The two pion contribution to such dispersion relations was recently worked out by GOLDBERGER and OEHME [4] in a way such that the dependence on one of the momentum transfer variables has been explicitly exhibited. However, because their starting point is a one dimensional dispersion relation, the dependence on the other momentum transfer variable (which dependence contributes to the angular variation of the scattering amplitude) is hidden in an arbitrary unknown function. Alternatively such a method only exhibits the properties of exchange forces (in lowest order due to the exchange of a charged pion between neutron and proton) and not the properties of the direct ones (neutral pion exchange in lowest order). We shall discuss more extensively the differences between our approach and that of GOLDBERGER, OEHEME and NAMBU at the end of this paper.

The two dimensional dispersion relation approach to nucleon-nucleon scattering has been applied by CHEW [5] to the determination of the pion-nucleon coupling constant g from the angular distribution in $\mathcal{N}$-$\mathcal{N}$ scattering; by CINI, FUBINI and STANGHELLINI [6] in order to obtain fixed angle dispersion relations, which are used both for the determination of g and for an analysis of the low energy deviation from the shape independent approximation in proton-proton scattering; the latter problem has also been treated by NOYES and WONG [7]

We shall proceed as follows: in Section 2 we shall define the kinematics and separate the causal amplitude into a suitable set of invariant operators

---

[2] M. CINI and S. FUBINI: *Theory of Low Energy Scattering in Field Theory*, in *Ann. Phys.* (to be published).

[3] M. L. GOLDBERGER, Y. NAMBU and R. OEHME: *Ann. Phys.*, **2**, 226 (1957), henceforth referred to as G.N.O.

[4] M. L. GOLDBERGER and R. OEHME: *Application of Dispersion Relations to Nucleon-Nucleon Scattering: the Two Pion Contribution*, EFINS 59-64 (to be published), henceforth referred to as G.O.

[5] G. F. CHEW: *Phys. Rev.*, **112**, 1380 (1958).

[6] M. CINI, S. FUBINI and A. STANGHELLINI: *Phys. Rev.*, **114**, 1633 (1959).

[7] H. P. NOYES and D. Y. WONG: *Phys. Rev. Lett.*, **3**, 191 (1959).

2977

(which we shall choose as linear combination of Fermi invariants, symmetric or antisymmetric under crossing). In Section 3 we shall write down the two dimensional representation for the scalar functions which multiply those invariant operators, and express them later on by means of dispersion relations at fixed energy. This will allow us to use unitarity in the nucleon-antinucleon channel and determine the corresponding two pion contributions. The way of dealing phenomenologically with the intermediate states with energy higher than two pion masses is then analysed. In Section 4 the way leading to integral equations for the individual angular momentum amplitudes is discussed, and the results obtained are briefly summarized and discussed. Appendix I contains a general analysis of the problem of the choice of a set of invariant operators and Appendix II contains some technical details on the separation of the s- and p-wave two pion intermediate states from the states with higher angular momentum.

2. – The scattering matrix.

2·1. *Kinematics.* – We wish to discuss the elastic scattering of two nucleons, with initial and final 4-momenta n_1, p_1 and n_2, p_2 respectively (see Fig. 1).

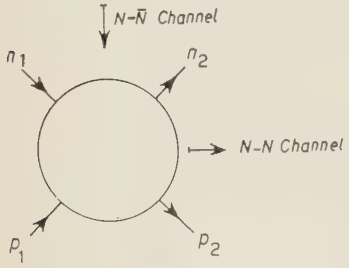

Fig. 1.

Our process will be characterized by three independent 4-vectors (because energy-momentum conservation gives: $n_1+p_1=n_2+p_2$), which we shall choose as:

$$(2.1)\qquad \begin{cases} N=\tfrac{1}{2}(n_1+n_2)\ ; \\ P=\tfrac{1}{2}(p_1+p_2)\ ; \\ \Delta=(n_1-n_2)=(p_2-p_1) \end{cases}$$

with $N\cdot\Delta=P\cdot\Delta=0$.

As the initial and final particles are on the mass shell, only two independent scalars can be constructed from these three vectors; we shall define the three scalars:

$$(2.2)\qquad \begin{cases} w=-(p_1+n_1)^2 \\ t\ =-(n_1-n_2)^2 \\ \bar{t}\ =-(p_1-n_2)^2, \end{cases}$$

where *e.g.* $p_1^2=\boldsymbol{p}^2-p_0^2=-m^2$, where m is the nucleon mass.

These are connected through the relation:

$$(2.3)\qquad w+t+\bar{t}=4m^2\,.$$

We shall also need in the following a set of four orthogonal 4-vectors, which we shall choose as:

$$M = N + P\,; \quad K = N - P\,; \quad \Delta\,; \quad L_\lambda = \varepsilon_{\lambda\mu\nu\varrho} M_\mu K_\nu \Delta_\varrho\,. \tag{2.4}$$

Definitions (2.1), (2.2), (2.4) give:

$$N^2 = P^2 = -\tfrac{1}{4}(w + \bar{t}); \quad \Delta^2 = -t; \quad M^2 = -w; \quad K^2 = -\bar{t}; \quad L^2 = -wt\bar{t}\,. \tag{2.5}$$

In the C.M. system of the two nucleons (2.2) reduces to:

$$\begin{cases} w = \quad 4(k^2 + m^2) = 4E_k^2 \\ t = -2k^2(1 - \cos\theta) \\ \bar{t} = -2k^2(1 + \cos\theta)\,, \end{cases} \tag{2.6}$$

where k, E_k and θ are, respectively, the momentum and the energy of each nucleon and the angle of scattering in the C.M. system.

The same 4-vectors n_1, n_2, p_1 and p_2 will describe also the process of elastic nucleon-antinucleon scattering; for instance, that process in which n_1, p_2 and $-n_2$, $-p_1$ are the initial and final momenta of the nucleon and antinucleon respectively. In the nucleon-antinucleon C.M. system (2.2) now gives:

$$\begin{cases} w = -2p^2(1 + \cos\psi) \\ t = \quad 4(p^2 + m^2) = 4E_p^2 \\ \bar{t} = -2p^2(1 - \cos\psi)\,, \end{cases} \tag{2.7}$$

where p, E_p and ψ are, respectively, the momentum and the energy of each nucleon or antinucleon and the angle of scattering between the two nucleons in the C.M. system.

2·2. *Scattering and causal matrices.* – We define a *transition amplitude* D through its connection with the S-matrix:

$$S_{\beta\alpha} = \delta_{\beta\alpha} + i\,\delta^4(p_\beta - p_\alpha)\,D_{\beta\alpha}\,. \tag{2.8}$$

In the case of elastic nucleon-nucleon and nucleon-antinucleon scattering the transition amplitude is connected with the differential cross-section in the C.M. system by the relation:

$$\sigma_{\beta\alpha}(\theta, \varphi) = \pi^2 E^2 |D_{\beta\alpha}|^2\,, \tag{2.9}$$

where E is the C.M. energy of each particle.

2279

The *scattering amplitude* T is such that

$$\sigma_{\beta\alpha}(\theta, \varphi) = |T_{\beta\alpha}|^2 \tag{2.10}$$

so that

$$D_{\beta\alpha} = (1/\pi E)\, T_{\beta\alpha}\,. \tag{2.11}$$

The *covariant Feynman amplitude* F is given by

$$F_{\beta\alpha} = 4\pi(E/m^2) T_{\beta\alpha}\,. \tag{2.12}$$

The *causal amplitude* M, with which the rest of this paper is concerned, can be defined as in G.N.O. (form. (2.14)) and coincides with the Feynman amplitude for physical scattering processes.

We shall deal in the following also with the nucleon-antinucleon absorption into two pions ($\mathcal{N}\bar{\mathcal{N}} \to \pi\pi$); for this process it will be convenient to introduce an *absorption amplitude* τ [8], which is connected with the scattering amplitude by:

$$T_{\beta\alpha}(\mathcal{N}\bar{\mathcal{N}} \to \pi\pi) = -\frac{1}{8\pi}\frac{m}{E}\sqrt{\frac{q}{p}}\,\tau_{\beta\alpha}\,, \tag{2.13}$$

where p and q are the C.M. momentum of the nucleons and pions respectively. (We note here that the relation (2.10) still holds, when $\sigma(\theta, \varphi)$ describes the differential cross-section for the process $\mathcal{N}\bar{\mathcal{N}} \to \pi\pi$.) We have therefore, from (2.10), (2.13):

$$\sigma_{\beta\alpha}(\mathcal{N}\bar{\mathcal{N}} \to \pi\pi) = \frac{q}{p}\left|\frac{m}{2E}\frac{\tau_{\beta\alpha}}{4\pi}\right|^2. \tag{2.14}$$

The absorption amplitude is directly related to the Feynman amplitude for the process ($\mathcal{N}\bar{\mathcal{N}} \to \pi\pi$):

$$\tau_{\beta\alpha} = -2\mu\, F_{\beta\alpha}(\mathcal{N}\bar{\mathcal{N}} \to \pi\pi)\,, \tag{2.15}$$

where μ is the π-meson mass.

2·3. *Separation of the causal amplitude M into invariants.* – The causal amplitude M is a covariant matrix in the spin and isotopic spin space of the incoming and outgoing particles. When using matrix elements $M_{\beta\alpha}$ for the elastic nucleon-nucleon and nucleon-antinucleon scattering, we shall assume

(8) G. F. CHEW, M. L. GOLDBERGER, F. E. LOW and Y. NAMBU: *Phys. Rev.*, **106**, 1377 (1957).

2280

in the following that the spin and isotopic spin operators in M are saturated as follows:

$$(2.16)\qquad \begin{cases} M_{\beta\alpha}(\mathcal{N}\mathcal{N}\to\mathcal{N}\mathcal{N}) = \overline{u}_i(n_2)\,\overline{u}_k(p_2)\,M^{kl}_{ij}\,u_j(n_1)\,u_l(p_1)\,, \\ M_{\beta\alpha}(\mathcal{N}\overline{\mathcal{N}}\to\mathcal{N}\overline{\mathcal{N}}) = \overline{v}_i(-n_2)\,\overline{u}_k(p_2)\,M^{kl}_{ij}\,u_j(n_1)\,v_l(-p_1) = \\ \qquad\qquad = \overline{v}_i(n')\,\overline{u}_k(p_2)\,M^{kl}_{ij}\,u_j(n_1)\,v_l(p')\,, \end{cases}$$

where M^{kl}_{ij}, by the general substitution law [9], is the same function for both processes. Note that the spinor saturation of M is between n_1 and n_2 and between p_1 and p_2 independent of whether they are nucleons or antinucleons. Since the operator M will be written as a sum of products of spin operators, we shall simply indicate the saturation of these operators by an index (n) or (p). The quantities $u(q)$ and $v(q)$ are positive energy spinors satisfying respectively the equations:

$$(2.17)\qquad \begin{cases} (i\gamma\cdot q + m)\,u(q) = 0\,, \\ (i\gamma\cdot q - m)\,v(q) = 0\,, \end{cases}$$

where $q_0 = +(\boldsymbol{q}^2+m^2)^{\frac{1}{2}}$.

Besides the spin and isotopic spin operators, M, being a covariant matrix, will depend only on the scalars that can be formed by means of the three independent vectors (2.1); in particular, we shall take M as dependent on the scalars w, t and $\bar{t}$ defined in (2.2). Therefore M can in principle be written as a linear combination of a set of invariant operators, O_j, whose coefficients o_j will be scalar functions of w, t and $\bar{t}$:

$$(2.18)\qquad M_{\beta\alpha} = \sum_j o_j(w t \bar{t})\langle\beta\,|\,O_j\,|\,\alpha$$

(or course O_j will contain, in the general case, not only the spin and isotopic spin operators but also the dynamical variables, as, for instance, in G.N.O.).

There is a large freedom in the choice of the O_j; each problem requires a choice of invariant operators most suitable to it. We shall see that our calculations, where use of the two dimensional dispersion relations is made, will require in an essential way a choice of invariant operators such that their coefficients can be expressed by a Mandelstam representation. Further a simplification occurs if these scalar functions behave simply under crossing $(t\rightleftarrows\bar{t})$, which corresponds in the nucleon-nucleon channel to the interchange of the two initial (or final) particles.

[9] J. M. Jauch and F. Rohrlich: *The Theory of Photons and Electrons* (Cambridge, Mass. 1955), pp. 161, 258.

Perturbation calculations up to the 4-th order indicate, as will be shown later, that the most useful set of invariants is given by what we shall call in the following « perturbative invariants ».

This set of O_j is given by (we disregard here the isotopic spin part of O_j):

$$\left\{\begin{array}{l} P_1 = 1^n 1^p\ ; \qquad P_2 = (i\gamma^n\cdot p\, 1^p + 1^n\, i\,\gamma^p\cdot N)\ ; \\ P_3 = (i\gamma^n\cdot P)(i\gamma^p\cdot N)\ ; \qquad P_4 = \gamma^n\cdot\gamma^p\ ; \qquad P_5 = \gamma_5^n\gamma_5^p\,. \end{array}\right. \tag{2.19}$$

These invariants, however, present no simple behaviour under crossing (which is equivalent to a Fierz transformation on them); we have therefore to find a new set of invariants, linear combinations of the P defined by (2.19), with suitable coefficients that do not spoil the analytic behaviour of their corresponding scalar functions, and which transform in the simplest way under a Fierz transformation. This had led us to the use of linear combinations of Fermi invariants.

We can express the perturbative invariants P_j in terms of the Fermi invariants F_j defined as usual by:

$$\left\{\begin{array}{l} F_1 = S = 1^n 1^p; \qquad F_2 = V = \gamma^n\cdot\gamma^p; \\ F_3 = T = \sum\limits_{\mu<\nu} (i\gamma_\mu^n\gamma_\nu^n)(i\gamma_\mu^p\gamma_\nu^p); \qquad F_4 = A = (i\gamma_5^n\gamma_\mu^n)(i\gamma_5^p\gamma_\mu^p); \qquad F_5 = P = \gamma_5^n\gamma_5^p\,, \end{array}\right. \tag{2.20}$$

[see Appendix I] by the relations:

$$\left\{\begin{array}{l} P_1 = S\,, \\ P_2 = \dfrac{1}{m}\left[\dfrac{(\bar t - w)}{4}\, S - m^2 V + \dfrac{t}{4}\, T + \dfrac{(\bar t - w)}{4}\, P\right], \\ P_3 = \tfrac{1}{4}\left[-(\bar t - w)V - tA + 4m^2 P\right], \\ P_4 = V\,, \\ P_5 = P\,, \end{array}\right. \tag{2.21}$$

and we note that no additional singularities are introduced in going from the P_j to the F_j.

2·4. *Crossing symmetry.* – It is easy to see that five independent invariant operators which are symmetric or antisymmetric under crossing (*i.e.* under a Fierz transformation $P(2,4)$ which brings from $[\bar u(n_2)O^{(n)}u(n_1)]\,[\bar u(p_2)O^{(p)}u(p_1)]$ to $[u(n_2)O^{(n)}u(p_1)]\,[u(p_2)O^{(p)}u(n_1)]$ and therefore exchanges t into $\bar t$) can be constructed as linear combinations of the Fermi invariants, combinations which

we shall denote henceforth by C_j. The choice of C_j will eventually depend on arguments of simplicity.

Let us define the index j in such a way that:

$$\text{(2.22)} \quad \begin{cases} C_j \text{ is antisymmetric under } P(2,4) \text{ if } j \text{ is odd } (j=1,3,5) \\ C_j \text{ is symmetric under } P(2,4) \text{ if } j \text{ is even } (j=2,4) \end{cases}$$

so that:

$$\text{(2.23)} \quad C_j \xrightarrow[P(2,4)]{} (-1)^j C_j \, .$$

We shall now go back to (2.18) and separate the spin and isotopic spin parts in O_j. Let us introduce the two projection operators in the isotopic spin space, P_T ($T=0,1$ is the total isotopic spin of the NN system), such that:

$$\text{(2.24)} \quad P_{T'} |NN\rangle = |NN(T=T')\rangle$$

(in terms of the isotopic spin matrices $\boldsymbol{\tau}^n$ and $\boldsymbol{\tau}^p$, P_0 and P_1 are given by:

$$\text{(2.25)} \quad P_0 = \tfrac{1}{4}(1 - \boldsymbol{\tau}^n \cdot \boldsymbol{\tau}^p) \, ; \qquad P_1 = \tfrac{1}{4}(3 + \boldsymbol{\tau}^n \cdot \boldsymbol{\tau}^p) \, ,$$

where, as usual, τ^n is to be saturated between $\bar{u}(n_2)$ and $u(n_1)$ and τ^p between $\bar{u}(p_2)$ and $u(p_1)$).

We can therefore write (2.18) as:

$$\text{(2.26)} \quad M_{\beta\alpha} = \sum_{1}^{5}{}_j \sum_{0,1}{}_T c_j^T(wt\bar{t}) \langle \beta | P_T C_j | \alpha \rangle \, .$$

As a $P(2,4)$ Fierz transformation is equivalent to an exchange $n_1 \rightleftarrows p_1$, the Pauli principle applied to the initial NN state will give:

$$\text{(2.27)} \quad \langle n_2 p_2 | M | n_1 p_1 \rangle = - \langle n_2 p_2 | M | p_1 n_1 \rangle \, ,$$

where position, spin and isotopic spin of the two incoming particles are interchanged.

By using the crossing symmetry (2.23) and by noticing that:

$$\text{(2.28)} \quad \langle n_2 p_2 | P_T | n_1 p_1 \rangle = - (-1)^T \langle n_2 p_2 | P_T | p_1 n_1 \rangle \, ,$$

we obtain, from (2.23), (2.26), (2.27) and (2.28), the following crossing conditions on the c_j^T:

$$\text{(2.29)} \quad c_j^T(wt\bar{t}) = (-1)^{j+T} c_j^T(w\bar{t}t) = \varepsilon_{j1} c_j^T(w\bar{t}t) \, ,$$

3333

which defines the meaning of the symbol ε_{jT}, which will be used in the following to simplify our notations.

We shall now briefly discuss the choice of the set of C_j's which we shall use in what follows. As our method will eventually lead to integral equations for the transition amplitudes corresponding to definite initial and final spin states (helicity states or singlet and triplet states), a simplicity criterion can be provided by the relations between the coefficients of the C_j's, c_j, and the above-mentioned transition amplitudes. A set which turns out to be convenient from this point of view is given by:

$$\text{(2.30)} \qquad \begin{cases} C_1 = \ (S - V - T + A + P)/4 \\ C_2 = (2S + V + A - 2P)/2 \\ C_3 = (2S - V - A - 2P)/2 \\ C_4 = (3S + T + 3P)/2 \\ C_5 = \ (S + V - T - A + P)/4 \end{cases}$$

(we recall that the C_j's with odd index j are odd under a Fierz transformation $P(2, 4)$ and those with even j are even).

The usefulness of the set (2.30) can be easily seen by expressing the C_j as Fermi operators, defined by a saturation between spinors different from the standard saturation (2.16). We shall here merely sketch the argument which leads to the connection of the C_j's, as given by (2.30), with the transition amplitudes for definite helicity states. Let us symbolize for simplicity the standard saturation (2.16) of the Fermi invariants between spinors by the expression (1, 2; 3, 4). If now we define a new set of Fermi invariants, F_j, by sandwiching the Fermi operators between initial-initial (and final-final) particles, we shall get, for instance, an expression of the type: (2, 4; 3, 1). It is easy to see that this permutation of the spinors can be obtained by the consecutive operation of a $P(1, 2)$ and a $P(2, 4)$ (Fierz) transformation to the standard order (1, 2; 3, 4). $P(1, 2)$ is diagonal [see ref. ([14])] and gives plus sign for S, A and P and minus sign for V and T; if we now apply the product matrix $P(1, 2)$, $P(2, 4)$ to the Fermi invariants we get the linear combinations given by (2.30). It is therefore demonstrated that those combinations reduce each to a single Fermi invariant, saturated between the two initial and final particles. With the saturation (2, 4; 3, 1) one finds that:

$$\text{(2.31)} \qquad \overline{S} = C_1; \qquad \overline{V} = C_2; \qquad \overline{T} = C_4; \qquad \overline{A} = C_3; \qquad \overline{P} = C_5 .$$

To go now from the C_j's to the scattering amplitudes corresponding to definite spin states, we have to saturate the invariant operators with spinors with definite helicity or with combinations of them corresponding to singlet and triplet states. It is clear that this connection will be much simplified, in the nucleon-nucleon C.M. system, by our new saturation; our invariant operators will be represented by single Fermi invariants, even or odd under the exchange $t \rightleftarrows \bar{t}$, and the γ matrices contained in them will now connect the two incoming (outgoing) particles, which have opposite momenta in the C.M.

2284

As an example, we shall give here the connection between the singlet and triplet transition amplitudes T_{ij} (as defined, for instance, in G.N.O.) and the coefficients c_j of the invariant operators C_j:

$$
(2.32)\quad \begin{cases}
T_{11} = \dfrac{m}{4\pi\eta}\left[\eta[2\eta-(\eta-1)\sin^2\theta]c_2 - 2(\eta^2-1)\cos\theta c_3 + [2+(\eta-1)\sin^2\theta]c_4\right]; \\
T_{1-1} = \dfrac{m}{4\pi\eta}(\eta-1)\sin^2\theta[\eta c_2 - c_4]\,, \\
T_{01} = \dfrac{\sqrt{2}m}{4\pi\eta}(\eta-1)\sin\theta[\eta\cos\theta c_2 - (\eta+1)c_3 - \cos\theta c_4]\,, \\
T_{10} = \dfrac{\sqrt{2}m}{4\pi\eta}(\eta-1)\sin\theta[(\eta+1)c_1 + \cos\theta c_2 - \eta\cos\theta c_4]\,, \\
T_{00} = \dfrac{m}{2\pi\eta}\left[-(\eta^2-1)\cos\theta c_1 + [\eta-(\eta-1)\cos^2\theta]c_2 + \eta[1+(\eta-1)\cos^2\theta]c_4\right]; \\
T_{ss} = \dfrac{m}{2\pi\eta}[c_3 - (\eta^2-1)\cos\theta c_4 + \eta^2 c_5]\,,
\end{cases}
$$

where $\eta = \sqrt{w}/2m$ and the six T_{ij} are reduced to five independent amplitudes by the relation:

$$
(2.33)\qquad (T_{11} - T_{1-1} - T_{00}) = \sqrt{2}\,\mathrm{ctg}\,\theta(T_{10} + T_{01})\,,
$$

which follows from the time reversal invariance of the theory.

By using (2.21) and (2.30) it is easy to find out the relations between the invariants P_j and the C_j's:

$$
(2.34)\quad \begin{cases}
P_1 = \dfrac{1}{4}[C_1 + C_2 + C_3 + C_4 + C_5]\,, \\
P_2 = \dfrac{1}{4}\left[\dfrac{1}{m}(6m^2 - w - 2t)C_1 - 2mC_2 + 2mC_3 + \dfrac{1}{m}(2m^2 - w)C_4 + \right. \\
\qquad\qquad \left. + \dfrac{1}{m}(2m^2 + w + 2t)C_5\right]\,, \\
P_3 = \dfrac{1}{4}[(5m^2 - 2w - 2t)C_1 - (3m^2 - w)C_2 + (m^2 - w)C_3 + \\
\qquad\qquad + m^2 C_4 - (3m^2 - 2w - 2t)C_5]\,, \\
P_4 = \dfrac{1}{2}[-2C_1 + C_2 - C_3 + 2C_5]\,, \\
P_5 = \dfrac{1}{4}[C_1 - C_2 - C_3 + C_4 + C_5]\,.
\end{cases}
$$

2285

2·5. *Isotopic spin in the nucleon-antinucleon channel.* – We shall find useful in the following to label our matrix elements according to the total isotopic spin I in the $N\bar{N}$ channel, while our label T corresponds to the total isotopic spin in the NN channel. The connection between these two sets of T- and I-labelled amplitudes can be easily obtained in the following way.

Let us divide $M_{\alpha\beta}(\mathcal{N}\mathcal{N} \to \pi\pi)$, which is a matrix in the isotopic spin space, into two parts:

$$M_{\alpha\beta}(\mathcal{N}\mathcal{N} \to \pi\pi) = N_+ \delta_{\alpha\beta} + \tfrac{1}{2}[\tau^n_\alpha, \tau^p_\beta] N_- , \tag{2.35}$$

where N_+ and N_- are proportional to the transition amplitudes with definite total isotopic spin $I = 0, 1$:

$$N_+ = (1/\sqrt{6}) N^0 ; \qquad N_- = (\tfrac{1}{2}) N^1 . \tag{2.36}$$

From (2.35) and the orthogonality of N_+ and N_-, which follows from (2.36), we obtain:

$$M(\mathcal{N}\bar{\mathcal{N}} \to \mathcal{N}\bar{\mathcal{N}}) = 3 N_+^+ N_+ + 2 N_-^+ N_- \boldsymbol{\tau}^n \cdot \boldsymbol{\tau}^p = 3 M^+ + 2 M^- \boldsymbol{\tau}^n \cdot \boldsymbol{\tau}^p . \tag{2.37}$$

As $M = P_0 M^0 + P_1 M^1$ (where the label 0, 1 now refers to the total isotopic spin T in the NN channel), using (2.25) it is easy to obtain the desired relation:

$$\begin{cases} M^0 = 3 M^+ - 6 M^- , \\ M^1 = 3 M^+ + 2 M^- . \end{cases} \tag{2.38}$$

3. – Two dimensional dispersion relations.

3·1. – Let us consider the fourth order Feynman graphs of Fig. 2.

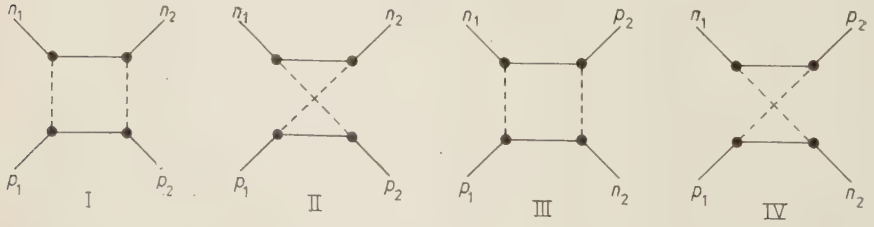

Fig. 2.

The actual computation of graph I (the results of the perturbative calculation will turn out to be a particular case of the results of this section) shows

2286

that the coefficients of its expansion in terms of the perturbative invariants (2.19) have the simple form

$$\int_{(2m)^2}^{\infty} \mathrm{d}x \int_{(2\mu)^2}^{\infty} \mathrm{d}y \, \frac{\sigma(xy)}{(x-w)(y-t)} \,. \tag{3.1}$$

The graph II gives just the same contribution to those coefficients (except for a plus-minus sign (*)) with w substituted by $\bar{t}$. This means, as we have discussed before, that the contributions of graphs I and II to the coefficients of the invariants C_j of (2.30) have the necessary analytic properties in order to satisfy a Mandelstam representation (except for one more subtraction due to the pole at infinity introduced by the transformation (2.34)).

Graph III can be obtained from graph I by exchanging n_2 into p_2 and viceversa. This means that the coefficients of the « perturbative » invariants with the γ matrices saturated between n_1 and p_2, and p_1 and n_2 (crossed perturbative invariants) will have the simple form:

$$\int_{(2m)^2}^{\infty} \mathrm{d}x \int_{(2\mu)^2}^{\infty} \mathrm{d}y \, \frac{\sigma(xy)}{(x-w)(y-\bar{t})} \,. \tag{3.2}$$

For graph IV the coefficients of the same invariants will have the form

$$\int_{(2m)^2}^{\infty} \mathrm{d}x \int_{(2\mu)^2}^{\infty} \mathrm{d}y \, \frac{\sigma(xy)}{(x-t)(y-\bar{t})} \,. \tag{3.3}$$

Now, what can be said about these crossed perturbative invariants? They will be related to the perturbative ones of (2.19) in a very complicated way in which extra singularities will appear. So we shall not be able to assert that the four graphs of Fig. 2 give coefficients of perturbative invariants satisfying a Mandelstam representation. However, the crossed perturbative invariants will be related to the crossed C_j invariants just in the same way as the perturbative ones where to the C_j. But the crossed C_j are just the C_j except for a $\pm$ sign: this means that the contributions of graphs III and IV to

(*) This symmetry can be understood easily from (2.21). In fact, the amplitude for graph II can be obtained from that of I by the substitution $n_1 \leftrightarrow -n_2$. This substitution makes $w \leftrightarrow \bar{t}$, changes the sign of S, A and P of (2.20), and leaves V and T unchanged. From (2.21) one sees that P_1, P_3 and P_j are antisymmetric for this exchange while P_2 and P_4 are symmetric. Besides, the isotopic state $(+)$ introduced in the last section is antisymmetric for that exchange while the $(\ )$ state is symmetric.

the coefficients of the C_j have again the correct singularities so to satisfy a Mandelstam representation.

So generalizing the results of the fourth order perturbative calculation we shall suppose the validity of the Mandelstam representation for the functions $c_j^T(wt\bar{t})$ of (2.26). We note that up to now there is no more indication for the validity of Mandelstam representation, even for the case of scalar particles, than that given by perturbative arguments.

Instead of writing the representation in the usual way, we shall put in evidence the kinematical coefficients coming from (2.34) by writing:

$$
\left\{
\begin{aligned}
c_1^T(w\,\bar{t}) &= \left\{\frac{1}{4}\left[p_1^T(wt\bar{t}) + \frac{6m^2 - w - 2t}{m}\,p_2^T(wt\bar{t}) + (5m^2 - 2w - 2t)\cdot\right.\right. \\
&\qquad \left.\left.\cdot\, p_3^T(wt\bar{t}) - 4p_4^T(wt\bar{t}) + p_5^T(wt\bar{t})\right]\right\} - (-1)^T\{t \leftrightarrow \bar{t}\} + \frac{D_1^T(t-\bar{t})}{w_D - w}\,, \\
c_2^T(wt\bar{t}) &= \left\{\frac{1}{4}\left[p_1^T - 2mp_2^T - (3m^2 - w)\,p_3^T + 2p_4^T - p_5^T\right]\right\} + \\
&\qquad + (-1)^T\{t \leftrightarrow \bar{t}\} + \frac{D_2^T(t-\bar{t})}{w_D - w}\,, \\
c_3^T(w\bar{t}) &= \left\{\frac{1}{4}\left[p_1^T + 2mp_2^T + (m^2 - w)\,p_3^T - 2p_4^T - p_5^T\right]\right\} - \\
&\qquad - (-1)^T\{t \leftrightarrow \bar{t}\} + \frac{D_3^T(t-\bar{t})}{w_D - w}\,, \\
c_4^T(wt\bar{t}) &= \left\{\frac{1}{4}\left[p_1^T + \frac{(2m^2 - w)}{m}\,p_2^T + m^2 p_3^T + p_5^T\right]\right\} + \\
&\qquad + (-1)^T\{t \leftrightarrow \bar{t}\} + \frac{D_4^T(t-\bar{t})}{w_D - w}\,, \\
c_5^T(wt\bar{t}) &= \left\{\frac{1}{4}\left[p_1^T + \frac{2m^2 + w + 2t}{m}\,p_2^T - (3m^2 - 2w - 2t)\,p_3^T + 4p_4^T + p_5^T\right]\right\} - \\
&\qquad - (-1)^T\{t \leftrightarrow \bar{t}\} + \frac{D_5^T(t-\bar{t})}{w_D - w}\,,
\end{aligned}
\right. \tag{3.4}
$$

where

$$
\left\{
\begin{aligned}
p^1 &= 3\,p^+ + 2\,p^-\,, \\
p^0 &= 3\,p^+ - 6\,p^-\,,
\end{aligned}
\right. \tag{3.5}
$$

with

$$
p_j^{\pm}(w\,\bar{t}) = \begin{pmatrix} 0 \\ -\frac{1}{2}(g^2\delta_{j5}/(\mu^2 - t)) \end{pmatrix} + \left[\int_{4\mu^2} \mathrm{d}t' \int_{4m^2} \mathrm{d}x\, \frac{\varkappa_j^{\pm}(t'x)}{(t'-t)(x-w)}\right] \mp (-1)^j[w \to \bar{t}], \tag{3.6}
$$

2288

$D_j(t-\bar{t})$ is the residue at the deuteron pole at $w_D=(2m-B)^2$, B being the magnitude of the deuteron binding energy. D_j is given in terms of B and the asymptotic ratio of S and D waves in the deuteron wave function: explicit expression for such residues, as coefficients of two dimensional invariants, are given in formula (4.43) of GNO. g is the usual renormalized rationalized pion nucleon coupling constant, *i.e.* $g^2/4\pi\sim 14.4$.

Clearly (3.4) to (3.6) are absolutely analogous to a subtracted Mandelstam representation for the $c_j(wt\bar{t})$ written in the usual form ([12]). The cut in w begins at $(2m)^2$ while that of t or $\bar{t}$ starts at $(2\mu)^2$ which corresponds to the lowest energy of the process $\mathcal{N}\overline{\mathcal{N}}\to 2\pi$. Of course the range from $(2\mu)^2$ to $(2m)^2$ corresponds to an unphysical region of energy for the $\mathcal{N}\overline{\mathcal{N}}$ system. Another feature is automatically taken into account in (3.4)-(3.6); this is the fact, true at all orders in perturbation theory, that t and $\bar{t}$ cannot both be in the region $(2\mu)^2$ to $(2m)^2$. By simple inspection of a general Feynman diagram one immediately realizes that if looking in one of the $\mathcal{N}\overline{\mathcal{N}}$ channels it does not have any baryonic line in an intermediate state, it presents at least two baryonic lines in the intermediate states of the other $\mathcal{N}\overline{\mathcal{N}}$ channel.

The lowest cut in t in (3.6), *i.e.* that going from $4\mu^2$ to $9\mu^2$, is due to the intermediate two pion contribution; let us single out this contribution by writing (3.6) in the form:

$$\rho_j^{\pm}(wt\bar{t})=\begin{pmatrix}0\\ -\frac{1}{2}\,(g^2\delta_{j5}/(\mu^2-t))\end{pmatrix}\dot{+}\left[\frac{1}{\pi}\int_{4\mu^2}\frac{\varrho_j^{\pm}(wt')}{t'-t}\,\mathrm{d}t'+\frac{1}{\pi}\int_{4m^2}\frac{\chi_j^{\pm}(xt)}{x-w}\,\mathrm{d}x\right]\pm(-1)^j\,[w\to\bar{t}]\,, \tag{3.7}$$

where $\varrho(t'w)$ has a cut in w starting at $(2m)^2$ and $\chi(xt)$ one in t that, however, begins only at $9\mu^2$. Following our general approach we shall make the assumption that in $\mathcal{N}$-$\mathcal{N}$ scattering (in which t and $\bar{t}$ are negative) the dependence of the last integral in (3.7) on t is sufficiently weak so as to contribute only to the lower partial waves. We shall discuss in Section **4** the consequences of such a hypothesis.

3·2. *Evaluation of the two pion contribution.* – We shall use now unitarity in the nucleon-antinucleon channel in which t is the energy and w and $\bar{t}$ are the two momentum transfers (see (2.7), where the relation bteween w, t and $\bar{t}$ and the momentum and scattering angle in the $\mathcal{N}\overline{\mathcal{N}}$ C.M. system is given).

The unitarity condition in terms of the transition matrix D defined by (2.8) is:

$$i(D^+_{\beta\alpha}-D_{\beta\alpha})=\sum_{\gamma}\delta^4(p_\gamma-p_\alpha)\,D^+_{\beta\gamma}D_{\gamma\alpha}\,. \tag{3.8}$$

Relation (3.8) leads, when written in terms of the causal matrix M and of the absorption matrix τ for the process $\mathcal{N}\bar{\mathcal{N}} \to 2\pi$ (see (2.13), (2.14), (2.15)), to the following relation:

$$(3.9) \qquad i\langle N\bar{N}|M^+ - M|N\bar{N}\rangle = \frac{1}{(2\pi)^2 t}\sum_{(2\pi)}\langle N\bar{N}|\tau^+|\pi\pi\rangle\langle\pi\pi|\tau|N\bar{N}\rangle + J_n\,,$$

where the sum is carried out over all 2π intermediate states that conserve four momenta. The contributions of the intermediate states in M^+M have been split into those coming from intermediate two pion states and those coming from higher energy intermediate states with baryonic number zero (J_n).

Also, one sees easily from (3.7) and the fact that all the invariants we have introduced are self-adjoint, that the two pion contribution to

$$(3.10) \qquad i(M^+ - M) = 2\sum_j (\operatorname{Im} c_j) C_j$$

is given by means of (3.4), (3.5) in terms of

$$(3.11) \qquad \operatorname{Im}(p_j) = \varrho_j(\omega t) \mp (-1)^t \varrho_j(\bar{t}t)\,.$$

Besides, because we have put in evidence in (3.4) the kinematical factors coming from the transformation from P_j to C_j, $\operatorname{Im} p_j$ turns out to be given by the coefficients of the perturbative invariants in the expression for $(i/2)(M^+ - M)$. Then, due to (3.9):

$$(3.12) \qquad \sum_j [\varrho_j(wt) \mp (-1)^j \varrho(\bar{t}t)] P_j = \frac{\mathcal{M}}{2(2\pi)^2 t}\,,$$

where

$$(3.13) \qquad \mathcal{M} = \sum_{(2\pi)}\langle \bar{p}_1 p_2|\tau^+|2\pi\rangle\langle 2\pi|\tau|n_1\bar{n}_2\rangle\,,$$

so that by evaluating $\mathcal{M}$ we shall be able to obtain from (3.12) the function ϱ_j. $\mathcal{M}$ corresponds to the graph of Fig. 3, in which the intermediate pions are on the mass shell, where $n = n_1$, $n' = -n_2$ are the momenta of the incoming nucleon and antinucleon, respectively and $p = p_2$, $p' = -p_1$ those of the outgoing nucleon and antinucleon. $2\pi|\tau|n_1 n_2$ is the matrix element for the process $\mathcal{N}\mathcal{N} \to 2\pi$ and is an analytic continuation of that corresponding to pion nucleon scattering.

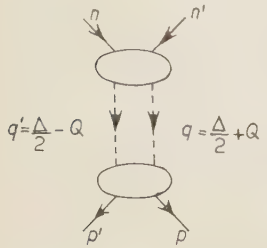

Fig. 3.

We write it in the usual way ([8]):

$$(3.14) \qquad \langle\pi_\alpha\pi_\beta|\tau|n_1\bar{n}_2\rangle = \bar{v}(n')\big[-(A_n^+\delta_{\alpha\beta} + \tfrac{1}{2}[\boldsymbol{\tau}_\beta, \boldsymbol{\tau}_\alpha]A_n^-) + i\gamma\cdot Q(B_n^+\delta_{\alpha\beta} + \tfrac{1}{2}[\boldsymbol{\tau}_\beta, \boldsymbol{\tau}_\alpha]B_n^-)\big]u(n)\,,$$

where α, β are the isotopic spin indices of the two pions and

$$Q = \frac{q - q'}{2} . \tag{3.15}$$

A_n and B_n will be functions of

$$\begin{cases} t = -(n + n')^2 , \\ s_n = -(n - q)^2 = -(n^2 + q^2 - 2nq\cos\varphi_n), \\ \bar{s}_n = -(n - q')^2 = -(n^2 + q^2 + 2nq\cos\varphi_n), \end{cases} \tag{3.16}$$

$$(t + s_n + \bar{s}_n = 2m^2 + 2\mu^2) , \tag{3.17}$$

where φ_n is the $\mathcal{N}\mathcal{N} \to 2\pi$ scattering angle; n and q the modulus of thenucleon and pion momentum, respectively, in the $\mathcal{N}\mathcal{N}$ C.M. system.

We see that the t defined here coincides with the t of (2.2), s_n and $\bar{s}_n$ depend on the scattering angle in the process $\mathcal{N}\mathcal{N} \to 2\pi$. Similar reasoning can be applied to

$$\langle \bar{p}_1 p_2 | \tau^+ | 2\pi \rangle .$$

We split the sum over intermediate states in (3.13) into a sum over the isotopic indices of the pions (which is trivially done) and an integration over their momenta; we obtain then

$$\mathcal{M} = 3\mathcal{M}^+ + 2\boldsymbol{\tau}^{(p)} \cdot \boldsymbol{\tau}^{(n)} \mathcal{M}^- , \tag{3.18}$$

$$\mathcal{M}^\pm = \frac{1}{2} \int \mathrm{d}^3\boldsymbol{q}\, \mathrm{d}^3\boldsymbol{q}'\, \bar{u}(p) \left(-A_p^{\pm *} + i\gamma \cdot Q B_p^{\pm *}\right) v(p') \cdot \tag{3.19}$$
$$\cdot \bar{v}(n') \left(-A_n^{\pm} + i\gamma \cdot Q B_n^{\pm}\right) u(n) \cdot \delta^4(q + q' - p - p') .$$

Note that, in the region we are interested in ($9\mu^2 \leqslant t \leqslant 4\mu^2$), q is real but p is pure imaginary. The unitarity condition has therefore to be extended to the complex p-plane by using $S^+(p^*)S(p) = 1$ (see, for instance, N. Van Kampen: *Phys. Rev.*, **89**, 1072 (1953)). The arguments of A^* and B^* in (3.19) contain therefore p^* and not p, which is equivalent to a substitution $s \rightleftarrows \bar{s}$, as is clear from (3.16). The results obtained by using this extension of the unitarity condition are completely equivalent to those that can be obtained by working always in the physical region ($t \geqslant 4m^2$), where p and q are both real (and so are therefore s and $\bar{s}$), and going then by analytical continuation in t to the region we are interested in ($4\mu^2 \leqslant t \leqslant 9\mu^2$).

In order to perform the integration over the two δ functions it is simpler to go into the $\mathcal{N}\mathcal{N}$ centre of mass system. In such a system $\boldsymbol{J}$ has no spatial components, so that

$$\frac{J_0^{\text{c.m.}}}{2} = \frac{\sqrt{-J^2}}{2} = \sqrt{\frac{t}{4}} . \tag{3.20}$$

Writing $\mathscr{M}^{\pm}$ as an operator in spinor space, with our usual notations, we have

$$\mathscr{M}^{\pm} = \frac{1}{16}(t(t-4\mu^2))^{\frac{1}{2}} \int (-A_p^{\pm *} + i\boldsymbol{\gamma}\cdot\boldsymbol{Q}B_p^{\pm *})(-A_n^{\pm} + i\boldsymbol{\gamma}\cdot\boldsymbol{Q}B_n^{\pm}) \, \mathrm{d}\Omega_Q , \tag{3.21}$$

where the integration is now extended only over the whole solid angle of $\boldsymbol{Q}$, its modulus being given by

$$\boldsymbol{Q}^2 = \frac{t}{4} - \mu^2 . \tag{3.22}$$

In order to proceed in the evaluation of $\mathscr{M}$ we must introduce in (3.21) some knowledge about A and B. From their Mandelstam representation we know the location of their singularities, so we can write for them the following expression:

$$\begin{cases} A^{\pm}(s\bar{s}t) = \dfrac{1}{\pi}\displaystyle\int_{(m+\mu)^2} \sigma_A^{\pm}(s', t)\left(\frac{1}{s'-s} \pm \frac{1}{s'-\bar{s}}\right)\mathrm{d}s' + \frac{1}{\pi}\int_{(2\mu)^2} \frac{\nu_A^{\pm}(t', s-\bar{s})}{t'-t}\,\mathrm{d}t' , \\ B^{\pm}(s\bar{s}t) = g^2\left(\dfrac{1}{m^2-s} \mp \frac{1}{m^2-\bar{s}}\right) + \dfrac{1}{\pi}\displaystyle\int_{(m+\mu)^2} \sigma_B^{\pm}(s', t)\left(\frac{1}{s'-s} \mp \frac{1}{s'+s}\right)\mathrm{d}s' + \\ \qquad\qquad + \dfrac{1}{\pi}\displaystyle\int_{(2\mu)^2} \frac{\nu_B^{\pm}(t', s-\bar{s})}{t'-t}\,\mathrm{d}t' , \end{cases} \tag{3.23}$$

where the upper sign corresponds to isotopic index (+) and the lower to the index (—).

We distinguish for A and B three contributions; first the pole that represents the graph of Fig. 4; next the cut in s and $\bar{s}$. This incorporates the π-$\mathcal{N}$ rescattering corrections to A and B and is that studied by CHEW, GOLDBERGER, LOW and NAMBU for π-$\mathcal{N}$ scattering ([8]); it is dominated by the 33 resonance. And lastly, the cut in t brings into the game the π-π interaction; this term has been considered by FRAZER and FULCO ([10]) in the analysis of the electromagnetic structure of the nucleon, and recently by BOWCOCK, COTTINGHAM and LURIÉ ([11]) in the analysis of π-$\mathcal{N}$ scattering, under the hypothesis of p-wave π-π resonance (*). In these last investigations is discussed the location of the singularities of ν_A and ν_B in s and $\bar{s}$ as derived from the Mandelstam representation for A and B. These singularities are cuts in s and $\bar{s}$ that, however begin only at $s = (m+2\mu)^2$ and $\bar{s} = (m+2\mu)^2$. The whole philosophy of our

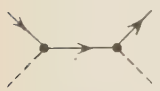

Fig. 4.

([10]) W. FRAZER and J. FULCO: *Phys. Rev. Lett.*, **2**, 365 (1959).

([11]) J. BOWCOCK, W. N. COTTINGHAM and D. LURIÉ: *Nuovo Cimento*, **16**, 918 (1960).

(*) Note that $\sigma_A(s't)$ and $\sigma_B(s't)$ also have cuts in t beginning at $16\mu^2$ (see ([11])).

2192

approach consists in making use of the weak dependence of every quantity in those variables for which the singularities are far from the region of interest. Or, alternatively, we lump the dependence of these variables into some constants which come from the lower terms of a development of the quantity in question.

The development parameter is just

$$s - \bar{s} = 4pq \cos\varphi \,, \tag{3.24}$$

φ being the c.m. scattering angle in the reaction $\mathcal{N}\bar{\mathcal{N}} \to 2\pi$. Then a weak dependence on $s - \bar{s}$ means that only low waves of the two pions occur in the process $\mathcal{N}\mathcal{N} \to 2\pi$. To fix better our ideas let us suppose that only s and p-waves occur in the development of the last terms in (3.23); it is clear however, that higher waves of the two pions shall be present by virtue of the strong s and $\bar{s}$ dependence of the other terms in (3.23).

We stress that the restriction made is justified only for the values of t in which we are interested, *i.e.* a total energy of the two pion system of a few pion masses. The inclusion of higher waves coming from the integrals over t' in (23) would be a simple extension of the following arguments.

We notice first that not only the last term in (3.23) contributes to the s and p-waves; the other terms that we shall call $\mathscr{A}^{\pm}\mathscr{B}^{\pm}$, where

$$\begin{cases} \mathscr{A}^{\pm}(s\bar{s}t) = \dfrac{1}{\pi}\displaystyle\int_{(m+\mu)^2} \sigma_A^{\pm}(s', t)\left(\frac{1}{s'-s} \pm \frac{1}{s'-\bar{s}}\right) \mathrm{d}s' \,, \\ \mathscr{B}^{\pm}(s\bar{s}t) = \dfrac{1}{\pi}\displaystyle\int_{0} \bar{\sigma}_B^{\pm}(s', t)\left(\frac{1}{s'-s} \mp \frac{1}{s'-\bar{s}}\right) \mathrm{d}s' \,, \end{cases} \tag{3.25}$$

with

$$\bar{\sigma}_B^{\pm}(s', t) = \pi g^2 \delta(s' - m^2) + \sigma_B^{\pm}(s', t) \tag{2.26}$$

also contribute to them. In Appendix II it is shown that the 2π s, p-wave contributions of $\mathscr{A}$ and $\mathscr{B}$ are given respectively by (omitting the $\pm$ indices when inessential)

$$\begin{cases} \alpha = \alpha_0(t) + \alpha_1(t)\dfrac{s-\bar{s}}{4} \,, \\ \beta = \beta_1(t) \,, \end{cases} \tag{3.27}$$

where

$$\begin{cases} \alpha_0^{+}(t) = \tfrac{1}{2}\,\mathscr{A}_1^{+} \,, \\ \alpha_1^{-}(t) = \dfrac{3}{2}\left(\dfrac{1}{pq}\,\mathscr{A}_1^{-} + \dfrac{m}{p^2}\,\mathscr{B}_2^{-}\right) \,, \\ \beta_1^{-}(t) = \tfrac{1}{2}\,(\mathscr{B}_0^{-} - \mathscr{B}_2^{-}) \,, \\ \alpha_0^{-} \qquad \alpha_1^{+} \quad \beta_1^{+} \qquad 0 \,. \end{cases} \tag{3.28}$$

6693

having

$$\left\{\begin{aligned} \mathscr{A}_J(t) &= \int_{-1}^{+1} \mathscr{A} P_J(\cos\varphi)\,\mathrm{d}\cos\varphi\,, \\ \mathscr{B}_J(t) &= \int_{-1}^{+1} \mathscr{B} P_J(\cos\varphi)\,\mathrm{d}\cos\varphi\,. \end{aligned}\right. \tag{3.29}$$

Let us denote by A_{sp} and B_{sp} the whole s and p-wave contribution to A and B respectively. Then, because we supposed that the last term in (3.23) contributes only to such waves

$$\left\{\begin{aligned} A_{sp} &= \alpha + \frac{1}{\pi}\int_{(2\mu)^2} \frac{\nu_A(t', s-\bar{s})}{t'-t}\,\mathrm{d}t'\,, \\ B_{sp} &= \beta + \frac{1}{\pi}\int_{(2\mu)^2} \frac{\nu_B(t', s-\bar{s})}{t'-t}\,\mathrm{d}t'\,, \end{aligned}\right. \tag{3.30}$$

so we can write

$$\left\{\begin{aligned} A &= \mathscr{A} - \alpha + A_{sp}\,, \\ B &= \mathscr{B} - \beta + B_{sp}\,. \end{aligned}\right. \tag{3.31}$$

In analogy with (3.27) we can write for A_{sp} and B_{sp} the development

$$\left\{\begin{aligned} A_{sp} &= \lambda_0(t) + \lambda_1(t)\frac{(s-\bar{s})}{4}\,, \\ B_{sp} &= \eta_1(t)\,, \end{aligned}\right. \tag{3.32}$$

with

$$\lambda_0^- = \lambda_1^+ = \eta_1^+ = 0\,. \tag{3.33}$$

We are now ready to go further in the evaluation of (3.21). For every A_n, B_n, A_p or B_p we shall use an expression of the form (3.31) with (3.27) and (3.32) where $s-\bar{s}$ will be either $s_n-\bar{s}_n$ or $s_p-\bar{s}_p$, respectively. In Appendix II it is shown that the iteration of the terms containing A_{sp} and B_{sp} with those containing $\mathscr{A}-\alpha$ and $\mathscr{B}-\beta$ is zero. This is physically clear because interference between terms containing only s and p-waves (as A_{sp} and B_{sp}), with $\mathscr{A}-\alpha$ and $\mathscr{B}-\beta$, which by construction do not contain them, must certainly vanish. Since α and A_{sp} (or β and B_{sp}) have the same form ((3.27), (3.32)) a consequence of the previous statement is that the iteration of α

22944

and β with $\mathscr{A}$ and $\mathscr{B}$ gives the same contribution as their iteration with α and β respectively (*).

Then we can write for (3.21)

$$\mathscr{M} = \frac{1}{8}\left(t\left(\frac{t}{4}-\mu^2\right)\right)^{\frac{1}{2}}\int\{(-\mathscr{A}_p^* + i\boldsymbol{\gamma}\cdot\boldsymbol{Q}\mathscr{B}_p^*)(-\mathscr{A}_n + i\boldsymbol{\gamma}\cdot\boldsymbol{Q}\mathscr{B}_n) + \tag{3.34}$$
$$+ (-[A_{sp}^* - \alpha^*]_p + i\boldsymbol{\gamma}\cdot\boldsymbol{Q}[B_{sp}^* - \beta]_p)(-[A_{sp} - \alpha]_n + i\boldsymbol{\gamma}\cdot\boldsymbol{Q}[B_{sp} - \beta]_n)\}\,\mathrm{d}\Omega_{\boldsymbol{Q}}\,.$$

It is not difficult to develop (3.34) into invariants. We obtain readily

$$\mathscr{M} = (a + 2mc + m^2 e)1^n\ 1^p - (b + md)[1^n\ i\gamma^p\cdot N + i\gamma^n\cdot P\ 1^p] + \tag{3.35}$$
$$+ e[i\gamma^p\cdot N\, i\gamma^n\cdot P] - f[\gamma^p\cdot\gamma^n]\,,$$

where

$$\left\{\begin{aligned}
a &= \frac{1}{8}\left(t\left(\frac{t}{4}-\mu^2\right)\right)^{\frac{1}{2}}\int[\mathscr{A}_p^*\mathscr{A}_n + A_{sp_p}^* A_{sp_n} - \alpha_p^*\alpha_n]\,\mathrm{d}\Omega_{\boldsymbol{Q}}\,,\\
b &= \frac{1}{8}\left(t\left(\frac{t}{4}-\mu^2\right)\right)^{\frac{1}{2}}\int[\mathscr{B}_p^*\mathscr{A}_n + \mathrm{Re}\,(B_{sp_p}^* A_{sp_n}) - \beta_p\alpha_n]\cdot\\
&\qquad\cdot\left[\frac{\boldsymbol{Q}\cdot\boldsymbol{M}}{\boldsymbol{M}^2} + \frac{\boldsymbol{Q}\cdot\boldsymbol{K}}{\boldsymbol{K}^2}\right]\mathrm{d}\Omega_{\boldsymbol{Q}}\,,\\
c &= \frac{1}{8}\left(t\left(\frac{t}{4}-\mu^2\right)\right)^{\frac{1}{2}}\int[\mathscr{B}_p^*\mathscr{A}_n + \mathrm{Re}\,(B_{sp_p}^* A_{sp_n}) - \beta_p\alpha_n]\cdot\\
&\qquad\cdot\left[\frac{\boldsymbol{Q}\cdot\boldsymbol{M}}{\boldsymbol{M}^2} - \frac{\boldsymbol{Q}\cdot\boldsymbol{K}}{\boldsymbol{K}^2}\right]\mathrm{d}\Omega_{\boldsymbol{Q}}\,,\\
d &= \frac{1}{8\boldsymbol{M}^2\boldsymbol{K}^2}\left(t\left(\frac{t}{4}-\mu^2\right)\right)^{\frac{1}{2}}\int[\mathscr{B}_p^*\mathscr{B}_n + B_{sp_p}^* B_{sp_n} - \beta_p\beta_n]\cdot\\
&\qquad\cdot\left[\frac{(\boldsymbol{Q}\cdot\boldsymbol{M})^2}{\boldsymbol{M}^2}(2\boldsymbol{K}^2 + \boldsymbol{M}^2) + \frac{(\boldsymbol{Q}\cdot\boldsymbol{K})^2}{\boldsymbol{K}^2}(2\boldsymbol{M}^2 + \boldsymbol{K}^2) - \boldsymbol{Q}^2(\boldsymbol{K}^2 + \boldsymbol{M}^2)\right]\mathrm{d}\Omega_{\boldsymbol{Q}}\,,\\
e &= \frac{1}{8\boldsymbol{M}^2\boldsymbol{K}^2}\left(t\left(\frac{t}{4}-\mu^2\right)\right)^{\frac{1}{2}}\int[\mathscr{B}_p^*\mathscr{B}_n + B_{sp_p}^* B_{sp_n} - \beta_p\beta_n]\cdot\\
&\qquad\cdot\left[\frac{(\boldsymbol{Q}\cdot\boldsymbol{M})^2}{\boldsymbol{M}^2}(2\boldsymbol{K}^2 - \boldsymbol{M}^2) + \frac{(\boldsymbol{Q}\cdot\boldsymbol{K})^2}{\boldsymbol{K}^2}(\boldsymbol{K}^2 - 2\boldsymbol{M}^2) + \boldsymbol{Q}^2(\boldsymbol{M}^2 - \boldsymbol{K}^2)\right]\mathrm{d}\Omega_{\boldsymbol{Q}}\,,\\
f &= \frac{1}{8}\left(t\left(\frac{t}{4}-\mu^2\right)\right)^{\frac{1}{2}}\int[\mathscr{B}_p^*\mathscr{B}_n + B_{sp_p}^* B_{sp_n} - \beta_p\beta_n]\cdot\\
&\qquad\cdot\left[\boldsymbol{Q}^2 - \frac{(\boldsymbol{Q}\cdot\boldsymbol{M})^2}{\boldsymbol{M}^2} - \frac{(\boldsymbol{Q}\cdot\boldsymbol{K})^2}{\boldsymbol{K}^2}\right]\mathrm{d}\Omega_{\boldsymbol{Q}}\,,
\end{aligned}\right. \tag{3.36}$$

(*) This reflects the fact that the interference of s and p-waves with the whole $\mathscr{A}$ and $\mathscr{B}$ is the same as their interference with only the s and p part of $\mathscr{A}$ and $\mathscr{B}$, *i.e.* α and β.

220

where $\boldsymbol{M}$ and $\boldsymbol{K}$ are the spatial components of M and K, as defined in (2.4), in the $\mathcal{N}\mathcal{N}$ centre of mass system. In such a system the time component of M and K vanish, so that

$$\boldsymbol{M}^2 = -w\,, \qquad \boldsymbol{K}^2 = -t\,. \tag{3.37}$$

Let us consider the integration over $\mathscr{A}$ and $\mathscr{B}$ in (3.36). We see that the dependence on Ω_Q for every $\mathscr{A}$ or $\mathscr{B}$ is explicitly exhibited in s and $\bar{s}$ (s_n, $\bar{s}_n$ and s_p, $\bar{s}_p$) in the denominators of (3.25). Then the integration over Ω_Q can be performed explicitly. We prefer, however, to express the results in parametric form

$$\int \varkappa(xt)\left(\frac{1}{x-\bar{t}} \pm \frac{1}{x-w}\right) \mathrm{d}x\,,$$

where the dependence on x of $\varkappa$ is determined. We shall see later the reason for this form. In order to integrate the terms in (3.36) containing $A_{sp}B_{sp}$ α and β, we take for them their expressions (3.27) and (3.32) in which their dependence on Ω_Q appears explicitly in $s_n - \bar{s}_n = 4\boldsymbol{Q}\cdot\boldsymbol{N}$ in one factor and $s_p - \bar{s}_p = 4\boldsymbol{Q}\cdot\boldsymbol{P}$ in the other. The integration over Ω_Q can then be performed easily. By collecting the results we find:

$$\begin{cases}
a^{\pm} = \dfrac{1}{\pi}\displaystyle\int_{4m^2} \varkappa_a^{\pm}(tx)\left[\frac{1}{x-\bar{t}} \pm \frac{1}{x-w}\right] \mathrm{d}x + \frac{\pi}{2}\left|t\left(\frac{t}{4} - \mu^2\right)\right|^{\frac{1}{2}} \cdot \\
\qquad\qquad \cdot \left|\lambda_0^{\pm 2} - \varkappa_0^{\pm 2} - \frac{1}{3}\left(\lambda_1^{\pm 2} - \varkappa_1^{\pm 2}\right)\left(\frac{t}{4} - \mu^2\right)\left(w - \frac{t}{4}\right)\right|\,, \\
b^{\pm} = \dfrac{1}{\pi}\displaystyle\int_{4m^2} \varkappa_b^{\pm}(tx)\left[\frac{1}{x-\bar{t}} \mp \frac{1}{x-w}\right] \mathrm{d}x + \frac{\pi}{6}\cdot \\
\qquad\qquad \cdot \left[\mathrm{Re}\,(\eta_1^{\pm *}\lambda_1^{\pm}) - \alpha_1^{\pm}\beta_1^{\pm}\right]\left(t\left(\frac{t}{4} - \mu^2\right)^3\right)^{\frac{1}{2}}\,, \\
c^{\pm} = \dfrac{1}{\pi}\displaystyle\int_{4m^2} \varkappa_c^{\pm}(tx)\left[\frac{1}{x-\bar{t}} \pm \frac{1}{x-w}\right] \mathrm{d}x\,. \\
d^{\pm} = \dfrac{1}{\pi}\displaystyle\int_{4m^2} \varkappa_d^{\pm}(tx)\left[\frac{1}{x-\bar{t}} \mp \frac{1}{x-w}\right] \mathrm{d}x\,, \\
e^{\pm} = \dfrac{1}{\pi}\displaystyle\int_{4m^2} \varkappa_e^{\pm}(tx)\left[\frac{1}{x-\bar{t}} \pm \frac{1}{x-w}\right] \mathrm{d}x\,, \\
f^{\pm} = \dfrac{1}{\pi}\displaystyle\int_{4m^2} \varkappa_f^{\pm}(tx)\left[\frac{1}{x-\bar{t}} \mp \frac{1}{x-w}\right] \mathrm{d}x + \frac{\pi}{6}\left[|\eta_1^{\pm}|^2 - \beta_1^{\pm 2}\right]\left(t\left(\frac{t}{4} - \mu^2\right)^3\right)^{\frac{1}{2}}\,,
\end{cases} \tag{3.38}$$

with

$$
\begin{cases}
\varkappa_a^{\pm}(tx) = \sqrt{t}\iint \mathrm{d}s'\,\mathrm{d}s''\,\sigma_A^{\pm}(s't)\,\sigma_A^{\pm}(s''t)\,K(s's''tx)\,, \\
\varkappa_b^{\pm}(tx) = \dfrac{\sqrt{t}}{2}\iint \mathrm{d}s'\,\mathrm{d}s''\,\bar{\sigma}_B^{\pm}(s't)\,\sigma_A^{\pm}(s''t)\left[\dfrac{Z(s's''t)}{x-4m^2+t}+\dfrac{Y(s's'')}{x}\right]K\,, \\
\varkappa_c^{\pm}(tx) = \dfrac{\sqrt{t}}{2}\iint \mathrm{d}s'\,\mathrm{d}s''\,\bar{\sigma}_B^{\pm}(s't)\,\sigma_A^{\pm}(s''t)\left[\dfrac{Z(s's''t)}{x-4m^2+t}-\dfrac{Y(s's'')}{x}\right]K\,, \\
\varkappa_d^{\pm}(tx) = \dfrac{\sqrt{t}}{4}\iint \mathrm{d}s'\,\mathrm{d}s''\,\bar{\sigma}_B^{\pm}(s't)\,\bar{\sigma}_B^{\pm}(s''t)\cdot \\
\qquad\qquad \cdot\left\{\dfrac{t-4m^2}{x^2(x-4m^2+t)^2}\dfrac{1}{K}+\left[\dfrac{Z^2}{(x-4m^2+t)^2}-\dfrac{Y^2}{x^2}\right]K\right\}, \\
\varkappa_e^{\pm}(tx) = \dfrac{\sqrt{t}}{4}\iint \mathrm{d}s'\,\mathrm{d}s''\,\bar{\sigma}_B^{\pm}(s't)\,\bar{\sigma}_B^{\pm}(s''t)\cdot \\
\qquad\qquad \cdot\left\{-\dfrac{2x-4m^2+t}{x^2(x-4m^2+t)^2}\dfrac{1}{K}+\left[\dfrac{Z^2}{(x-4m^2+t)^2}-\dfrac{Y^2}{x^2}\right]K\right\}, \\
\varkappa_f^{\pm}(xt) = \dfrac{\sqrt{t}}{4}\iint \mathrm{d}s'\,\mathrm{d}s''\,\bar{\sigma}_B^{\pm}(s't)\,\bar{\sigma}_B^{\pm}(s''t)\left\{\dfrac{1}{x(x-4m^2+t)}\dfrac{1}{K}\right\},
\end{cases}
\tag{3.39}
$$

with

$$
K(s's''tx) = \big[t\big(x-[\sqrt{s'}+\sqrt{s''}]^2\big)\big(x-[\sqrt{s'}-\sqrt{s''}]^2\big)-4m^2(s'-s'')^2- \\
-4x\big\{s's''+[\mu^2-m^2]^2-(\mu^2+m^2)(s'+s'')+\mu^2x\big\}\big]^{-\frac{1}{2}}. \tag{3.40}
$$

$$
Z(s's''t) = s'+s''-2(\mu^2+m^2)+t\,, \qquad Y(s's'') = s'-s'' \tag{3.41}
$$

where the integrations over s' and s'' begin at m^2 and go up to a curve (in the $s'-s''$ plane) given by:

$$
s's''+(s'+s'')\left(\frac{t}{2}-\mu^2-m^2\right)+(m^2-\mu^2)^2-\frac{x_0}{2}(t-4\mu^2)+ \\
+\sqrt{[s'^2+s'(t-2\mu^2-2m^2)+(m^2-\mu^2)^2][s''^2+s''(t-2\mu^2-2m^2)+(m^2-\mu^2)^2]}=0\,. \tag{3.42}
$$

This limits, for any fixed x and t, the possible intermediate masses $\sqrt{s'}$ and $\sqrt{s''}$ of Fig. 5 that can contribute to (3.39). Alternatively, the same integration region of (3.38) and (3.39) can be obtained by limiting the integration over x for every value of s', s'' and t in the form

$$
\int_{m^2}^{\infty}\mathrm{d}s'\int_{m^2}^{\infty}\mathrm{d}s''\int_{x_1}^{\infty}\mathrm{d}x
$$

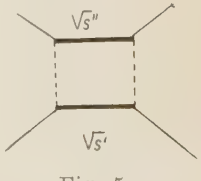

Fig. 5.

where x_0 is just the value given by solving (3.42) for x. This means that for every pair of intermediate masses $\sqrt{s'}$ and $\sqrt{s''}$ the integration over x is limited to lie above a curve in the $x-t$ plane given by (3.42) (see ref. [12]).

If we take $\sigma_A^{\pm}=\sigma_B^{\pm}=0$, so that only the δ functions of $\bar{\sigma}$ in (3.26) remain in (3.39) the expressions for the $\varkappa$ are just real analytic expressions for $t>4\mu^2$, $x>4m^2$. This is, on the other hand, just the perturbative fourth order (renormalized) contribution. That the fourth order terms have this form was already utilized in the discussion at the beginning of Section 3·1.

We are now able to give explicit expressions for the functions ϱ_j of (3.7). In fact, from (3.12), (3.35) and (3.38) we obtain readily:

$$
\left\{
\begin{aligned}
\varrho_1^{\pm}(wt) &= \frac{1}{2(2\pi)^2 t}\left[\pm\frac{1}{\pi}\int_{(2m)^2}\frac{\varkappa_a^{\pm}+\frac{2m\varkappa_c^{\pm}}{x-w}+m^2\varkappa_e^{\pm}}{x-w}\,\mathrm{d}x + \right.\\
&\qquad\left. +\frac{\pi}{4}\left(t\left(\frac{t}{4}-\mu^2\right)\right)^{\frac{1}{2}}\begin{pmatrix}|\lambda_0^{+}|^2-\alpha_0^{+2}\\ -(w/6)((t/4)-\mu^2)(|\lambda_1^{-}|^2-\alpha_1^{-2})\end{pmatrix}\right],\\
\varrho_2^{\pm}(wt) &= \frac{1}{2(2\pi)^2 t}\left[\pm\frac{1}{\pi}\int_{(2m)^2}\frac{\varkappa_b^{\pm}+m\varkappa_d^{\pm}}{x-w}\,\mathrm{d}x - \right.\\
&\qquad\left. -\frac{\pi}{12}\sqrt{t\left(\frac{t}{4}-\mu^2\right)^3}\begin{pmatrix}0\\ \mathrm{Re}\,(\eta_1^{-*}\lambda_1^{-})-\alpha_1^{-}\beta_1^{-}\end{pmatrix}\right],\\
\varrho_3^{\pm}(wt) &= \frac{1}{2(2\pi)^2 t}\left[\pm\int_{(2m)^2}\frac{\varkappa_e^{\pm}}{x-w}\,\mathrm{d}x\right],\\
\varrho_4^{\pm}(wt) &= \frac{1}{2(2\pi)^2 t}\left[\pm\int_{(2m)^2}\frac{\varkappa_f^{\pm}}{x-w}\,\mathrm{d}x-\frac{\pi}{12}\sqrt{t\left(\frac{t}{4}-\mu^2\right)^3}\begin{pmatrix}0\\ |\eta_1^{-}|^2-\beta_1^{-2}\end{pmatrix}\right],\\
\varrho_5^{\pm}(wt) &= 0\,.
\end{aligned}
\right. \tag{3.43}
$$

This means, by looking at (3.38), (3.39)-(3.41) that we have obtained for all $\varrho_j^{\pm}$ expressions that depend on σ_A and σ_B on one side and on functions $\lambda_0^{\pm}(t)$, $\lambda_1(t)$, $\eta_1(t)$ on the other (α_0^{-}, α_1 and β_1^{-} are given by (3.28), (3.29) as functions of σ_A and σ_B). The former are given by π-$\mathcal{N}$ scattering; if for instance we take into account only the $(\frac{3}{2},\frac{3}{2})$ resonance in π-$\mathcal{N}$ rescattering corrections as done by Chew, Goldberger, Low and Nambu [8] one finds

$$
\left\{
\begin{aligned}
\sigma_A^{-}(st) &= 2\sigma_B^{-}(st) = -\frac{8\pi}{3}\left|\sqrt{\frac{s}{}}+m\right|\left|\frac{3}{E+m}\left(1+\frac{t}{2k^2}\right)+\frac{\sqrt{s}-m}{E-m}\right|\frac{\sin^2\delta_{33}(s)}{k}\,,\\
\sigma_B^{+}(st) &= -2\sigma_B^{-}(st) = -\frac{8\pi}{3}\left|\frac{3}{E+m}\left(1+\frac{t}{2k^2}\right)-\frac{1}{E-m}\right|\frac{\sin^2\delta_{33}(s)}{k}\,,
\end{aligned}
\right. \tag{3.44}
$$

[12] S. Mandelstam: *Phys. Rev.*, **115**, 1741, 1752 (1959).

2208

where

$$E = \frac{s + m^2 - \mu^2}{2\sqrt{s}}, \qquad k^2 = \frac{\frac{1}{4}(s - m^2 - \mu^2)^2 - \mu^2 m^2}{s}.$$

and δ_{33} is the usual $(\frac{3}{2}, \frac{3}{2})$ π-$\mathcal{N}$ phaseshift.

The functions $\lambda_0^-(t)$, $\lambda_1^-(t)$, $\eta_1^-(t)$ come instead from the $\mathcal{N}\mathcal{N} \to 2\pi$ process; unhappily we have not much information about it. The fact that they represent the whole 2π s and p-wave contribution to such a reaction would allow, however, the use of unitarity in order to specify their properties. For its discussion we refer to the work of Bowcock, Cottingham and Lurié [11] in which (under the assumption of a sharp resonance in p-wave pion-pion scattering), $\lambda_1^-(t)$, and $\eta_1^-(t)$ ($\lambda_0^+ = 0$) are obtained in terms of certain constants. In a future paper, consequences of the π-π resonance in $\mathcal{N}$-$\mathcal{N}$ scattering, will be investigated.

4. – Discussion and conclusions.

We shall briefly sum up and discuss the results obtained in the preceding paragraph. We shall use the information that we have get on the structure of the c_j's in order to discuss the possibility of obtaining integral equations for the partial wave amplitudes in $\mathcal{N}\mathcal{N}$ scattering.

A detailed derivation and discussion of these partial wave integral equations will be given in a later paper. We shall here shortly note the main features of these equations.

It is clear that our c_j's, satisfying a Mandelstam representation, present singularities only on the real k^2 axis. Going to the T_{ij} by means of (2.32) does not introduce any extra singularity, with the exception of a kinematical singularity (due to the $\sqrt{w}$ present in η_j) which can be, however, singled out in the singlet case. Partial wave integral equations will be satisfied by amplitudes proportional to the a_L^J, b_L^J and C_L (as defined, for instance, in G.N.O., formula (B, 11) in Appendix II) and presenting the right analytic and convergence properties. It is easy to see from the above mentioned formula in G.N.O. and from (2.32) that these functions will be obtained by multiplying the amplitudes a, b and C by the kinematical factor: $\sqrt{(k^2 + m^2)}/k^2$. The resulting amplitudes, which can be expressed in terms of the projections of the c_j's over partial waves, will present the following singularities in the k^2 plane:

a) a cut for positive values of k^2, starting from 0;

b) a cut going from $-\mu^2/4$ to $-\infty$, due to the one meson pole;

c) a cut going from $-\mu^2$ to $-\infty$, due to the two pion contribution;

d) farther cuts on the negative real axis, due to many-pion states.

22290

The jump of the amplitude at the cut *a*) is just given by the imaginary part of the amplitude considered, for positive values of the energy; the jumps at *b*) and *c*) can be calculated starting from the formulae given in the previous paragraph, and the two pion contribution can be given explicitly in terms of pion-nucleon and pion-pion interaction; the higher cuts will contribute with a weak dependence on the energy, which will be approximate by a low order polynomial in k^2. This means that the different amplitudes will contain some constants, which will enter as parameters into our theory. The number of them will clearly depend on the region of the variables in which we wish to reach definite conclusions, *i.e.* the energy up to which one is interested in. The theory is however meaningful only if the number of parameters is rather restricted. This philosophy has as background the assumption that the weight functions (of the Mandelstam representations) in all the phenomena we are interested in have no « strange » behaviour, so that the main features are still understandable just from the positions of the singularities. This is a theoretical assumption whose consequences are reflected in our results in which the whole aspect of low energy $\mathcal{N}$-$\mathcal{N}$ scattering is given in terms of only a few parameters.

We want to discuss here briefly the difference between our approach and that of GOLDBERGER, OEHME and NAMBU ([3,4]). They used dispersion relations at fixed momentum transfer t of the form

$$(4.1) \qquad F(tw) = \frac{R_1}{w_D - w} + \frac{R_2}{\mu^2 - \bar{t}} + \frac{1}{\pi}\int_{(2m)^2} \frac{\mathrm{Im}\, F(x,t)}{x - w}\,\mathrm{d}x + \frac{1}{\pi}\int_{(2,)^2} \mathrm{d}.\, \frac{\mathrm{Im}\, F^c(x,t)}{x - \bar{t}}\,.$$

GOLDBERGER and OEHME have analysed the last integral by considering the two pion contributions to it.

Let us analyse the relation (4.1) in some detail. First we note that it is surely most appropriate to use it in the case of forward scattering ($t = 0$) in which, by virtue of the optical theorem, the imaginary part of the amplitudes in the first and second integrals in (4.1) is connected to $\mathcal{N}$-$\mathcal{N}$ and $\mathcal{N}$-$\overline{\mathcal{N}}$ total scattering cross-sections respectively. In this case (4.1) is transformed in a sum rule similar to that analysed by PUPPI and STANGHELLINI for π-$\mathcal{N}$ scattering ([13]) (*).

But if we want to obtain more information from the theory (*i.e.* phase shifts) we are forced to use the dispersion relations also for $t \neq 0$, for instance, by doing a development in partial waves. This means to integrate t over the

([13]) G. PUPPI and A. STANGHELLINI: *Nuovo Cimento*, **5**, 1305 (1957).

(*) *Added in proof.* – An analysis in this direction has been recenly attempted by Y. HARA and H. MIYAZAWA (Tokyo University preprint).

2300

appropriate Legendre functions. It is clear, however, that in regions in which there are singularities in t (poles or cuts) such developments have no meaning.

This means that in some way one musti dentify in (4.1) the terms which, having singularities in t, would give contribution to many waves in $\mathcal{N}$-$\mathcal{N}$ scattering. For instance, neglect of the high energy contribution in the first integral in (4.1) can be misleading if one does not single out the strong t dependence that such contributions have; *i.e.* the high energy contribution would generate a function of t (not developable) that would prevent a development in partial waves. This is also true for the low energy contribution, we have seen in Section 3 that the fourth order perturbative contribution of diagram I of Fig. 2 is just that term which is strongly dependent on both t and w (low lying singularities in both variables). There is a term analogous to this one that has instead a strong dependence in w and $\bar{t}$; this is given by the perturbative graph III of Fig. 2. This contribution is considered by Goldberger and Oehme and comes from the two pion contribution to the last integral in (4.1). The reason why in such an approach the graph III is taken into account while I is not included, comes from the asymmetry of eq. (4.1) in the treatment of t and $\bar{t}$.

* * *

We wish to thank warmly Professor S. Fubini for his continuous interest in this investigation and many enlightening discussions. We thank also Professor M. Fierz for useful discussions; one of us (E.L.) wishes to thank him for his hospitality at the Theoretical Study Division of CERN.

Appendix I

The invariant operators in the nucleon-nucleon and nucleon-antinucleon elastic scattering.

In order to build up all the possible independent invariant operators for $\mathcal{N}\mathcal{N}$ and $\mathcal{N}\bar{\mathcal{N}}$ elastic scattering, we have at our disposal two γ matrices [γ^n and γ'', to be saturated between spinors as in (2.16)] and the three independent vectors (2.1): P, N and λ. It is clearly possible to construct from these five 4-vectors quite a few scalar quantities (matrices in the spin space of the two fermions) but many of them can be further reduced, by using the Dirac equation (2.17), to simpler ones. At the end of this process of reduction, we are left with a set of 16 possible invariants [this can be most easily seen by using the separation (as given by Michel [14]), of all the forms that can

(14) L. Michel: *Proc. Phys. Soc.*, A **63**, 514 (1950); *Compt. Rend.*, **232**, 391 (1951); *Journ. Phys. et Rad.*, **12**, 793 (1951).

be obtained by using two γ matrices, into five « classes » characterised by « class » number Q ($Q = 0, 1, 2, 3, 4$ indicating that the two γ matrices combine to give, respectively, a scalar, vector, tensor, axial, pseudoscalar matrix)]. These 16 invariants belong to three different classes [as we have no independent pseudovector at our disposal, no combination of γ matrices present in the classes with $Q = 3$ and $Q = 4$ can be saturated in order to give eventually a scalar]; five of them are the Fermi invariants ($Q = 0$) and the others are:

$$\text{(AI.1)} \quad \begin{cases} Q = 1: & (1^n i\gamma^p \cdot N); \quad (i\gamma^n \cdot P\, 1^p); \quad (\gamma^n \gamma^p i\gamma^\mu \cdot N); \quad (\gamma^n i\gamma^\mu \cdot P\, \gamma^\mu); \\ & (\gamma^\mu \gamma_5^\nu \gamma^\mu \gamma_5^\nu i\gamma^\mu \cdot N); \ (\gamma^n \gamma_5^\mu i\gamma^\mu \cdot P \gamma^\mu \gamma_5^p); \ (\gamma_5^\mu \gamma_5^p i\gamma^\mu \cdot N); \ (\gamma_5^n i\gamma^n \cdot P \gamma_5^p). \\ Q = 2: & (i\gamma^n \cdot P\, i\gamma^p \cdot N); \quad (\gamma^n i\gamma^n \cdot P\, \gamma^p i\gamma^p \cdot N); \quad (\gamma_5^n i\gamma^n \cdot P\, \gamma_5^p i\gamma^p \cdot N)\,. \end{cases}$$

The requirement of time reversal invariance (as expressed, for instance, in G.N.O.) allows us to rule out $(\gamma_5^n \gamma_5^p i\gamma^p \cdot N)$ and $(\gamma_5^n i\gamma^n \cdot P\, \gamma_5^p)$; time reversal invariance plus use of the Dirac equation helps us to reduce $(\gamma^n \gamma^p i\gamma^p \cdot N)$, $(\gamma^n i\gamma^n \cdot P \gamma^p)$, $(\gamma^n \gamma_5^n \gamma^p \gamma_5^p i\gamma^p \cdot N)$ and $(\gamma^n \gamma_5^n i\gamma^n \cdot P\, \gamma^p \gamma_5^p)$.

The invariant $(\gamma^n i\gamma^n \cdot P\, \gamma^p i\gamma^p \cdot N)$ can be expressed in terms of the remaining ones by developing γ^n and γ^μ in terms of the four orthogonal 4-vectors defined by (2.4): M, K, Δ and L. We are therefore left with the five Fermi invariants and four other invariants:

$$\text{(AI.2)} \quad \begin{cases} Q = 1: & (1^n i\gamma^p \cdot N); \quad (i\gamma^n \cdot P\, 1^p)\,, \\ Q = 2: & (i\gamma^n \cdot P i\gamma^p \cdot N); \quad (\gamma_5^n i\gamma^n \cdot P \gamma_5^p i\gamma^p \cdot N)\,. \end{cases}$$

If we assume now charge symmetry, only the symmetric combination $(1^n i\gamma^p \cdot N + i\gamma^n \cdot P\, 1^p)$ can be present in the development of M into invariant operators. Thus we now have the five Fermi invariants and three other invariants, which latter coincide with three of the invariants introduced and used by G.N.O. (the other two being S and P). These invariants cannot be reduced further by the use of the Dirac equation; they are however not linearly independent and can be expressed always in terms of only five linearly independent invariant operators. This can be done in two ways: either expressing $(1^n i\gamma^p \cdot N + i\gamma^n \cdot P\, 1^p)$, $(i\gamma^n \cdot P i\gamma^p \cdot N)$ and $(\gamma_5^n i\gamma^n \cdot P\ \gamma_5^p i\gamma^p \cdot N)$ in terms of Fermi invariants, or expressing V, T and A in terms of the G.N.O. invariants. The former way is, at least in principle, trivial, but gives rise to a rather cumbersome calculation; as an even number of Fierz transformations can be applied to an invariant without altering it, a repeated application of the Michel tables for Fierz transformations of invariants belonging to different Q can be made, followed by a suitable application of the Dirac equation. At the end, our three G.N.O. invariants will be reduced to linear combinations of Fermi invariants. To go the other way round, we can express each γ matrix in V, T and A in terms of the four orthogonal 4-vectors (2.4); a repeated application of the Dirac equation will now allow us to express the three Fermi invariants we started from in terms of the G.N.O. invariants.

It is therefore clear that the $\mathcal{N}.\mathcal{N}$ and $\mathcal{N}.\overline{\mathcal{N}}$ elastic scattering can be always described in terms of only five independent invariant functions, which we shall take, as explained in the text, as linear combinations of Fermi invariants.

2302

The connection between the Fermi and the G.N.O. sets is given by the following table:

$$
\left\{
\begin{aligned}
&S = G_1\,,\\
&V = 1/(w\bar{t})\,[m^2(\bar{t}-w)\,G_1 - m(\bar{t}+w)\,G_2 + (\bar{t}-w)\,G_3 + tG_4]\,,\\
&T = -4\left[\frac{(\bar{t}-w)}{4t}\left(1-\frac{4m^4}{w\bar{t}}\right)G_1 + \frac{m}{t}\left(\frac{m^2(w+\bar{t})}{w\bar{t}}-1\right)G_2 - \right.\\
&\qquad\qquad \left. - \frac{m^2(\bar{t}-w)}{w t\bar{t}}\,G_3 - \frac{m^2}{w\bar{t}}\,G_4 - \frac{(w-\bar{t})}{4t}\,G_5\right],\\
&A = -\left[\frac{m^2(\bar{t}-w)^2}{w t\bar{t}}\,G_1 - \frac{m(\bar{t}^2-w^2)}{w t\bar{t}}\,G_2 - \frac{(w+\bar{t})^2}{w t\bar{t}}\,G_3 - \right.\\
&\qquad\qquad \left. + \frac{(\bar{t}-w)}{w\bar{t}}\,G_4 - \frac{4m^2}{t}\,G_5\right],\\
&P = G_5\,.
\end{aligned}
\right. \tag{AI.3}
$$

where $G_2 = (1^n\, i\gamma^p\cdot N + i\gamma^n\cdot P\, 1^p)$; $G_3 = (i\gamma^n\cdot P\, i\gamma^p\cdot N)$ and $G_4 = (\gamma_5^n i\gamma^n\cdot P\,\gamma_5^p i\gamma^p\cdot N)$.

From Table (AI.3) and the definition (2.19) of the perturbative invariants P_j it is easy to find out the transformation table (2.21) between the perturbative and the Fermi set of invariant operators.

Appendix II

Separation of the S and P-wave two pion contribution to the unitarity condition.

The absorption matrix (2.13) can be expressed in terms of two independent scalar functions A and B:

$$\tau = -A + i\gamma\cdot Q\,B\,. \tag{AII.1}$$

We want now to separate, out of A and B, those parts that contribute to the nucleon-antinucleon absorption into S and P two pion states, from the rest, which gives absorption into two pion states with angular momentum higher than 1. In order to do so, let us write A and B in the form

$$A = (\mathscr{A} - \alpha) + A_{sp}\,, \qquad B = (\mathscr{B} - \beta) + B_{sp}\,, \tag{AII.2}$$

where $\mathscr{A}$ and $\mathscr{B}$ are defined as in (3.25) and A_{sp} and B_{sp} contain all of the S and P-wave two pion contribution. The definition of α and β has therefore to be such that the S and P-waves coming from them have to cancel exactly those coming from $\mathscr{A}$ and $\mathscr{B}$.

2303

The S and P-wave contributions of $(-\mathscr{A}+i\gamma\cdot Q\mathscr{B})$ to τ will be proportional to:

$$\text{(AII.3)} \qquad \int(-\mathscr{A}+i\gamma\cdot Q\,\mathscr{B})\,\mathrm{d}\Omega\,, \qquad \int(-\mathscr{A}+i\gamma\cdot Q\,\mathscr{B})\,Q_\mu\,\mathrm{d}\Omega\,.$$

Expanding $\mathscr{A}$ and $\mathscr{B}$ into Legendre polynomials, the coefficients in the development being given by:

$$\text{(AII.4)} \quad \mathscr{A}_J(t)=\int_{-1}^{+1}\mathscr{A}\,P_J(\cos\varphi)\,\mathrm{d}\cos\varphi\,, \qquad \mathscr{B}_J(t)=\int_{-1}^{+1}\mathscr{B}\,P_J(\cos\varphi)\,\mathrm{d}\cos\varphi\,,$$

it is easy to see from (AII.3) that only that part of $\mathscr{A}$ which does not depend on the nucleon-pion angle [proportional to $(s-\bar{s})$] will contribute to the S-wave, and only that part of $\mathscr{A}$ linearly dependent on — and that of $\mathscr{B}$ independent of — $(s \quad s)$ will contribute to the P-wave. We shall therefore define $\alpha_0(t)$, $\alpha_1(t)$ and $\beta_1(t)$ by means of the relations:

$$\text{(AII.5)} \qquad \begin{cases} \displaystyle\int\mathscr{A}\,\mathrm{d}\Omega=\int\alpha_0(t)\,\mathrm{d}\Omega=\pi\alpha_0(t)\,, \\ \displaystyle\int(-\mathscr{A}+i\gamma\cdot Q\,\mathscr{B})\,Q_\mu\,\mathrm{d}\Omega=\int\left(-\alpha_1\frac{s-\bar{s}}{4}+i\gamma\cdot Q\,\beta_1\right)Q_\mu\,\mathrm{d}\Omega\,, \end{cases}$$

[we have, of course, $\alpha=\alpha_0(t)+\alpha_1(t)((s-\bar{s})/4)$, $\beta=\beta_1(t)$].

From this definition it is easy to get α_0, α_1 and β_1 in terms of $\mathscr{A}$ and $\mathscr{B}$:

$$\text{(AII.6)} \qquad \begin{cases} \alpha_0(t) - \tfrac{1}{2}\,\mathscr{A}_0(t)\,, \\ \alpha_1(t) - \tfrac{3}{2}\left(\dfrac{1}{pq}\,\mathscr{A}_1(t)+\dfrac{m}{p^2}\,\mathscr{B}_2(t)\right), \\ \beta_1(t) - \tfrac{1}{2}\left(\mathscr{B}_0(t) \quad \mathscr{B}_2(t)\right). \end{cases}$$

This result could also have been derived starting from the expressions for A and B in terms of partial waves that can be obtained from FRAZER and FULCO [15].

We shall have to deal, in using the unitarity condition, with the integral $\int\tau^{-}_{\gamma\gamma}\tau_{\gamma\gamma}$ over two pion intermediate states; if now we write down explicitly the whole of the interference terms present in this integral (by which we mean those terms containing products of $\mathscr{A}$, $\mathscr{B}$, α and β with A_{sp} and B_{sp}), it will be quite straightforward to see that it is zero, as it is indeed required on physical grounds. It is enough for this to note that relation (AII.5b) can also be written as:

$$\text{(AII.7)} \qquad \int\left(-\mathscr{A}-\alpha_1\frac{s-\bar{s}}{4}\right)Q_\mu\,\mathrm{d}\Omega=\int(\mathscr{B}-\beta)i\gamma\cdot Q\,Q_\mu\,\mathrm{d}\Omega\,.$$

[15] W. R. FRAZER and J. R. FULCO: *Phys. Rev.*, **117**, 1603 (1960).

2304

We have in so far disregarded isotopic spin. It is easy to see that the Pauli principle for the two pion states implies:

(AII.8) $$\mathscr{A}_0^{(-)} = \mathscr{B}_0^{(+)} = 0 , \qquad \mathscr{A}_1^{(+)} = \mathscr{B}_1^{(-)} = 0 .$$

RIASSUNTO

Si studia l'interazione nucleone-nucleone ad energie inferiori alla soglia per processanelastici, usando un metodo basato sulla rappresentazione bidimensionale dell'ami piezza di diffusione, nella forma recentemente proposta da Cini e Fubini. L'idea essenziale di questo metodo è quella di tener conto interamente delle singolarità presenti nell'ampiezza di diffusione, per valori delle variabili vicini a quelli corrispondenti alla regione fisica (regione la cui ampiezza dipende naturalmente dall'energia dei nucleoni incidenti); per ottenere questo, si sfrutta completamente la simmetria della rappresentazione di Mandelstam. Le funzioni spettrali vengono calcolate facendo uso della condizione di unitarietà sia nel canale nucleone-nucleone che in quello nucleone-antinucleone. In quest'ultimo canale si calcola il contributo dovuto a due pioni intermedi, in termini della diffusione pione-nucleone e di alcune ampiezze corrispondenti a bassi momenti orbitali nel processo di annichilamento in due pioni. Si discute poi sulla costruzione di equazioni integrali per le ampiezze di diffusione corrispondenti alle varie onde parziali. L'ampiezza totale di diffusione nucleone-nucleone è separata in operatori, ciascuno dei quali è rappresentato da una combinazione lineare di operatori di Fermi, combinazione scelta in modo tale che i corrispondenti coefficienti hanno semplici proprietà di scambio e soddisfano una rappresentazione di Mandelstam al quarto ordine perturbativo.

The Angular Distribution of Secondary π-Mesons from 4.5 GeV π^- and 6 GeV Proton Interactions in Emulsion.

H. H. Aly and C. M. Fisher

H. H. Wills Physical Laboratory, University of Bristol - Bristol

(ricevuto il 30 Marzo 1960)

Summary. — The angular distributions of π-mesons produced in two hundred 4.5 GeV π^- and two hundred 6 GeV proton interactions with emulsion nuclei have been investigated. It is found that the pions from the 6 GeV proton induced interactions are consistent with an isotropic distribution in the C-system whilst the pions from the 4.5 GeV π^- induced interactions have an anisotropic distribution peaked in the forward direction. The degree of anisotropy is larger with smaller N_h values.

In a previous paper, Aly *et al.* [1] hereafter referred to as paper I, an analysis of the interactions of 4.5 GeV π^--mesons with emulsion nuclei was described. A similar experiment has been undertaken to investigate the nature of 6 GeV proton interactions. As a result of these experiments an interesting property of the angular distribution of the secondary π-mesons in the centre-of-momentum systems, hereafter referred to as the C-systems, of the interactions has been revealed. It is the purpose of the present paper to describe these results.

The observations were made in two stacks of stripped Ilford G-5 emulsions, one exposed to the external 4.5 GeV π^- beam and the other to the internal 6 GeV proton beam of the Berkeley Bevatron. In each experiment 200 interactions were found by «along the track» scanning. The interactions, recognized by the production of heavily ionizing tracks or at least two shower tracks, were analysed in two groups having $N_h \gtrless 7$ where N_h is the number of

[1] H. H. Aly, J. G. Duthie and C. M. Fisher: *Phil. Mag.*, **45**, 993 (1959).

heavily ionizing prongs, *i.e.* tracks having $b^* > 1.4$ where b^* is the ratio of the blob density of the track to that of a beam track in the vicinity.

The procedure adopted in both experiments was the same as was described in paper I. The angles of emission of all shower particles, having $b^* \leqslant 1.4$, were determined and a sample of shower particles from each experiment identified using the method described by DANIEL *et al.* [2] depending on the variation of the ionization with velocity in nuclear emulsion. The results for the 4.5 GeV π^- interactions are given in « I ». In the 6 GeV proton induced interactions 48 tracks were investigated of which 14 were identified as protons, 31 as pions and 3 could not be identified. Of the tracks identified as protons all but one had angles of emission of less than 10° with the primary direction. The laboratory distributions were thus readily corrected for the « proton contamination » in the manner described in « I ».

Two methods were adopted to investigate the *C*-system angular distributions which do not require a knowledge of the Lorentz factor γ_c of the *C*-system. However it is assumed that the particles are created in a single collision system.

i) The Duller-Walker [3] distributions in terms of the variables $\log F(\theta)/(1-F(\theta))$ and $\log \operatorname{tg} \theta$, where $F(\theta)$ is the fraction of the total number of particles having angles of emission less than θ, are shown in Fig. 1. For an isotropic distribution in the *C*-system the

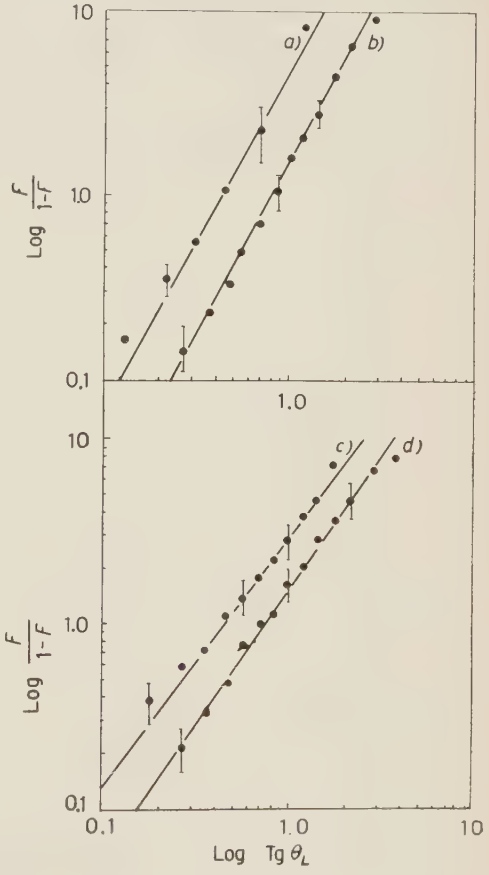

Fig. 1. – $\operatorname{Log}(F/(1-F))$ plots for: *a*) 6 GeV proton interactions having $N_h \leqslant 7$; *b*) 6 GeV proton interactions having $N_h > 7$; *c*) 4.5 GeV π^- interactions having $N_h \leqslant 7$ and *d*) 4.5 GeV π^- interactions having $N_h > 7$.

(2) R. R. DANIEL, J. H. DAVIES, J. H. MULVEY and D. H. PERKINS: *Phil. Mag.*, **43**, 753 (1952).

(3) N. M. DULLER and W. D. WALKER: *Phys. Rev.*, **93**, 215 (1954).

2307

relation between these variables will be

$$(1) \qquad 2 \log \gamma_c \operatorname{tg} \theta = \log \frac{F(\theta)}{1 - F(\theta)} - 2 \log \left(1 - \frac{\delta}{2(1 - F(\theta))}\right),$$

where $\beta_c / \bar{\beta}_s = 1 - \delta$ and β_c is the velocity of the C-system in the laboratory whilst $\bar{\beta}_s$ is the velocity of the shower particles in the C-system. Values of $\bar{\beta}_s$, were obtained from the scattering measurements as described in paper I. No dependence on the angle of emission θ was observed and the mean value obtained for shower particles identified as π-mesons were $\bar{\beta}_s^*$ (4.5 GeV π^-) = $= 0.865 \pm 0.024$ and $\bar{\beta}_s^*$ (6 GeV protons) $= 0.88 \pm .03$. Using the value of β_c for a single nucleon collision partner we obtain $\delta \simeq 0.05$ in both experiments. If the relation (1) is plotted then a curve is obtained similar to curve $A2$ of Duller and Walker [3]. This is well represented by a straight line of slope ~ 1.9. The results of the experimental distributions are given in the Table I. The effect of missing due to pions emitted backwards in the C-system and appearing as « grey » tracks in the laboratory is taken into account in these distributions by increasing the total number of tracks by 5% of the number of grey prongs. This is a small correction based on the results of KAMAL [4].

TABLE I.

		σ	S	P
4.5 GeV π^-	$N_h > 7$	$.47 \pm .02$	$1.48 \pm .2$	—
	$N_h \leqslant 7$	$.52 \pm .03$	$1.37 \pm .2$	.01
6 GeV protons	$N_h > 7$	$.41 \pm .03$	$1.87 \pm .2$	—
	$N_h \leqslant 7$	$.44 \pm .02$	$1.85 \pm .2$	.27

σ = dispersion of differential distribution;
S = slope of Duller-Walker distribution;
P = Pearson probability of agreement with isotropy.

The distribution of pions from the 6 GeV proton induced interactions is consistent with isotropic emission in the C-system. The distribution of pions from the 4.5 GeV π^- induced interactions shows a deviation from isotropy. It is interesting to note that the deviation from isotropy is larger for smaller N_h values. This may indicate that in high N_h interactions secondary processes are involved which tend to make the distribution more isotropic. In the 6 GeV proton case this effect is absent as might be expected.

[4] A. KAMAL: *Thesis* (University of Bristol, 1957).

2308

ii) A further method of investigating the C-system distribution is provided by the differential angular distribution in the variable $x = \log \operatorname{tg} \theta$ (LINDERN (5)). If the distribution in the C-system is isotropic this plot will have dispersion $\sigma = 0.394$ about its mean value provided $\delta = (\overline{\beta}_s/\beta_c) - 1 = 0$. If $\delta \neq 0$ the dispersion will be changed by a factor $(1 - \delta)^{\frac{1}{2}}$. Thus for $\delta = 0.05$, $\sigma = .384$ for an isotropic distribution. The experimental distributions are shown in Figs. 2 and 3.

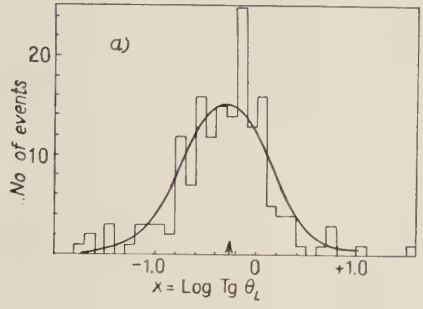

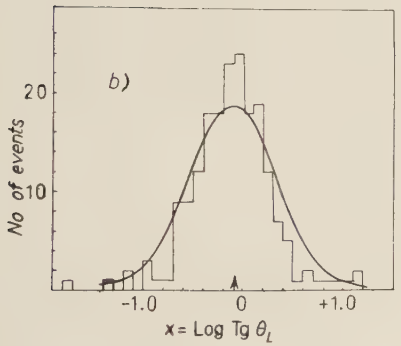

Fig. 2. – Differential distribution in $\log \operatorname{tg} \theta_L$ for 6 GeV proton interactions having: *a*) $N_h \leqslant 7$ and *b*) $N_h > 7$. The mooth curves are Gaussians having the same dispersions as the histograms.

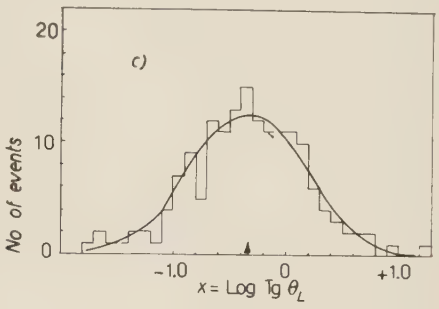

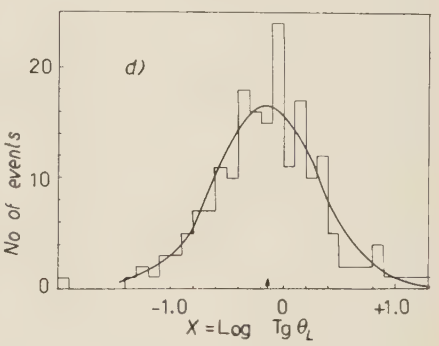

Fig. 3. – Differential distribution in $\log \operatorname{tg} \theta_L$ for 4.5 GeV pion interactions having: *c*) $N_h \leqslant 7$ and *d*) $N_h < 7$. The smooth curves are Gaussians having the same dispersions as the histograms.

It is apparent that the distribution from the proton interactions is consistent with isotropic emission in the C-system for events having $N_h > 7$ and deviates only slightly from isotropy for events having $N_h \leqslant 7$, whilst

(5) L. VON LINDERN: *Nuovo Cimento*, **5**, 491 (1957).

the π^--meson distributions are anisotropic the deviations from isotropy being largest for small N_h events. The corrections for « grey » pions would tend to increase the dispersions because they are emitted backwards in the C-system, however this correction is small and is not included in these results.

It was shown in paper « I » that for low N_h events at least, the median angle of the laboratory distribution is consistent with the assumptions of *a*) single nucleon collision partner and *b*) that equal numbers of particles are emitted, on average, backwards and forwards in the C-system of a 4.5 GeV π^- nucleon interaction. A similar result has been obtained for 6 GeV proton interactions. If we assume that, for events having $N_h \leqslant 7$ the interaction is with a single nucleon then the angles may be transformed to the C-system using the relation

$$\gamma_c \operatorname{tg} \theta = \frac{\sin \theta}{\beta_c/\bar{\beta}_s^* + \cos \bar{\theta}} \tag{2}$$

where θ is the laboratory angle of emission and $\bar{\theta}$ is the corresponding angle in the C-system. Using the values of $\bar{\beta}_s^*$ deduced from the scattering measurements as described in « I », the laboratory distributions, corrected for the proton component were transformed to the C-system. The distributions obtained are shown in Fig. 4.

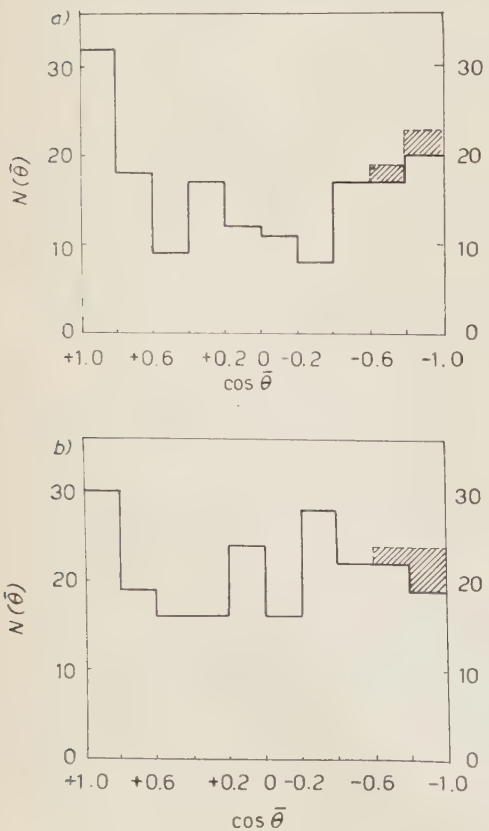

Fig. 4. – Angular distribution of secondary pions in the C-system of an interaction with a single nucleon: *a*) 4.5 GeV π^- interactions having $N_h \leqslant 7$; *b*) 6.0 GeV proton interactions having $N_h \leqslant 7$.

Clearly there will be a loss of particles emitted backwards in the C-system and appearing as grey tracks. From considerations of the velocity transformation it is evident that all particles emitted with $\cos \bar{\theta}$ greater than -0.6 appear as shower particles in the laboratory. Thus any correction for « grey » π-mesons is restricted to the region $-.6 > \cos \bar{\theta} \geqslant -1.0$. The correction for

grey tracks estimated from the results of Kamal is shown in Fig. 4 as a shaded region. We may perform a χ^2 test on the part of these distributions having $-.6 < +\cos\bar{\theta} < +1.0$ to examine their departure from isotropy. The result is that the proton distribution gives agreement with isotropy on the 30% level whilst the pion distributions yields a probability of less than 1%. This confirms the previous indications that the pion distribution is anisotropic whilst the proton distribution is consistent with isotropy.

In Section **10** of paper « I » the angular distribution of shower particles in the effective *C*-system of a composite 4.5 GeV pion nucleus interaction was given which includes events of all N_h. The transformation was chosen such that the distribution has equal numbers of tracks in the backwards and forward directions. This distribution therefore does not represent the distribution in the *C*-system of a pion-nucleon interaction.

It is clear from Fig. 4 that the anisotopy of the distribution of secondary pions from the pion induced interactions is in the form of a peak in the forward direction, a result which may explain why the collision partner for this group of events ($7 \leqslant N_h$) was found to be less than one proton mass unit (see paper «I »). This distribution is also in agreement with that obtained by the Berkeley group working with a hydrogen filled diffusion chamber (MAENCHEN *et al.* (6), WALKER (7)).

To summarize the results of this investigation we therefore have that the *C*-system angular distribution of secondary pions produced in 6 GeV proton interactions with emulsion nuclei deviates only slightly from isotropy whilst the distribution of pions from 4.5 GeV π^--interactions is anisotropic with a peak in the forward direction.

Discussion.

KALBACH *et al.* (8) have investigated the angular distribution of secondary pions from proton-proton interactions in emulsion at 6 GeV. These authors obtain an anisotropic distribution peaking in the backwards and forwards directions of the *C*-system, however the anisotropy was found to be smallest where the statistics are best. It is evident that if a small anisotropy exists in the elementary nucleon-nucleon collision then it may be reduced by secondary scattering interactions within the nucleus to give the result observed in the present experiment.

(6) G. MAENCHEN, W. B. FOWLER, W. M. POWELL and R. W. WRIGHT: *Phys. Rev.*, **108**, 850 (1957).

(7) W. D. WALKER: *Phys. Rev.*, **108**, 872 (1957).

(8) R. M. KALBACH, J. J. LORD and C. H. TSAO: *Phys. Rev.*, **113**, 330 (1959).

Results obtained by FRIEDLANDER ([9]) in an investigation of 9 GeV proton interactions in emulsion are consistent with isotropic emission in the C-system.

The results may easily be understood in terms of the isobar model of Sternheimer and Lindenbaum ([10]). If the result of a proton nucleon interaction is to produce, on average, two isobars which decay isotropically in their rest systems then the resulting C-system distribution will be approximately isotropic if the velocities of the isobars in the C-system are small compared with the velocities of the pions into which they decay. If the velocities of the isobars increase with the available energy quicker than the velocities of their decay products, then at higher energies the distribution will become anisotropic. Observations by the Polish Group (CIOK *et al.* ([11])) have provided strong evidence in favour of a two centres model for some high energy interactions. The application of such a model has been discussed in some detail by COCCONI ([12]), KRAUSHAAR and MARKS ([13]) and others.

The observed anisotropy in the 4.5 GeV π^- interactions can be explained if the process is one of inelastic excitation of the target nucleon with a recoil pion. The recoil pion will give rise to a peak in the forward direction whilst the isobar decays isotropically in the C-system. This model was discussed in detail by STERNHEIMER and LINDENBAUM ([10]).

* * *

We would like to thank Professor C. F. POWELL for extending to us the hospitality of his laboratory at Bristol.

The experiment was made possible by Professor W. H. BARKAS and others of the staff of the Radiation Laboratory, Berkeley who exposed the stacks and Dr. A. ENGLER of the Clarendon Laboratory, Oxford who loaned us plates exposed to the 6 GeV proton beam.

We are particularly thankful to Dr. D. H. PERKINS of this laboratory for his useful criticism and suggestions.

One of us (H.H.A.) would like to thank the government of Iraq and the other (C.M.F.) the Department of Scientific and Industrial Research for maintenance grants.

([9]) E. M. FRIEDLÄNDER: *Nuovo Cimento*, **4**, 794 (1959).

([10]) R. M. STERNHEIMER and S. J. LINDENBAUM: *Phys. Rev.*, **109**, 1723 (1958); **106**, 1107 (1957).

([11]) P. CIOK, T. COGHEN, J. GIERULA, R. HOŁYŃSKI, A. JURAK, M. MIĘSOWICZ, T. SANIEWSKA and J. PERNEGR: *Nuovo Cimento*, **10**, 741 (1958).

([12]) G. COCCONI: *Phys. Rev.*, **111**, 1699 (1958).

([13]) W. L. KRAUSHAAR and L. J. MARKS: *Phys. Rev.* **93**, 326 (1954).

RIASSUNTO (*)

Si sono studiate le distribuzioni angolari dei mesoni π prodotti in duecento interazioni di π^- di 4.5 GeV e in duecento interazioni di protoni di 6 GeV con nuclei della emulsione. Si trova che i pioni da interazioni indotte da protoni di 6 GeV sono coerenti con una distribuzione isotropica nel sistema C, mentre i pioni da interazioni indotte da π^- di 4.5 GeV hanno una distribuzione anisotropica con picco nella direzione anteriore. Il grado di anisotropia aumenta al diminuire dei valori N_h.

(*) *Traduzione a cura della Redazione.*

2343

(La responsabilità scientifica degli scritti inseriti in questa rubrica è completamente lasciata dalla Direzione del periodico ai singoli autori)

Proton Magnetic Resonance Study of Hydrates by Spinning Crystals.

R. CHIDAMBARAM

Department of Physics, Indian Institute of Science - Bangalore

(ricevuto l'11 Maggio 1960)

Sample spinning has been employed in nuclear magnetic resonance by earlier investigators with different objectives in view as, for example, to overcome partially field inhomogeneity in high-resolution work ([1,2]), to reduce the proton spin-lattice relaxation time in solid chlorobenzenes for particular proton magnetic resonance frequencies ([3]), and to prove the invariance of the second moment of a resonance line to motional narrowing ([4,5]). ANDREW has also indicated that the observation of the spectrum on a rapidly rotated specimen should assist in determining the sources of spectral broadening ([6]).

It is the purpose of this note to suggest that sample spinning can also be of assistance in structural investigations of crystals. An important application is to hydrates in which, by this technique, the resonance of the water molecule protons may often to a large extent be isolated from the resonances due to single protons or reorienting ammonium ions, if present. The basis of the method is that if a single crystal is spun about an axis, about which the nuclear magnetic resonance is not symmetric, then, in the vicinity of resonance, the r.f. voltage across the sample coil would be modulated at twice the frequency of the spin even in the absence of an external field modulation. The frequency of the spin should be much lower that the width of the resonance so that there may be no effects due to motional narrowing.

Let us consider the case of an identical interacting spin-$\frac{1}{2}$ pair (for example, the protons in a bound water molecule), all the pairs in the crystal being similarly oriented in space. The line shape function can be written ([7]), assuming Gaussian broadening, as

$$(1) \qquad g(h) = \frac{1}{2\beta\sqrt{2\pi}} \sum_{i=1,2} \exp\left[-\{h + (-1)^i \alpha(3\cos^2\varphi\cos^2\delta - 1)\}^2/2\beta^2\right],$$

([1]) F. BLOCH: *Phys. Rev.*, **94**, 496 (1954).
([2]) W. A. ANDERSON and J. T. ARNOLD: *Phys. Rev.*, **94**, 497 (1954).
([3]) D. E. WOESSNER and H. S. GUTOWSKY: *Journ. Chem. Phys.*, **29**, 804 (1958).
([4]) E. R. ANDREW, A. BRADBURY and R. G. EADES: *Nature*, **182**, 1659 (1958).
([5]) I. J. LOWE: *Phys. Rev. Lett.*, **2**, 285 (1959).
([6]) E. R. ANDREW: *Arch. Sci. (Geneva)*, **12**, 103 (1959).
([7]) G. E. PAKE: *Journ. Chem. Phys.*, **16**, 327 (1948).

where h is the difference between the applied field H and the resonance field H^* for an isolated nucleus: $(H - H^*)$; $\alpha = \frac{3}{2}\mu r^{-3}$; μ is the magnetic moment of the nucleus and r is the pair separation; δ is the angle between $\boldsymbol{r}$ and the plane containing the static field H and perpendicular to the axis of the r.f. coil; φ is the angle between the projection of $\boldsymbol{r}$ on the above plane and $\boldsymbol{H}$; β is the broadening factor which is assumed to be independent of φ in the following discussion.

If now the crystal is rotated about an axis coinciding with the axis of the r.f. coil at an angular frequency ω_r ($\ll 1/T_2$), φ in eq. (1) may be replaced by $\omega_r t$. If we write

$$(2) \qquad \begin{cases} h_1 \equiv \left(h + \alpha - \dfrac{3\alpha}{2}\cos^2\delta\right)\Big/\sqrt{2}\beta\,, \\ h_2 \equiv \left(-h + \alpha - \dfrac{3\alpha}{2}\cos^2\delta\right)\Big/\sqrt{2}\beta\,, \\ \varepsilon \equiv 3\alpha\cos^2\delta/2\sqrt{2}\beta\,, \end{cases}$$

eq. (1) reduces to

$$(3) \qquad g(h,t) = \frac{1}{2\beta\sqrt{2\pi}} \sum_{i=1,2} \exp\left[-\{h_i - \varepsilon\cos 2\omega_r t\}^2\right].$$

Using a phase-sensitive detector with a reference synchronised to the *fourth* harmonic of the frequency of spin, we can obtain an output signal at this frequency. The amplitude of the fourth harmonic can be shown from eq. (3) to be

$$(4) \qquad s_4(h) = \frac{1}{2\beta\sqrt{2\pi}} \sum_{i=1,2} \exp\left[-h_i^2\right] \{\sum_{r=1}^{\infty} (-1)^{r-1}\varepsilon^{2r} \sum_{k=0}^{r} (-1)^k A_k^r h_i^{2k}\}\,,$$

where

$$(5) \qquad A_k^r = \frac{r}{2^{r-k-1}(r+1)!\,k!\,(r-k)!} \cdot \frac{(2k-1)(2k+1)\ldots(2r-1)}{(2k-1)}\,.$$

An alternative form for $s_4(h)$ is the following:

$$(6) \qquad s_4(h) = \frac{1}{\beta\sqrt{2\pi}} \sum_{i=1,2} \exp\left[-h_i^2\right] \left\{\sum_{r=0}^{\infty} \frac{(-2)^r (h_i\varepsilon)^{2r}}{(2r)!} \cdot \frac{d^r}{d(\varepsilon^2/2)^r} \left(\exp\left[-\varepsilon^2/2\right] I_1(\varepsilon^2/2)\right)\right\}.$$

where I_1 is the modified Bessel function of the first order. It can be seen from eqs. (4) and (6) that $s_4(h)$ has two maxima at

$$(7) \qquad h = \pm\,\alpha(1 - \tfrac{3}{2}\cos^2\delta)\,,$$

(provided we neglect the very small effect of the presence of one maximum on position of the other) and that the height of each peak is given by

$$(8) \qquad p = \frac{1}{\beta\sqrt{2\pi}} \exp\left[-\varepsilon^2/2\right] I_1(\varepsilon^2/2)\,.$$

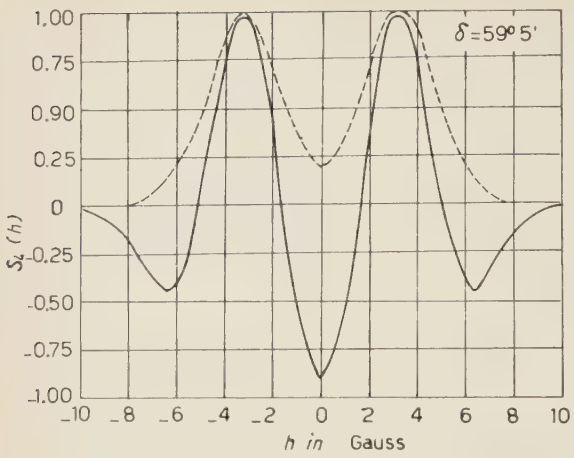

Fig. 1. – The fourth harmonic $s_4(h)$ output signal shape for a hydrate proton pair with $\alpha = 5.36$ G and $\beta = 1.5$ G. The broken curve is the sum of two Gaussians with $\beta = 1.5$ G and centred at the peak positions of $s_4(h)$.

The peaks correspond to resonances at $\varphi = \pm 45°, \pm 135°$, at constant δ in a static crystal, as is to be expected on physical considerations. The assumption of Gaussian broadening with a β independent of φ is unlikely to cause a significant error in eq. (7). It is preferable to use the fourth harmonic rather than the second harmonic because the latter does not appear to have maximum amplitude at a h which is a convenient function of α and δ.

Fig. 1 gives the $s_4(h)$ output curve calculated from eq. (4) for $\alpha = 5.36$ G (corresponding to the protons in a water molecule), a broadening factor $\beta = 1.5$ G and $\delta = 59° 5'$ ($\varepsilon = 1$). The peaks are seen to be sharper than those of Gaussians with the same β, indicated in the figure by the broken curve. Fig. 2 gives the variation of peak separation and peak height (p) with δ for the above values of α and β.

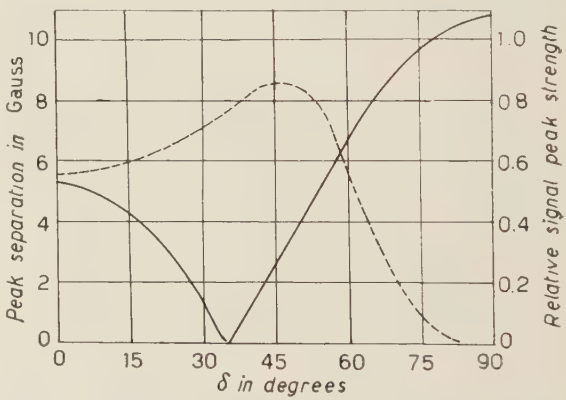

Fig. 2. – Variation of the peak separation (——) and the peak height p (– – –) with δ for a hydrate proton pair with $\alpha = 5.36$ G and $\beta = 1.5$ G.

The method of investigation described above appears well-suited for the study of hydrate protons in the presence of isolated protons or reorienting ammonium ions since the latter have approximately axially symmetric resonances in many cases and their contributions to the fourth harmonic output signal are likely to be small. It is felt that this method supplementing the normal static crystal method may be useful in structural investigations and we are shortly undertaking experiments in this direction.

* * *

The author is indebted to Professor R. S. Krishnan for his kind interest and encouragement, to Dr. G. Suryan for many helpful discussions and to Mr. A. K. Rajagopal and Mr. R. Sankar for generous assistance with the mathematics. He is also thankful to the Department of Atomic Energy for a Research Fellowship.

2316

IL NUOVO CIMENTO Vol. XVII, N. 1 1° Luglio 1960

Measurement of the Muon Mass by Critical Mesic X-Ray Absorption.

I: Scintillation Spectrometry (*).

J. Lathrop, R. A. Lundy (**), V. L. Telegdi (***),
R. Winston and D. D. Yovanovitch

The Enrico Fermi Institute for Nuclear Studies,
The University of Chicago - Chicago, Ill.

(ricevuto il 23 Maggio 1960)

Several authors have used the classical technique of critical absorption for establishing bounds for the transition energies E_{if} of mesic X-rays, and hence for the meson masses involved [1]. The K-edge taken as an infinitely sharp discontinuity in the absorption coefficient σ, of the absorber, is used as a reference energy E_K; one concludes that $E_{if} > E_K$, if the X-ray is « strongly absorbed », and $E_{if} < E_K$, if it is « transmitted ».

Actually, the K-edge is not a discontinuous jump of σ at the E_K, but rather a region where σ varies by a large factor (~ 5) over a narrow range (*e.g.* $\sim E_K/10^3$ for Pb). Provided that this variation of σ is known in detail, one can determine an E_{if} falling in this range very accurately (say, to $\pm E_K/10^4$) by measuring σ (E_{if}). We have applied this principle to the $3D \to 2P$ transition of mesic phosphorus, which according to the early work of Koslov [2] lies near E_K for Pb. Our work was stimulated by the remarks of Petermann and Yamaguchi [3] and made possible by the recent work of Bearden [4] on the Pb K-edge [5].

Fig. 1*a* shows positions of the two main fine structure components of the $3D \to 2P$ transition with respect to Bearden's Pb K-edge for three assumed muon masses; the insert in this figure is a fine structure level diagram of this $3D \to 2P$ transition. Fig. 1*b* shows the absorption curves predicted for the three situations indicated in Fig. 1*a*. These curves illustrate the sensitivity of the method

(*) Research supported by a joint program of the Office of Naval Research and the U. S. Atomic Energy Commission.

(**) National Science Foundation predoctoral fellow, 1959-60.

(***) Natioaal Science Foundation senior fellow, 1959-60. Temporary address, CERN, Geneva, Switzerland.

(1) For a summary, see D. West: *Rep. on Progr. Phys. London*, **21**, 271 (1958).

(2) S. Koslov, V. Fitch and J. Rainwater: *Phys. Rev.*, **95**, 291 (1954); S. Koslov: *Thesis* (Columbia, 1954); Nevis Report no. 19 (unpublished).

(3) A. Petermann and Y. Yamaguchi: *Phys. Rev. Lett.*, **2**, 359 (1959).

(4) A. J. Bearden: *Phys. Rev. Lett.*, **4**, 240 (1960).

(5) A preliminary account of the present work was given at the 1960 N.Y. Meeting of the A.P.S.

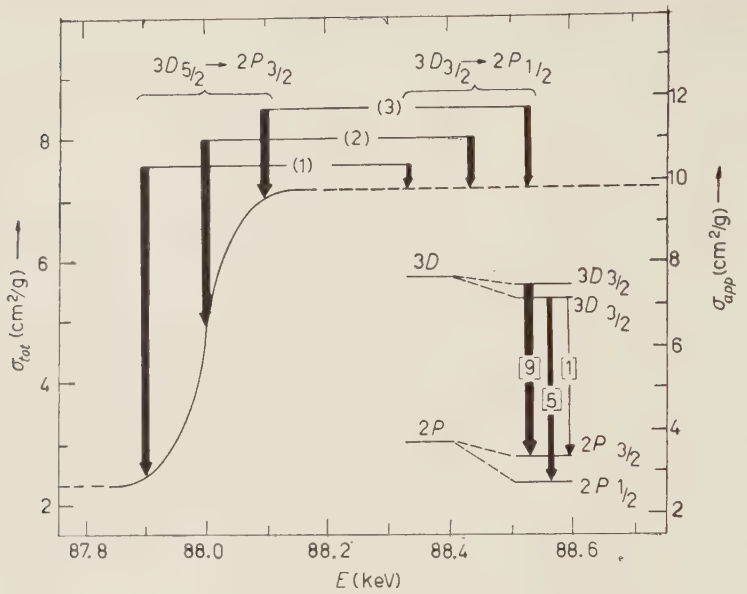

Fig. 1*a*. – Positions of the two main components of the $3D \rightarrow 2P$ transition of μ-mesic phosphorus with respect to the Pb *K*-edge, assuming for m_μ the values: 1) (206.56) m_e; 2) (206.74) m_e; 3) (206.92) m_e: σ_{tot} are the total absorptionc oefficients as measured by BEARDEN [4], σ_{app} are the « apparent » absorption coefficients defined in the text. The insert is the relevant level diagram (not to scale) with the relative line intensities indicated by number in [ ].

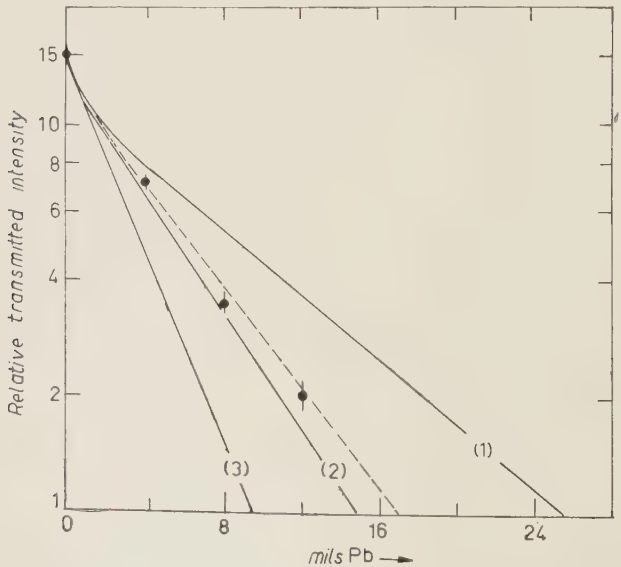

Fig. 1*b*. – Curves (1) through (3) are Pb absorption curves predicted from the σ_{app} of Fig. 1*a*, for the three muon masses assumed there. The full circles with flags are our experimental points with their statistical standard deviations; the dashed curve corresponds to assumption (2) but includes a correction for 10 % Compton degradation in the target.

N.B. - 1 mil Pb = $2.86 \cdot 10^{-2}$ g/cm².

inasmuch as they correspond to variations of the muon mass in steps of 0.1%.

μ-mesic X-rays in the energy range (10÷160) keV from a 2 g/cm²/P target were analysed, with and without Pb absorbers, with a NaI(Tl) spectrometer peaks of interest amount to about 10% and are due to accidentals and the Compton pedestals from higher transitions (mainly $2P \rightarrow 1S$). They were investigated in separate runs with extended energy range.

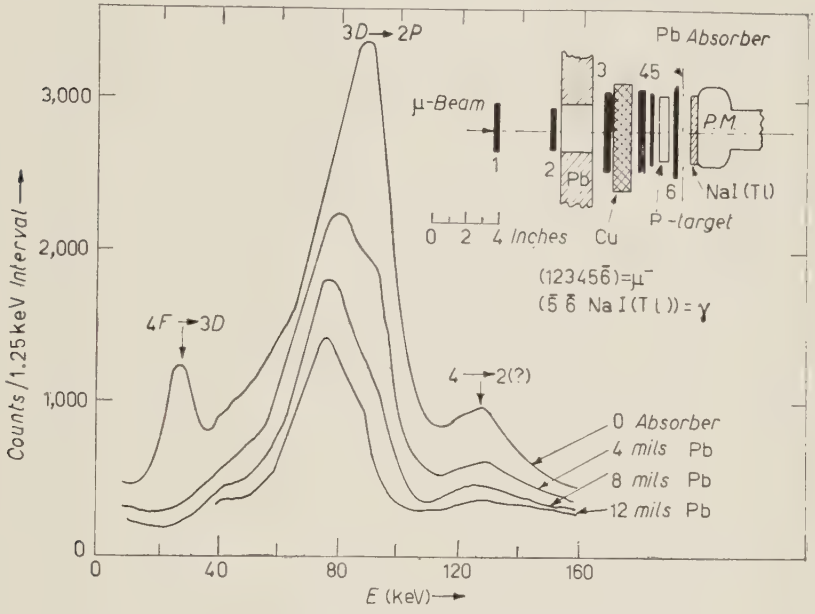

Fig. 2. – Typical μ-mesic X-ray spectra from P observed, without and through Pb absorbers, by means of the NaI(Tl) spectrometer schematically indicated in the insert. The assignment of the small peak at ~127 keV to a $4 \rightarrow 2$ transition is tentative.

(4 in. diameter, 0.25 in. thick). Fig. 2 reproduces the spectra recorded with 0, 4, 8, and 12 mils of Pb; the insert shows the experimental setup used. Each spectrum in Fig. 2 corresponds to $1.2 \cdot 10^6$ μ^--stops. The energy scale was calibrated with ^{170}Tm (53 and 84 keV lines). The zero absorber curve in Fig. 2 shows an essentially symmetric peak at 88 keV, corresponding to the $3D \rightarrow 2P$ line sought, while the 12-mils absorber curve shows a skew peak near 74 keV which we attribute to a combination of the Pb-K_α fluorescence radiation with the transmitted fraction of the $3D \rightarrow 2P$ line. The 4- and 8-mils curves are readily understood as intermediate situations. The backgrounds underlying the

The *apparent* transmission corresponding to the geometry used was extracted from the data in Fig. 2 in two independent ways after subtracting the background: (*A*) The spectra in the (60÷110) keV range were decomposed into two gaussians centered about 74 and 88 keV, of widths corresponding to resolutions of 24 and 22% respectively, experimentally determined for the same geometry ([6]). The area of the 88 keV gaussian was taken as the transmitted $3D \rightarrow 2P$ intensity. (*B*) Counts falling into the (88÷100) keV energy band were taken as due to transmitted $3D \rightarrow 2P$

([6]) Using «impregnated» targets; see text.

photons. A correction of 5% was applied in both cases to account for the Pb-K_β fluorescence radiation ($\sim$ 85 keV) which would tend to simulate transmitted 88 keV X-rays (7). Methods (*A*) and (*B*) gave within $\pm 5\%$ identical results and were, hence, averaged to obtain following trasmissions: 4 mils absorber, $(44 \pm 2)\%$; 8 mils Pb, $(21 \pm 2)\%$ and 12 mils Pb, $(12 \pm 3)\%$. The relative transmission intensities are plotted as full circles in Fig. 1*b*. The curves in that figure were computed using the apparent absorption coefficient σ_{app} (r.h.s. scale of Fig. 1*a*) for our geometry rather than the true absorption coefficient σ_{tot} measured by Bearden in good geometry. One has $\sigma_{tot} = \alpha\sigma_{app} + \sigma_{coh}$, where α represents the effect of oblique absorber traversals, while σ_{coh} is the attenuation coefficient for coherent scattering. The relation between σ_{tot} and σ_{app} was established empirically by measuring the transmission of the radiation from two *P* targets (identical with the mesic target proper), uniformly impregnated with the ^{170}Tm and ^{57}Co (122 keV) activities respectively. Only the high energy side of the NaI photopeaks was used to exclude the effects of the target degradation. Values of σ_{app} at 53, 84, and 122 keV were so obtained and extrapolated to the energies just above and just below the *K*-edge, yielding

$$\sigma_{app} = (9.8 \pm 0.6)\ \mathrm{cm^2/g}\,,$$

and

$$\sigma_{app} = (2.6 \pm 0.2)\ \mathrm{cm^2/g}\,,$$

respectively. Assuming σ_{coh} to be constant across the *K*-edge, we find

$$\sigma_{coh} = (0.4 \pm 0.2)\ \mathrm{cm^2/g}\,,$$

in reasonable agreement with theory (8). The experimental value $\alpha^{-1} = 1.35 \pm 0.05$ agrees well with the value 1.38 predicted numerically for this geometry.

Fig. 1*b* shows that the experimental points lie closest to curve (2), *i.e.* that the $3D_{\frac{5}{2}} \to 2P_{\frac{3}{2}}$ component falls near the center of the *K*-edge. The Compton degradation within the target, so far neglected, tends to simulate a smaller σ_{app} for the situation considered in Fig. 1*a*. The fraction of photons of 88 keV degraded by $\leqslant 8$ keV in our target, *i.e.* into an energy band that would fall under the transmitted « 88 keV » photopeak, is $\leqslant 20\%$, while our best estimate of this fraction is 10%. Using this estimate, one predicts for situation (2) in Fig. 1*a* the dashed curve in Fig. 1*b*.

One obtains the best fit for our points, assuming a 10% degradation correction, when the $3D_{\frac{5}{2}} \to 2P_{\frac{3}{2}}$ line is assumed to lie at 87 992 keV on Bearden's curve. This corresponds, accepting the calculation of reference (3), to $m_\mu = 206.74\ m_e$.

Uncertainties in this value arise primarily from our limited knowledge of the Compton degradation in the target. Assuming either zero or maximum (20%) degradation, we obtain the limits

$$(1) \qquad m_\mu = (206.74 \pm^{0.03}_{0.04})\ m_e\,,$$

This is to be compared with

$$(2) \quad m_\mu = (\mathrm{QED}) = (206.77 \pm 0.013)\ m_e\,,$$

the muon mass derived from Columbia's corrected value (9) for the muon magnetic moment, assuming that quantum electrodynamics (QED) predicts the muon *g*-factor correctly.

Several minor effects have been neglected in the analysis leading to eq. (1). The h.f. splitting (coupling muon-nucleus)

(7) We are indebted to Prof. G. WENTZEL for drawing our attention to this point. Fortunately, the K_β fluorescence yield is small.

(8) K. SIEGBAHN: *Beta and Gamma Ray Spectroscopy* (New York, 1955).

(9) R. L. GARWIN, G. W. HUTCHINSON, S. PENMAN and M. M. SHAPIRO: *Phys. Rev. Lett.*, **2**, 516 (1959).

2320

is significantly larger ([10]) ($\sim$ 20 eV) than the radiation width only for the $3D_{\frac{3}{2}} \to 2P_{\frac{1}{2}}$ transition. This transition lies, however, in a region of the Pb absorption curve where the latter is assumed to be constant for the lack of detailed information. Small variations in σ_{tot} within a few hundreds of eV from the K-edge (Kronig effect) are indeed known for other elements ([11]) but would not have been detected for Pb with Bearden's resolution ([12]). Whether the $3D_{\frac{3}{2}} \to 2P_{\frac{1}{2}}$ « line » falls onto such a variation in σ_{tot} is an open question but, in any case, the h.f.s. may decrease the consequences of such a coincidence. One may also consider a h.f. type coupling between the muon and an unpaired electron in the P atom ([7]). This coupling is, however, even for $1s$ electrons about a factor $(m_\mu/m_e)^3(m_e/M_p)$ smaller than the h.f.s. effect just considered.

([10]) The h.f.s. entry of Table I in ref. ([3]) is distorted by a misprint. In connection with the energies of the three lines, the h.f.s. effects were not discussed in ref. ([3]).

([11]) See, for instance, L. G. PARRAT: *Rev. Mod. Phys.*, **31**, 616 (1959).

([12]) A. J. BEARDEN: private communication.

* * *

We are grateful to Dr. A. BEARDEN for making his results available prior to publication. We are grateful to Professor G. WENTZEL for much constructive criticism, and to Dr. S. PENMAN for useful discussions.

Measurement of the Muon Mass by Critical Mesic X-Ray Absorption.

II. – Proportional Counter Spectrometry (*).

J. Lathrop, R. A. Lundy (**), S. Penman, V. L. Telegdi (***),
R. Winston and D. D. Yovanovitch

The Enrico Fermi Institute for Nuclear Studies,
The University of Chicago - Chicago, Ill.

A. J. Bearden
University of Wisconsin - Madison, Wisc.

(ricevuto il 23 Maggio 1960)

The work of West and associates [1] has clearly demonstrated the advantages of proportional counters (P.C.) over NaI(Tl) crystals in the spectrometry of low-energy mesic X-rays. For a study of the critical absorption of the 88 keV $3D \to 2P$ transition of mesic phosphorus — such as has recently been completed here [2] by means of a NaI(Tl) spectrometer — the use of a P.C. offers the following specific advantages:

(*a*) Cleaner separation of the photopeak due to the transmitted 88 keV line from the photopeak due to the 74 keV Pb-K_α fluorescence excited in the absorbers;

(*b*) Smaller contamination of the « 88 keV » photopeak by $3D \to 2P$ radiation Compton degraded in the phosphorus target.

Both (*a*) and (*b*) are consequences of the $(3 \div 4)$ times better energy resolution (at 88 keV) given by the P.C. The Xe-K_α escape peaks which accompany the photopeaks of a Xe-filled P.C. share their advantages and afford in addition the possibility of independent checks.

P.C. spectrometry should enable one to decrease appreciably some of the systematic uncertainties encountered in I and thus to obtain a more accurate value of the muon mass. We describe here an independent measurement of the relevant absorption coefficient by this technique. This measurement is further based on

(*) Research supported by a joint program of the Office of Naval Research and the U. S. Atomic Energy Commission.

(**) National Science Foundation predoctoral fellow, 1959-60.

(***) National Science Foundation senior fellow, 1959-60. Temporary address, CERN, Geneva, Switzerland.

(1) D. West, R. Batchelor and E. F. Bradley: *Proc. Phys. Soc. London*, A **68**, 801 (1955); D. West and E. F. Bradley: *Phil. Mag.*, **1**, 97 (1956); **2**, 957 (1957).

(2) J. Lathrop, R. A. Lundy, V. L. Telegdi, R. Winston and D. D. Yovanovitch: preceding work. This experiment will be referred to here as I.

a more refined determination of the effective absorber thicknesses than I (see « Calibration », below).

A P.C. was substituted for the NaI(Tl) assembly in a setup very similar to the one shown as an insert in Fig. 2 of I. It consisted of 2 in. diameter, 11 in. long Al pipe of 1/32 in. wall thickness, provided with a 0.005 in. W center wire, and filled with 2.5 atm of Xe and 2.5 cm Hg of CH_4. The two end sections of the pipe were wrapped with deteriorated. During the experiment, such a purification had to be performed every 24 h.

The P.C. was operated at 4 500 V, and gave pulses with less than 2 μs jitter. A prompt coincidence of 3 μs resolution with the signal indicating a muon stop in the target was made, and used to gate a 100 channel pulse-height analyzer ([3]). The threshold of this gate corresponded to an X-ray energy of < 10 keV, and was kept constant. The

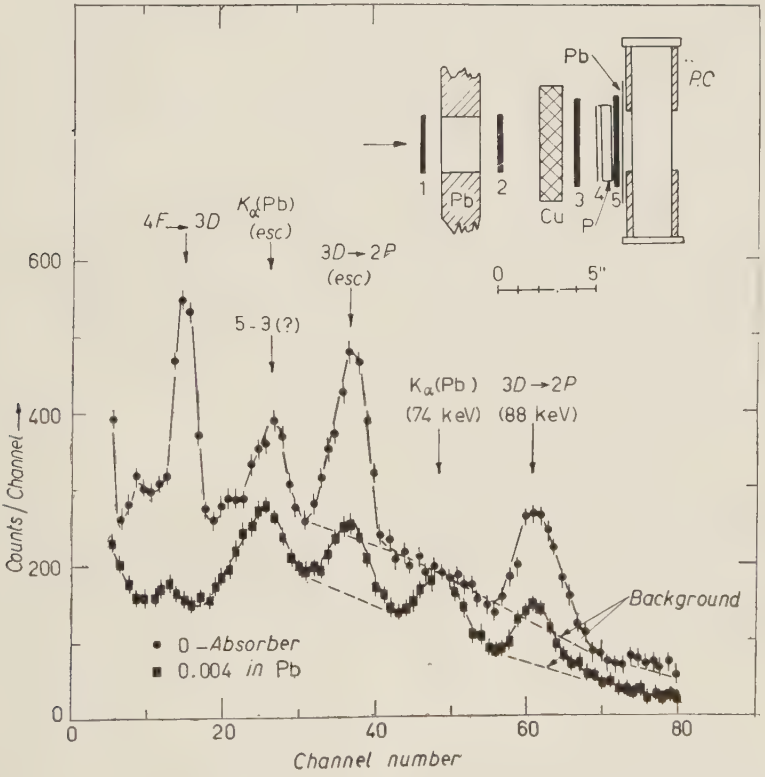

Fig. 1. – Typical μ-mesic spectra from phosphorus target observed without and through Pb absorber, by means of Xe-filled (2.5 atm) P.C. The errors indicated are statistical standard deviations.

Cd foils, leaving an unshielded effective volume of only 3 in. length in the middle. The P.C. was permanently attached to a purifying system which enabled one to pass the filling mixture readily over hot (350 °C) Ca whenever the resolution integrating time constants of the P.C. and of the preamplifier and amplifier following it were so chosen that the

([3]) One section of an RIDL 400-channel analyzer.

instantaneous counting rates of the experiment ($1.5 \cdot 10^3$ P.C. pulses/s) entailed no impairment of energy resolution nor appreciable dead-time losses.

Mesic X-ray spectra from a 2 g/cm^2 red phosphorus target, in the energy range (10÷114) keV, were recorded with Pb absorbers of zero, 4 and 8 mils thickness ([4]). Each run included $3 \cdot 10^5$ muon stops in the target, and took about 2 h. After each run, the P.C. spectrometer was calibrated with an ^{241}Am source (60 keV); and the variation in gain was kept to $< 1\%$ in the course of the entire experiment. Typical zero and 4 mils absorber spectra, each resulting from $1.5 \cdot 10^6$ muon stops, are reproduced in Fig. 1. Essentially the same peaks as in Fig. 2 of I are observed, except that the $3D \to 2P$ photopeak (88 keV) and the Pb-K_α photopeak (74 keV) are accompanied by escape peaks lying ~ 30 keV (the Xe-K_α energy) lower. The peak tentatively assigned to a $5 \to 3$ transition appears in the zero absorber spectrum, but overlaps with the Pb-K_α escape peak in the 4 mils spectrum. The peaks of interest to the transmission measurement are seen to ride on a sloping background, the energy dependence of which appears to follow the efficiency curve of our P.C.

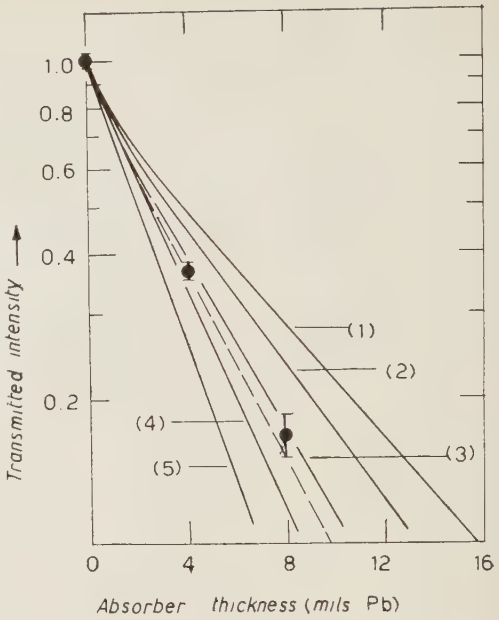

Fig. 2. – Curves (1) though (5) are Pb absorption curves calculated from Bearden's values of σ_{tot} across the Pb K-edge (corrected for our geometry), corresponding to the following assumed muon masses: 1) 206.62 m_e; 2) 206.68 m_e; 3) 206.74 m_e; 4) 206.80 m_e; and 5) 206.86 m_e. The dashed curve corresponds to $m_\mu = 206.76\ m_e$ and is the best fit to our experimental points as quoted in the last column of Table I.

TABLE I. – *List of experimental trasmitted intensities of $3D \to 2P$ mesonic transition in phosphorus for given* Pb *absorber thicknesses and of relevant correction factors.* The last column gives corrected transmitted intensities as plotted on Fig. 2.

Pb absorber thickness	Transmitted intensity (experimental values)	Correction factors: $f_{K\beta}$	Correction factors: f_{Compt} (*)	Correction factors: f_{coh}	Corrected transmitted intensity
0 mils	1.00±0.04	1.00	1.00	1.00	1.00±0.04
4 mils	0.42±0.03	0.95±0.01	0.94	0.97±0.01	0.36±0.03
8 mils	0.22±0.02	0.90±0.01	0.89	0.94±0.03	0.17±0.02

(*) The Compton correction factors correspond to upper limit estimates of the effect. In the final mass evaluation the full magnitude of the effect is allowed as its uncertainty.

([4]) Pb sheets identical with those used by Bearden in his K-edge measurement [ref. ([5])] were employed.

This background is due partly (30%) to non beam-coincident events (accidentals) and partly to prompt photons of uncertain origin (*e.g.* from the de-excitation of μ-capture products, π-mesic background, e-bremsstrahlung, etc.).

The data analysis is summarized in Table I. After background subtraction, the sum of counts in the $3D \to 2P$ photo and escape peaks was normalized to the number obtained with zero absorber. To these normalized experimental values (column I) we applied corrections for (i) the Pb-K_β fluorescence radiation (the yield of which was determined separately with the help of the 120 keV gammas from ^{57}Co); (ii) coherent scattering by Pb; and (iii) Compton scattering. The relevant factors used are listed in Table I, and yield the corrected intensities listed in its last column. These are plotted in Fig. 2 as full circles, with errors which include statistical standard deviations as well as systematic uncertainties in the listed corrections.

1. – Calibration.

To relate the known ([5]) Pb absorption coefficients σ_{tot} to our experimental results it suffices (neglecting coherent scattering in the Pb foils and Compton degradation in the P target) to determine the relative transmitted intensity T *vs.* Pb foil thickness x for a γ-source for which the mass absorption coefficient is known, which reproduces the muon stop distribution in the P target, and for which the detection efficiency in the P.C. is identically to that at 88 keV photon energy. In fact, knowing $T(\sigma x) \equiv \equiv T(\varrho)$ (ϱ dimensionless) one can predict, for our experimental set-up, the transmitted intensity for photons having arbitrary mass absorption coefficients. In practice, this calibration was performed with a 60 keV point source (^{241}Am), with the Xe pressure reduced to 1.1 atm to bring about the same efficiency as obtains for 88 keV photons at 2.5 atm. The absorption measurements were carried out for a series of source positions throughout the target volume, weighting the results with the known muon stop distribution. Finally, the absolute absorption coefficient σ_{tot} for the 60 keV radiation was determined in good geometry. The result of the calibration was a plot of $T(\varrho)$ *vs.* $\ln \varrho$, giving an essentially straight line. The effect of the geometry of the setup is summarized by a factor $f = 1.47$ (accurate to $\pm 4\%$) by which the actual thicknesses of the Pb foils have to be multiplied to obtain their *effective* thicknesses ([6]). A correction for Compton degradation in the target in the calibration runs affects f by $< 1\%$.

Fig. 2 shows transmission curves predicted for a set of assumed muon masses, using the calculations of Petermann and Yamaguchi ([7]), ref. ([5]), and this f. We emphasize that the plotted experimental points are corrected for Pb-K_β fluorescent radiation, coherent scattering, and for Compton degradation in the target. The fraction of photons which are Compton degraded and which one would tend to include in the observed « 88 keV » photo and escape peaks is estimated as $\leqslant 7\%$. The dashed curve in Fig. 2 is a best fit to our experimental points, and corresponds to a μ^- mass.

$$(1) \qquad m_\mu = (206.76 \pm^{0.02}_{0.03}) \, m_e \, ,$$

the asymmetry in the assigned errors being due to an allowance for our imperfect knowledge of the actual magnitude of the Compton degradation in the P target. The cautionary remarks at

([5]) A. J. Bearden: *Phys. Rev. Lett.*, **4**, 240 (1960).

([6]) The work of ref. ([2]), done in different geometry, gave $f = 1.35$.

([7]) A. Petermann and Y. Yamaguchi: *Phys. Rev. Lett.*, **2**, 359 (1959).

the end of ref. [2], concerning the possible effects of various minor atomic phenomena on this type of experiment, fully apply here as well.

(1) is in excellent agreement with the mass value obtained in I, and lies even closer to

$$(2) \quad m_\mu(\mathrm{QED}) = (206.77 \pm 0.013)\ \mathrm{m_e}\,,$$

the value derived from Columbia's μ^+ moment measurement [8], assuming that quantum electrodynamics (QED) predicts the muon g-factor g_μ correctly [9]. Conversely, accepting (1) and the result of ref. [8], one finds

$$(3) \quad (g_\mu/2 - 1) = 0.00113 \pm^{0.00012}_{0.00017}\,,$$

while QED predicts to lowest order

$$(4) \quad (g_\mu/2 - 1)_{\mathrm{QED}} = \alpha/2\pi = 0.00116\,.$$

[8] R. L. Garwin, G. W. Hutchinson, S. Penman and M. M. Shapiro: *Phys. Rev. Lett.*, **2**, 516 (1959). Also Nevis Report no. 79 (July 1959) (unpublished).

[9] In comparing (1) and (2), we rely implicitly on the *TCP* theorem which guarantees identical magnetic moments for anti-particles. Cfr. G. Grawert, G. Lüders and H. Rollnik: *Fortschr. d. Phys.*, **7**, 318 (1959).

The best present estimate for the π^+-μ^+ mass difference is [10]

$$(5) \quad m_{\pi^+} - m_{\mu^+} = (66.41 \pm 0.10)\ \mathrm{m_e}\,,$$

which yields with (1)

$$(6) \qquad m_\pi = (273.17 \pm 0.11)\ \mathrm{m_e}\,,$$

in agreement with the accepted value

$$(7) \qquad m_\pi = (273.27 \pm 0.11)\ \mathrm{m_e}\,,$$

and with the limits [10]

$$(273.18 \pm 0.11)\ \mathrm{m_e} \leqslant m_\pi \leqslant \leqslant (273.51 \pm 0.04)\ \mathrm{m_e}\,.$$

* * *

We are greatly indebted to Dr. R. West (Harwell) for much helpful advice on proportional counter design, and to Prof. C. S. Wu for very useful correspondence. We wish to thank Prof. G. Wentzel for several illuminating discussions, and Dr. K. M. Crowe for the loan of a tank of Xe gas.

[10] K. M. Crowe: *Nuovo Cimento*, **5**, 541 (1957).

2326

Cosmic Ray Intensity Increase on May 4, 1960.

O. R. Santochi, J. R. Manzano and J. G. Roederer
Comision Nacional de Energía Atómica - Buenos Aires

(ricevuto il 17 Giugno 1960)

On May 4, 1960, the Ellsworth neutron monitor (*) detected a sudden, big increase of about 110% in quarter hourly counting rate, in the interval (1030÷÷1045) UT. After this initial peak, intensity dropped to the previous level after about two hours. Ellsworth was located in the 09 impact zone for a solar event occuring at 1030 (1).

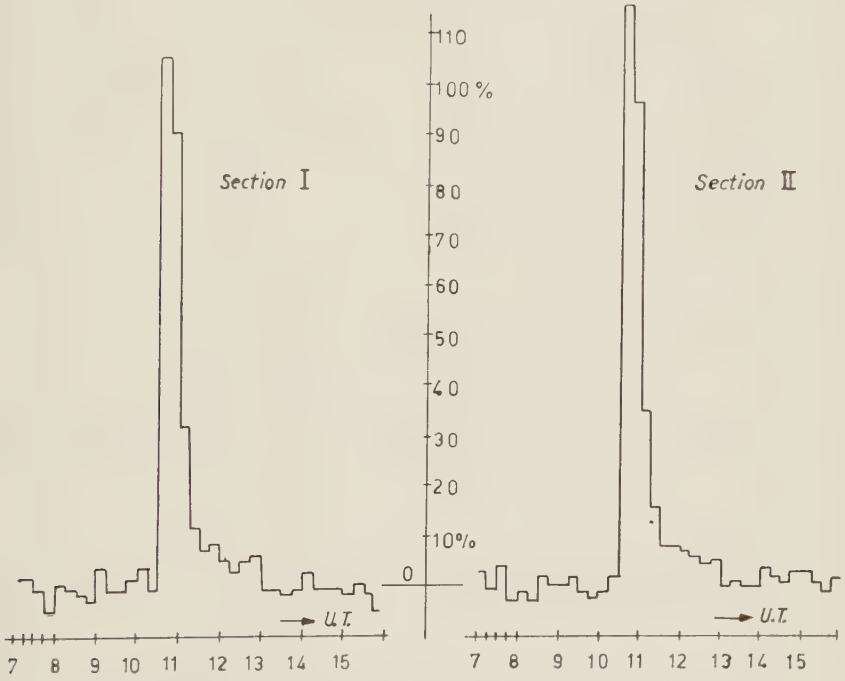

Fig. 1. – Percentage intensity variation referred to preflare level, for sections I and II of the Ellsworth neutron monitor. 15 min interval data.

(*) Geomagnetic coordinates: Lat. 67° S, Long. 14.7° E. Operated in collaboration with the Instituto Antártico Argentino and the University of California.

(1) J. W. Firor: *Phys. Rev.*, **94**, 1017 (1954).

Fig. 1 gives the 15 min counting rate percentage intensity variation of neutron monitor sections I and II, referred to the preflare level. Unfortunately, only 15 min readings are available. Section II shows a relative increase systematically higher than section I:

$$\delta I_{II}/\delta I_I = 1.10 \pm 0.02 .$$

additional flux. Indeed, for other time variations, like the July 1959 Forbush decreases, which have a flatter spectrum [2], percentage variations of sections II and I of the Ellsworth neutron monitor show a ratio 1.03 ± 0.02.

In order to determine the approximate time of the beginning of the increase, we plotted the integrated additional

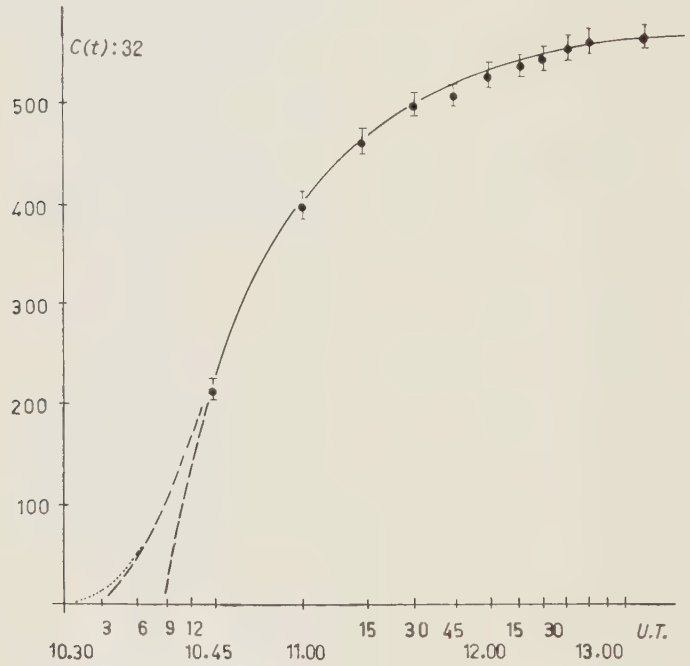

Fig. 2. – Integrated additional counting rate (sum of both sections) for 15 min readings. The extrapolation of the curve to zero counting rate gives an idea of the time of the beginning of the increase.

According to the geometry of this neutron monitor (section II lying above section I, Berkeley type), the coupling function for section I should be slightly displaced towards higher energies than that of section II, due to the increased absorbing material above section I with respect to section II. The fact that both sections do show an appreciable difference during this increase is an indication for a steep energy spectrum, or, what is the same for a small absorption length of the

counting rate

$$C(t) = \int_{t_0}^{t} (I - I_0)\, dt', \qquad (\mathrm{I} + \mathrm{II}),$$

where I is the 15 min counting rate and I_0 the mean counting rate before

(2) J. G. ROEDERER, O. R. SANTOCHI, J. C. ANDERSON, J. M. CARDOSO and J. R. MANZANO: *Preliminary report on cosmic ray intensity during magnetic storms in July* 1959, preprint C.N.E.A., 1959.

2328

the increase. Fig. 2 shows the result.

If we assume tentatively a very fast increase, the time of rise lasting not more than a couple of minutes, one may extrapolate the curve to 0 counting rate in order to get some information about the probable starting time. We obtain the values 1033 and 1039 UT as estimated lower and upper time limits for a sudden intensity rise. Taking this into account, the lower and upper limits of maximum intensity increase would have been of 138% and 277%, respectively, averaged over the time interval between start and 1045 UT. These considerations, of course, do not exclude the possibility of a slower rise starting at any time between 1030 and 1033.

Finally, neutron monitors of Mina Aguilar (geom. Lat. 11.6° S, Long. 3.1° E) and Buenos Aires (geom. Lat. 23.3°s, Long. 9.4° E) did not show any abnormal behaviour on the 4th of May. As it now seems to be usual for all interesting cosmic ray events, Ushuaia had a power supply failure starting exactly at 1030 UT. Ushuaia was located in the 04 impact zone.

* * *

This report was possible only due to the extremely efficient work of our technicist, Mr. R. Rastelli, who keeps operating the Ellsworth neutron monitor in spite of innumerable difficulties.

2329

Finite Value of the Wave Function Renormalization Constant in Quantum Electrodynamics.

I. Bialynicki-Birula (*)

University of Rochester - Rochester, N. Y.

(ricevuto il 20 Giugno 1960)

In a recent paper by Johnson and Zumino [1] the question has been raised whether there exists a special gauge which gives finite value of the electron wave function renormalization constant. The aim of this note is to prove that there exists a class of gauges which give a finite (as far as ultraviolet [2] divergences are concerned) value for this constant in every order of perturbation theory. It was noticed by Zumino [3] that one can get finite value for the Z constant [4] in the second order using Landau's gauge defined by the transverse form of the photon propagator,

$$(1) \quad D^T_{\mu\nu}(k) = (-g_{\mu\nu} + k_\mu k_\nu k^{-2})k^{-2} .$$

The second order result remains unchanged if Landau's gauge is modified in the following way,

$$(2) \quad D^M_{\mu\nu}(k) = D^T_{\mu\nu}(k) - k_\mu k_\nu k^{-4} f(e, k) ,$$

where the function $f(e, k)$ is given by a power series in renormalized charge,

$$(3) \qquad f(e, k) = f_1(k)e^2 + f_2(k)e^4 + \dots .$$

Our procedure will be to show that the $f_i(k)$ coefficients can be chosen in such a way that Z is finite in every order of perturbation theory. The proof will proceed by induction. Let us assume that Z is finite up to the $2n$-th order and let us consider the vertex part up to the $2(n+1)$-th order. This vertex part is a sum of the contributions from all irreducible diagrams and from skeleton diagrams with inserted self-energies and vertex parts. After mass renormalization all inserted electron self-energies and vertex parts become finite on the basis of our induction assumption. All inserted photon self-energies become finite after charge renormalization because the divergent factor Z_3 is absorbed into the charge at the vertices joined by the photon propagator under consideration. The arguments show that

(*) On leave of absence from Warsaw University, Warsaw, Poland.

(1) K. Johnson and B. Zumino: *Phys. Rev. Lett.*, **3**, 351 (1959).

(2) We will not discuss here the infrared divergence, assuming that it is removed by a small photon mass λ.

(3) B. Zumino: *Journ. Math. Phys.*, **1**, 1 (1960).

(4) Z *denotes* Z_1 and Z_2; which are equal due to the Ward identity.

the divergence is only logarithmic (5) for both irreducible and reducible diagrams since it appears at the final integration. This divergence can be always cancelled by an appropriate choice of the function $f_n(k)$ which appears for the first time in the calculation of the $2(n+1)$-th order correction to the vertex part. The contribution from $f_n(k)$ can be obtained by inserting the modified photon propagator (2) into the lowest order vertex part. This term has the form

$$(4) \qquad -\frac{(e^2)^{n+1}}{(2\pi)^4 i}\int \frac{\mathrm{d}^4 k}{k^4}\, \boldsymbol{k}\, \frac{1}{\boldsymbol{p}-\boldsymbol{k}-m}\cdot \gamma^\mu \frac{1}{\boldsymbol{q}-\boldsymbol{k}-m}\, \boldsymbol{k} f_n(k)\,.$$

This integral is also logarithmically divergent so the divergent terms of the vertex part in $2(n+1)$-th order can be cancelled if we choose the function $f_n(k)$ in the form of polynomial

$$(5)' \qquad f_n(k) = a_{n0} + a_{n1} \ln k^2 + \ldots + a_{nn} (\ln k^2)^n\,,$$

with the properly adjusted coefficients a_{ni}. Our argument shows that these coefficients are *finite*. Using this procedure we can make Z finite in every order, computing step by step the functions $f_i(k)$. This prescription is not unique because we can always change the $f_n(k)$ function in such a way that the divergent part of the integral (3) is not affected. It corresponds to a gauge transformation which multiplies Z by a finite factor.

* * *

The author is greatly indebted to Drs. C. J. Goebel, J. C. Taylor and E. C. G. Sudarshan for many helpful discussions and essential suggestions.

(5) By logarithmic divergence we mean any divergence of the form $\int \mathrm{d}^4 k k^{-4} (\ln k^2)^m$.

2331

Equivalence Principle «Paradox» in the Motion of a Gyroscope.

L. I. Schiff (*)

Faculté des Sciences - Orsay (**)

(ricevuto il 4 Luglio 1960)

In this note we describe an apparent violation of the equivalence principle that arises in connection with the precession of the spin axis of a gyroscope moving in a uniform gravitational field. The «paradox» is then resolved by a realistic specification of what is meant by the term uniform.

The rate of change of the spin angular momentum $\boldsymbol{S}_0$ of a gyroscope, as measured by a co-moving observer, has been derived in a recent paper [1]. If the gyroscope moves in the gravitational field external to a non-rotating, spherically symmetric mass m, and is acted on by a non-gravitational force $\boldsymbol{F}$ that exerts no torque on the gyroscope, the spin equation of motion is

$$(1) \qquad (\mathrm{d}\boldsymbol{S}_0/\mathrm{d}t) = \boldsymbol{\Omega} \times \boldsymbol{S}_0 ,$$

where

$$(2) \qquad \boldsymbol{\Omega} = (1/2m_0c^2)(\boldsymbol{F} \times \boldsymbol{v}) + (3Gm/2c^2r^3)(\boldsymbol{r} \times \boldsymbol{v}) .$$

Here G is the Newtonian gravitational constant, c is the speed of light, m_0 is the rest mass of the gyroscope, $\boldsymbol{r}$ is its position vector with respect to the center of the attracting mass m, and $\boldsymbol{v} = (\mathrm{d}\boldsymbol{r}/\mathrm{d}t)$ The first term on the right side of (2) is the special-relativistic Thomas precession, and the second term is the general-relativistic de Sitter-Fokker effect.

It might be supposed that a uniform gravitational field can be obtained by allowing m and r to become very large in such a way that the local acceleration of gravity

$$(3) \qquad g = Gm/r^2 ,$$

retains a definite value. Then if the motion is quasi-static,

$$(4) \qquad \boldsymbol{F} = m_0 g \hat{\boldsymbol{r}} ,$$

where $\hat{\boldsymbol{r}} = \boldsymbol{r}/r$, and

$$(5) \qquad \boldsymbol{\Omega} = (2g/c^2)(\hat{\boldsymbol{r}} \times \boldsymbol{v}) .$$

As a simple example of eq. (5), we assume that $\hat{\boldsymbol{r}}$ is directed vertically upward along the positive z-axis and $\boldsymbol{v}$ is directed horizontally along the positive x-axis. Then Ω is along the positive y-axis, and has the magnitude

(*) Supported in part by the United States Air Force through the Air Force Office of Scientific Research.

(**) Permanent address: Institute of Theoretical Physics, Department of Physics, Stanford University, Stanford, Cal.

(1) L. I. Schiff: *Proc. of the National Academy of Sciences* (June 1960).

$(2gv/c^2)$. If then $\boldsymbol{S}_0$ is vertical and the gyroscope moves a distance Δx, the upper end of its spin axis tilts forward through the angle

$$(6) \qquad \theta_T = |\Delta \boldsymbol{S}_0|/|\boldsymbol{S}_0| = (2g\,\Delta x/c^2)\,.$$

According to the equivalence principle, this tilt angle should agree with that found when the gyroscope is subjected to an upward acceleration g in the absence of the gravitational field. This may be obtained from eqs. (1) and (2) by setting $m=0$, retaining the expression (4) for $\boldsymbol{F}$, and replacing $\boldsymbol{v}$ by $\boldsymbol{v}+gt\hat{\boldsymbol{r}}$. It follows that the tilt angle measured by a co-moving observer is $(g\,\Delta x/2c^2)$, which is one quarter that given by eq. (6).

This « paradox » may be resolved by noting that the gravitational field is not strictly uniform so long as m and r are finite. The essential parameter in the Schwarzschild metric is (Gm/c^2r), which is always less than or of order unity. In all practical cases, it is very much smaller than unity, and indeed the derivation of eqs. (1) and (2) is only valid when this is the case. But from eq. (3), we see that

$$(7) \qquad P \equiv (Gm/c^2r) = (gr/c^2)\,,$$

so that this parameter becomes arbitrarily large if g is fixed and r increases without limit.

A measure of the non-uniformity of the field is provided by the angle of divergence $\theta_D = (\Delta x/r)$ between the field lines at the ends of the path of the gyroscope. It should be noted that this path must cut across the field lines, since $\boldsymbol{\Omega}$ given by (5) is zero if $\boldsymbol{v}$ is parallel to $\hat{\boldsymbol{r}}$. Now θ_D may be expressed in terms of the tilt angle (6) and the Schwarzschild parameter (7), as $\theta_D = (\theta_T/2P)$. Since $P \ll 1$, we see that $\theta_D \gg \theta_T$. Thus if the precession of the gyroscope axis is to be significant, the gravitational field cannot be regarded as uniform, and the equivalence principle is not applicable.

We conclude that the tilt angle is actually given by eq. (6). Of this amount, one quarter may be calculated from the equivalence principle. The other three quarters may be thought of physically as the result of an almost completely unsuccessful attempt of the spin axis of the moving gyroscope to follow the changing direction of the gravitational field. The coupling between the gravitational field and the inertial coordinate system of the gyroscope is very weak, of order the Schwarzschild parameter P, so that the tilt angle is very much smaller than the divergence angle.

LIBRI RICEVUTI E RECENSIONI

Libri ricevuti.

R. B. Adler and Lan Jen Chu: *Electromagnetic Energy Transmission and Radiation*: J. Wiley and Sons, New York, 1960.

M. Bayet: *Physique Nucléaire*; Masson et Cie., Paris, 1960; NF. 65.

R. H. Bube: *Photoconductivity of Solids*; J. Wiley and Sons Inc. Publishers, New York, 1960; $ 14.75.

M. Duquesne, R. Gregoire et M. Lefort: *Travaux pratiques de physique nucléaire et de radiochimie*; Masson et Cie., Paris, 1960; pp. 324; NF. 39.

Jones and Hawkins: *Engineering Thermodynamics* (an instructory text book); J. Wiley and Sons, New York, 1960.

F. L. Hill: *Introduction to Statistical Thermodynamics*; Addison-Wesley Pub. Co. Inc. Reading (Mass.), 1960; pp. xiv-508; $ 9.75.

J. G. Jones and G. A. Atkins: *Engineering Thermodynamics*; J. Wiley and Sons, New York, 1960.

J. S. Levinger: *Nuclear Photo-Disintegration*; Oxford Library of the Physical Sciences, 1960, pp. 144; sh 15.

M. W. Wolkenstein: *Structur und Physikalische Eigenschaften der Molekule*; G. B. Teubner Verlagsgesellschaft, Leipzig, 1960, pp. xiv-770; D.M. 58.

Applied Gamma Ray; C. E. Grouthanel Ed., pp. xii-443; s 50.

Formation and Trapping of Free Radicals; Ed. Arnold M. Bass and H. P. Broida, 1960, s 16.00.

Nuclear Spectroscopy, Vol. 9*a* of Pure and Applied Physics, Part A, 1960; $ 16.

Nuclear Spectroscopy, Vol. 9*b* of Pure and Applied Physics, Part B, 1960; $ 14.00 (pre Pub.); (after Pub.) $ 16.00 Ed. Fay Ajzenberg Selove.

Symposium of Plasma Dynamics; Editor F. H. Clauser by the Air Force Office of Scientific Research, Pergamon Press, London; Addison Wesley Pub. Co. Reading (Mass.), 1960, pp. ix-369; $ 12.50; s 84.

Recensioni.

International Review of Cytology, volume VIII, 1959. Editors: G. H. Bourne and J. F. Danielli. Academic Press, New York and London.

L'ottavo volume di questa Rivista raccoglie, come i precedenti, una serie di sintetici articoli di aggiornamento su disparati problemi di biologia cellulare. Gli argomenti trattati nei tredici articoli non sono legati da alcun nesso logico; vi si possono tuttavia riconoscere alcuni degli orientamenti attuali della ricerca biologica.

L'estendersi e il perfezionarsi della ricerca al microscopio elettronico hanno riportato il metodo morfologico a un livello di prima importanza nell'interpretazione dei fenomeni vitali. Le immagini

fornite dal microscopio elettronico, spesso soggette fino a poco tempo fa all'imputazione di artefatti, vengono ora guardate con maggior fiducia, per la generale corrispondenza trovata fra queste e i risultati di altri mezzi più indiretti di indagine. Ne è conseguenza l'interpretazione funzionale, dinamica, che viene oggi facilmente data alle immagini elettroniche. I primi quattro articoli della Rivista rispecchiano questa tendenza. *The structure of cytoplasm* di C. Oberling, è una rassegna delle attuali conoscenze sulla morfologia, particolarmente submicroscopica, del citoplasma; in *Wall organization in plant cells* di R. D. Preston, viene avanzata una interpretazione della struttura e della biosintesi delle fibrille che compongono la membrana di cellule vegetali, in base a dati ricavati dall'analisi chimica, dall'esame al microscopio elettronico, e da diagrammi di diffrazione di raggi X. In *The cell surface of Paramecium* di C. F. Ehret ed E. L. Powers, viene discussa l'interpretazione della complessa struttura rivelata dal microscopio elettronico in corrispondenza alla superficie di un organismo unicellulare, mentre in *Submicroscopic morphology of the synapse* di E. De Robertis, è avanzata un'ipotesi sulla conduzione nervosa a livello delle sinapsi, basata in gran parte sui dati morfologici forniti dal microscopio elettronico.

Due articoli sul problema della permeabilità cellulare testimoniano un altro orientamento della ricerca biologica moderna: lo sforzo di definire con rigore i limiti di applicabilità delle leggi fisiche e chimico-fisiche ai sistemi viventi: *Osmotic properties of living cells* di D. A. T. Dick, è un tentativo di interpretare la permeabilità delle cellule animali in base alle sole proprietà osmotiche dei costituenti elementari del protoplasma; in *Sodium and potassium movements in nerve, muscle and red cells* di I. M. Glynn, viene riconosciuta la necessità di ammettere un'attività biologica della membrana per giustificare a distribuzione degli ioni di potassio e sodio in cellule specializzate; in *Trace elements in cellular function* di B. L. Vallee e F. L. Hoch, la distribuzione nella cellula di metalli, legati in complessi metallo-proteici per costituire composti dotati di attività biologica specifica, viene studiata a mezzo della spettrografia di emissione, metodo finora poco usato nella ricerca biochimica. Anche l'estendersi di applicazioni tecniche più pertinenti alla Fisica testimonia la sentita necessità di porre i risultati della ricerca biologica in termini esatti.

I rimanenti articoli trattano argomenti di Citologia speciale (*The mammalian reticulocyte* di L. M. Lowenstein, *The physiology of chromatophores* di M. Fingerman, *Pinocytosis* di H. Holter) o di Istologia (*The fibrous components of connective tissue with special reference to the elastic fiber* di D. A. Hall, *Experimental heterotopic ossification* di J. B. Bridges). *A survey of metabolic studies on isolated mammalian nuclei* di D. B. Roodyn, è una raccolta bibliografica dei dati sulla composizione e sulle proprietà enzimatiche del nucleo, ricavati dall'analisi di nuclei isolati per omogeneizzazione e centrifugazione frazionata.

G. Marin

N. R. Hanson – *Patterns of Discovery*. Cambridge University Press, 1958, pp. 240.

Lo scopo di questo libro è così indicato dall'autore nella introduzione: « The approach and method of this essay is unusual. I have chosen not to isolate general philosophical issues — the nature of observation, the status of facts, the logic of causality, and the character of physical theory — and use the conclusions of such inquiries as lenses through which to view particle theory. Rather the reverse: the inadequacy of philosophical discussions of

2335

this subjects has inclined me to give a different priority. Particle theory will be the lens through which this perennial philosophical problem will be viewed ». Dopo una dichiarazione programmatica di questo genere si dovrebbe richiedere la recensione del volume da parte di un filosofo. Tuttavia essendo il saggio indirizzato esplicitamente sia alle persone con interessi prevalentemente filosofici che ai fisici, un giudizio da parte di un fisico appare opportuno.

L'idea di illustrare e chiarificare concetti come osservazione, causalità o teoria fisica, mediante un processo costruttivo descrivendo come questi si determinano naturalmente nei processi mentali del fisico, non è nuova e non mancano saggi particolarmente significativi nella letteratura sull'argomento: ad esempio alcuni capitoli di Analysis of Matter di Bertrand Russel. Ci sembra invece che N. R. Hanson non riesca a svolgere efficacemente il suo programma in questo volume Patterns of Discovery. Il difetto principale del libro è rappresentato da una descrizione eccessivamente dettagliata di situazioni particolari in cui va perduto il vero scopo della discussione. Dato il metodo esemplificativo usato nella trattazione dei diversi problemi il lettore sente alla fine di ogni capitolo la necessità di una sintesi delle osservazioni fatte che tuttavia manca completamente. Se si considera la dichiarazione programmatica dell'autore riportata precedentemente si è indotti a pensare che un qualsiasi tentativo di sintesi in termini logici sia stato volutamente evitato dall'autore.

Al contrario gli esempi usati nell'illustrare la discussione sono ben scelti e appropriati: progredendo nella lettura del saggio si nota un po' con rammarico che vi è molto materiale interessante male organizzato. Ad esempio nell'ultimo capitolo è posto il problema del significato della coincidenza della meccanica classica e della meccanica quantistica per grandi numeri quantici. Un possibile modo di rispondere al problema consiste nel riconoscere in questa coincidenza identità strutturale di « frasi » (nel senso della logica simbolica) appartenenti 3 linguaggi diversi. Questa conclusione è raggiunta in definitiva anche dal presente autore: tuttavia il lettore vi è portato attraverso discussioni dettagliate dei concetti dinamici della meccanica classica e della meccanica quantistica il cui effetto è di sviare notevolmente l'attenzione dal problema posto,

Il Volume è diviso in sei capitoli e due Appendici. Gli argomenti trattati sono nell'ordine: Observation - Facts - Causality - Theories - Classical Particle Physics - Elementary Particle Physics.

G. Jona-Lasinio

PROPRIETÀ LETTERARIA RISERVATA

Direttore responsabile: G. POLVANI

Tipografia Compositori - Bologna

Questo Fascicolo è stato licenziato dai torchi il 30-VII-1960

2336

NICOLA ZANICHELLI, EDITORE - BOLOGNA

Pubblicazioni di Matematica, Fisica, Fisica matematica, Fisica tecnica e Storia della scienza.

Estratto dal Catalogo Generale 1959

MATEMATICA

CHISINI, Oscar - *Lezioni di geometria analitica e proiettiva.*

In 8°; pag. VIII + 496 . . . . . L. 3 000

CHISINI, Oscar - *Esercizi di geometria analitica e proiettiva.*

In 8°; pag. VI + 296; . . . . . L. 2 000

ENRIQUES, Federigo - *Le superficie algebriche.*

In 8°; pag. XIV + 464 . . . . . L. 3 000
Legato . . . L. 5 000

LORIA, Gino - *Curve sgembe speciali, algebriche e trascendenti.*

Volume II; in 8°; pag. 254 . . . . . L. 800

RIMINI, Cesare - *Fondamenti di analisi matematica con applicazioni.*

Volume I; in 8°; pag. XVIII + 550 . . . . . L. 4000
Volume II; in 8°; pag. XVI + 704 . . . . . L. 6000

SANSONE, Giovanni - *Equazioni differenziali nel campo reale.*

Volume I; in 8°; pag. XVIII + 400 . . . . . L. 4 000
Volume II; in 8°; pag. XVI + 476 . . . . . L. 4 000

TRICOMI, Francesco - *Funzioni ellittiche.*

In 8°; pag. X + 344 . . . . . L. 4 500

TRICOMI, Francesco - *Funzioni analitiche.*

In 8°; pag. VIII + 134 . . . . . L. 1 500

(*segue*)

FISICA, FISICA MATEMATICA E FISICA TECNICA

BORDONI, Ugo - *Fondamenti di fisica tecnica.*

Volume I; in 8° pag. VIII + 398 . . . . . L. 5 000

BRONZI, Goffredo - *La tecnica dei radiotrasmettitori.*

In 8°; pag. XX + 404 . . . . . L. 4 000

FINZI, Bruno - *Meccanica razionale.*

Volume I; in 8°; pag. XII + 344 } . . . . . L. 7 000
Volume II; in 8°; pag. XII + 426 } Legati . . . L. 11 000

FINZI, Bruno e PASTORI, Maria - *Calcolo tensoriale e applicazioni.*

In 8°; pag. VIII + 428 . . . . . L. 2 000

FOÀ, Emanuele - *Fondamenti di Termodinamica.*

In 8°; pag. VIII + 256 . . . . . L. 3 000
Legato . . . L. 5 000

LEVI-CIVITA, Tullio e AMALDI, Ugo - *Lezioni di Meccanica razionale.*

Volume I: Cinematica, Principi e Statica.
In 8°; pag. XVIII + 816 . . . . . L. 5 000
Legato . . . L. 7 000

Volume II: Dinamica dei sistemi con un numero finito di gradi di libertà.
Parte I; in 8°; pag. XII + 510 . . . . . L. 4 000
Legato . . . L. 6 000
Parte II; in 8° pag. VI + 672 . . . . . L. 5 000
Legato . . . L. 7 000

LEVI-CIVITA, Tullio e AMALDI, Ugo - *Compendio di Meccanica razionale.*

Volume I: Cinematica, Principi e Statica.
In 8°; pag. XII + 424 . . . . . L. 2 000

Volume II: Dinamica, Cenni di Meccanica dei sistemi continui.
In 8°; pag. VIII + 310 . . . . . L. 2 000

PERSICO, Enrico - *Introduzione alla Fisica Matematica, a cura di Tino Zeuli.*

In 8°; pag. XVI + 434 . . . . . L. 4 000

PERSICO, Enrico - *Gli atomi e la loro energia.*

In 8°; pag. XVI + 490 con 150 figure e una tavola fuori testo . . . Legato . . . . L. 5 500

RIMINI, Cesare - *Elementi di Elettrotecnica generale e di Teoria delle macchine.*

In 8°; pag. XX + 806 . . . . . L. 4 000

RIMINI, Cesare - *Fondamenti di Radiotecnica generale.*

In 8°; pag. XX + 784 . . . . . L. 4 500
Legato . . . L. 6 500

TORALDO DI FRANCIA, Giuliano - *Onde elettromagnetiche.*

In 8°; pag. XIV + 286 . . . . . L. 3 000
Legato . . . L. 5 000

(segue)